

1-1-2010

# Synthesis and Investigation of Perfluorinated Polystannanes

Miles Damion  
*Ryerson University*

Follow this and additional works at: <http://digitalcommons.ryerson.ca/dissertations>

 Part of the [Inorganic Chemistry Commons](#)

---

## Recommended Citation

Damion, Miles, "Synthesis and Investigation of Perfluorinated Polystannanes" (2010). *Theses and dissertations*. Paper 1354.

This Thesis is brought to you for free and open access by Digital Commons @ Ryerson. It has been accepted for inclusion in Theses and dissertations by an authorized administrator of Digital Commons @ Ryerson. For more information, please contact [bcameron@ryerson.ca](mailto:bcameron@ryerson.ca).

# SYNTHESIS AND INVESTIGATION OF PERFLUORINATED POLYSTANNANES

by

Damion Miles

A thesis

presented to Ryerson University

in partial fulfillment of the

requirements for the degree of

Master of Science

in the Program of

Molecular Science

Toronto, Ontario, Canada, 2010  
© Copyright by Damion Miles 2010



## **Author's Declaration**

I hereby declare that I am the sole author of this thesis.

I authorize Ryerson University to lend this thesis to other institutions or individuals for the purpose of scholarly research.

Name: \_\_\_\_\_ Signature: \_\_\_\_\_

I further authorize Ryerson University to reproduce this thesis by photocopying or by other means, in total or in part, at the request of other institutions or individuals for the purpose of scholarly research.

Name: \_\_\_\_\_ Signature: \_\_\_\_\_



## **DEDICATIONS**

I would like to dedicate this thesis to the two people who shaped the person who I am, my grandmothers, Petita “Tita” Miles and Ruby “Ms. Tiny” Brown. This thesis represents the love, hard work and sacrifice of the two greatest influences in my daily life.

## ACKNOWLEDGEMENT

I would like to take this opportunity to thank my supervisor, Dr. Daniel Foucher for taking me on as a graduate student. Looking back I would also like to thank him for challenging me to reach my potential in the last two years. He was always there when I needed him, constantly providing vital feedback throughout the course of this work. I feel this has not only made me a better chemist but a better person and I will forever be grateful to him for that.

I would also like to thank Dr. Andrew Mc Williams, Dr. Robert Gossage for being such great committee members and for always providing insight into my thesis. The meeting with you guys was very educational for me and was instrumental in pointing me in the right directions.

Special thanks to the labmates who made my time in the lab very memorable. Patricia “Trish” Stanescu, Victoria Aldeva, Jon “Jonnie Boy” Ward, Sossina Gezahegn, Sarah Komejan, Maja “May” Chojnacka, Tayseer Mahdi and Sanja Resanovic. Thank you all. Aman Khan, you have been a brother to me throughout this time.

Thanks you also to the Dr. Alex Young and Dr. Alan Lough from the University of Toronto for the great mass spectrometry and X-ray crystallographic work. I could also count on you guys to provided accurate data within a short time.

To my family, I work hard not only for myself but also for you guys. Roxon, Renesia, Chantel, Justene, Rajheem, Jamie and Nehander you guys mean the world to me and hope I have set a good example as an older brother. Special Thanks to my parents Hugh Brown and Merna Muir for giving me the gift of life. Last but not least I would like to thank my aunt Etta Miles for putting up with me in the last ten years. I love you all.

## TABLE OF CONTENT

### Abstract

### Section 1: Introduction

- 1.1.a: History of Synthetic Materials.....1
- 1.1.b: Organic Carbon Based Chemistry.....2
- 1.1.c: Application of Carbon Chemistry and Group 14 elements.....2
- 1.1.d: Organic Carbon Based Polymers and Their Application.....3

### Section 1.2: Organic Conducting polymers

- 1.2.a: Conducting Polymers and the Band Gap Theory.....4-5
- 1.2.b: Organic  $\pi$  Conjugated Conducting Polymers..... 5-7

### Section 1.3: Group 14 Polymers and History of Polystannanes

- 1.3.a: Group 14 Inorganic Polymers.....7-9
- 1.3.b: Synthetic History of Polystannanes.....9-14
- 1.3.c: Current Synthetic Methods for Group 14 Polymers..... 14
- 1.3.d: Wurtz Coupling of Polystannanes.....14-16
- 1.3.e: Electrochemical Synthesis of Polystannanes.....16-17
- 1.3.f: One Electron Coupling of Polystannanes using Samarium Iodide.....17-18
- 1.3.g: Dehydrocoupling of Polystannanes.....19-21
- 1.3.h: Electronic Properties of Polystannanes.....21-22

### Section 1.4: Characterization of Polystannanes

- 1.4.a: NMR spectroscopy.....22-23
- 1.4.b: Gel Permeation Chromatography (GPC).....23-24
- 1.4.c: Thermal Gravimetric Analysis (TGA) and Differential Scanning Calorimetry (DSC) Analysis of Polystannanes.....24-26

## Section 1.5 Fluorine chemistry

- 1.5.a:** Properties of Fluorinated Compounds.....27
- 1.5.b:** Synthesis of Fluorinated Compounds.....28-29

## Section 1.6 Objective

- 1.6.a:** Thesis Objective.....30-32

## Section 2.0: Experimental and Method

- 2.1:** Methods.....33-34
- 2.2:** Synthesis of Perfluorinated Tetraarylstannanes, Diaryldichlorostannanes, Diaryltin dihydride and Diarylpolystannanes
- 2.2.1:** Synthesis of *Tetrakis[4-trifluoromethylphenyl]Stannane 1* by.....35-36  
the Organolithium route
- 2.2.2a:** Synthesis of *Tetrakis[3,5-bis(trifluoromethylphenyl)Stannane*.....36  
by Organolithium route **2**
- 2.2.2b:** Synthesis of *Tetrakis[3,5-bis(trifluoromethylphenyl)Stannane*.....37-38  
by Grignard Route **2**
- 2.2.3:** Synthesis of compound *Tetrakis[pentafluorophenyl]*.....38-39  
*stannane 3* using the organolithium route
- 2.2.4:** Synthesis of *Di-[4-(trifluoromethyl)phenyl]dichlorostannane*.....39-40  
**4** by reaction between **1** and SnCl<sub>4</sub>
- 2.2.5:** Synthesis of *Di-[3,5-bis-(trifluoromethyl)phenyl]*.....40-41  
*dichlorostannane 5* by reaction between **1** and SnCl<sub>4</sub>
- 2.2.6:** Synthesis of *Di-[Pentafluorophenyl]dichlorostannane 6*.....41-42  
using reaction between **3** and SnCl<sub>4</sub>
- 2.2.7:** Synthesis of *[4-(trifluoromethyl)phenyl]tin trihydride*.....42-43  
**8** by chlorine substitution by using LiAlH<sub>4</sub>
- 2.2.8:** Synthesis of *[3,5-bis-(trifluoromethyl)phenyl]tin*.....43-44  
*trihydride 9* by chlorine substitution by using LiAlH<sub>4</sub>

<b>2.2.9:</b>	Synthesis of <i>Poly(di[4-(trifluoromethyl)phenyl]stannane</i> .....	45
	by Wurtz Coupling <b>10</b>	
<b>2.2.10:</b>	Synthesis of <i>Poly[di(3,5-bis-(trifluoromethyl)phenyl)]</i> .....	46-47
	<i>stannane</i> by Wurtz Coupling <b>11</b>	
<b>2.2.11:</b>	Synthesis of <i>poly([4-(trifluoromethyl)phenyl])</i> .....	47-48
	<i>stannane</i> by Dehydrocoupling <b>12</b>	
<b>2.2.12:</b>	Synthesis of <i>Poly[(3,5-bis-(trifluoromethyl)phenyl)]</i> .....	48
	<i>stannane</i> by Dehydrocoupling <b>13</b>	

### **Section 3.0: Results and Discussion**

<b>3.1:</b>	Fluorinated Tetra(aryl) Tin Compounds.....	49-52
<b>3.2:</b>	Fluorinated Tin Dichlorides by Redistribution.....	52-57
<b>3.3:</b>	Tin Dihydrides Synthesis Using LiAlH <sub>4</sub> .....	58-60
<b>3.4a:</b>	Polymerization of Tin Dichlorides Using Wurtz.....	61-62
<b>3.4b:</b>	Polymerization of Tin Trihydrides using Dehydrocoupling.....	62-63
<b>3.5:</b>	UV/VIS Spectroscopy of Polystannanes.....	63-67
<b>3.6:</b>	GPC Analysis of Polymers From Wurtz and.....	67-70
	Dehydrocoupling reaction	
<b>3.7:</b>	NMR Analysis of Polymers From Wurtz and.....	70-72
	Dehydrocoupling reaction	
<b>Conclusion</b> .....		73-75
<b>Future Work</b> .....		75-76
<b>References</b> .....		77-80
<b>Appendices</b> .....		80-125

## TABLE OF TABLES

<b>Table 1</b>	Some common polymers containing carbon backbone.....3 and their use
<b>Table 2</b>	Calculated band parameter for polystannane and.....9 other Group 14 elements
<b>Table 3</b>	Selected polystannanes and the Catalyst used in their.....21 synthesis along with UV/VIS and $M_n$ data
<b>Table 4</b>	Molecular weight data and $^{119}\text{Sn}$ -NMR chemical.....23 shift of selected polystannanes
<b>Table 5</b>	GPC results from the different methods for polystannane.....24 Synthesis
<b>Table 6</b>	Decomposition temperatures of selected polystannanes.....25 measured by TGA analysis
<b>Table 7</b>	Shows the Thermal properties of polystannanes.....26 measured by DSC
<b>Table 8</b>	Physical properties of the C-F bond.....27
<b>Table 9</b>	Comparison of experimental and literature $^{119}\text{Sn}$ -NMR.....49 shift for tetraaryl stannanes
<b>Table 10</b>	MS fragmentation patterns for <i>tetrakis[3,5-Bis(trifluoromethyl).....52</i> <i>phenyl]stannane</i> after TOF-MS
<b>Table 11</b>	X-ray data for <i>di-[4-(trifluoromethyl)phenyl]dichlorostannane</i> ,.....56 <i>di-[3,5 (trifluoromethyl)phenyl]dichlorostannane</i> and <b>7</b>
<b>Table 12</b>	Fragmentation of <i>di-[3,5-(trifluoromethyl)phenyl].....57</i> <i>dichlorostannane</i> after TOF-MS
<b>Table 13</b>	UV/VIS data for polymers synthesized by Wurtz and.....64 Dehydrocoupling

## TABLE OF FIGURES

<b>Figure 1</b>	Electronic band gap illustration of an insulator,.....5 semi-conductor, and conductor	5
<b>Figure 2</b>	Some of the earliest organic conducting polymers.....6 synthesized	6
<b>Figure 3</b>	Conductivity of some organic polymer before and after.....7 doping	7
<b>Figure 4</b>	The band gap of the first 5 elements of the Group 14.....8	8
<b>Figure 5</b>	The X-ray structure showing bond angles and length of.....11 organotin compounds of different chain length	11
<b>Figure 6</b>	Relationship between structure and NMR shift for tin.....12 compounds	12
<b>Figure 7</b>	UV/VIS spectra for $\text{Ph}_3\text{Sn}(\text{Sn}^t\text{Bu}_2)_n\text{-SnPh}_3$ , where $n = 1-4$ .....13	13
<b>Figure 8</b>	GPC chromatogram for MPrPSi in THF with different molar.....16 ratio of 18-crown-6-ether/MePrSiCl <sub>2</sub>	16
<b>Figure 9</b>	Mechanism for metal catalyzed dehydrocoupling of.....19 polystannanes	19
<b>Figure 10</b>	DSC chromatogram for poly(dibutyl)stannane after first.....26 heating and cooling cycle	26
<b>Figure 11</b>	Fluorinated phenyl substituents.....30	30
<b>Figure 12</b>	Steps for the synthesis of polymers using Wurtz coupling or.....31 dehydrocoupling reactions	31
<b>Figure 13</b>	Synthesis of <i>tetrakis[4-trifluoromethylphenyl]stannane</i> .....35 <b>1</b> using the organolithium route	35
<b>Figure 14</b>	Synthesis of <i>tetrakis[3,5-Bis(trifluoromethyl)phenyl]</i> .....36 <i>stannane 2</i> using the Grignard route	36
<b>Figure 15</b>	Synthesis of <i>tetrakis[3,5-Bis(trifluoromethyl)phenyl]</i> .....37 <i>stannane 2</i> using the organolithium route	37
<b>Figure 16</b>	Synthesis of <i>Tetrakis[pentafluorophenyl]stannane 3</i> using.....38 the organolithium route	38

<b>Figure 17</b>	Synthesis of <i>di</i> -[4-(trifluoromethyl)phenyl]dichloro.....39 <i>stannane 4</i> using <b>1</b> and SnCl <sub>4</sub>	39
<b>Figure 18</b>	Synthesis of <i>di</i> -[3,5-(trifluoromethyl)phenyl]dichloro.....40 <i>stannane 5</i> using <b>2</b> and SnCl <sub>4</sub>	40
<b>Figure 19</b>	Synthesis of <i>Di</i> -[Pentafluorophenyl]dichlorostannane <b>6</b> via.....41 redistribution reaction between <b>3</b> and SnCl <sub>4</sub>	41
<b>Figure 20</b>	Synthesis of <i>Bis</i> [(trifluoromethyl) phenyl] tin dihydride <b>8</b> .....42 by reaction between <b>4</b> and LiAlH <sub>4</sub>	42
<b>Figure 21</b>	Synthesis of <i>Bis</i> (3,5(trifluoromethyl)phenyltin Trihydride <b>9</b> .....43 by reaction between <b>5</b> and LiAlH <sub>4</sub>	43
<b>Figure 22</b>	Synthesis of <i>Poly</i> ( <i>di</i> [4-(trifluoromethyl)phenyl]stannane .....45 <b>10</b> by Wurtz coupling of <b>4</b>	45
<b>Figure 23</b>	Synthesis of <i>Poly</i> ( <i>di</i> [3,5-(trifluoromethyl)phenyl]stannane.....46 <b>11</b> by Wurtz coupling of <b>5</b>	46
<b>Figure 24</b>	Synthesis of <i>Poly</i> [(trifluoromethyl)phenyl]stannane.....47 <b>12</b> by dehydrocoupling of <b>8</b>	47
<b>Figure 25</b>	Synthesis of <i>Poly</i> [3,5(trifluoromethyl)phenyl]stannane.....48 <b>13</b> by dehydrocoupling of <b>9</b>	48
<b>Figure 26</b>	A plot of the <sup>1</sup> H-NMR spectrum for tetra aryl stannanes.....50 ( <b>1-2</b> ) and dichlorostannanes ( <b>4-5</b> )	50
<b>Figure 27</b>	Crystal structure for <i>Tetrakis</i> [3,5- <i>Bis</i> (trifluoromethyl)phenyl].....51 <i>stannane 2</i>	51
<b>Figure 28</b>	Stack plot of the <sup>119</sup> Sn-NMR chemical shift for aryl.....53 tin dichlorides	53
<b>Figure 29</b>	A plot of the relationship between the <sup>119</sup> Sn-NMR.....54 shift and number of CF <sub>3</sub> for aryltin dichlorides	54
<b>Figure 30</b>	X-ray crystal structure for <i>Di</i> -[4-(trifluoromethyl)phenyl]dichloro.....55 <i>stannane 4</i> and <i>di</i> -[3,5-(trifluoromethyl)phenyl]dichlorostannane <b>5</b>	55
<b>Figure 31</b>	<sup>1</sup> H-NMR spectrum for the tin trihydride <b>9</b> showing the.....59 phenyl and hydride region	59
<b>Figure 32</b>	<sup>119</sup> Sn-NMR spectrum for the tin hydride <i>Bis</i> [(trifluoromethyl).....60 <i>phenyl</i> ]tin Trihydride <b>8</b>	60

<b>Figure 33</b>	Schematic diagram for the Wurtz coupling of <b>4</b> and <b>5</b> .....	61
	to yield polymers <b>10</b> and <b>11</b>	
<b>Figure 34</b>	Schematic diagram for the dehydrocoupling of <b>8</b> and <b>9</b> .....	62
	to yield polymers <b>12</b> and <b>13</b>	
<b>Figure 35</b>	Structure for network polymers <i>Poly[(trifluoromethyl)phenyl]</i> .....	65
	<i>stannane 12</i> and <i>poly[3,5(trifluoromethyl)phenyl]stannane 13</i>	
<b>Figure 36</b>	UV/VIS spectrum for <i>Poly[(trifluoromethyl)phenyl]stannane</i> .....	66
	<b>12</b> after dehydrocoupling	
<b>Figure 37</b>	UV/VIS spectrum for <i>Poly[3,5(trifluoromethyl)phenyl]</i> .....	67
	<i>stannane 13</i> after 1 and 2 scans of UV/VIS	
<b>Figure 38</b>	GPC of <i>Poly(di[3,5-(trifluoromethyl)phenyl]stannane 10</i> .....	69
	with RI (red) and LALS and RALS detectors	
<b>Figure 39</b>	A plot of the <sup>119</sup> Sn-NMR signals for <b>10</b> and <b>11</b> .....	70
<b>Figure 40</b>	<sup>1</sup> H-NMR spectrum for compound <b>11</b> after Wurtz coupling.....	71
<b>Figure 41</b>	<sup>19</sup> F-NMR spectrum of polymer <i>Poly[3,5(trifluoromethyl)phenyl]</i> .....	72
	<i>stannane 13</i> after dehydrocoupling	

## TABLE OF REACTIONS

<b>Reaction 1</b>	Preparation of diethyltin diiodide from ethyl iodide.....10 and tin metal
<b>Reaction 2</b>	Hydrostannolysis reaction used to synthesize.....13 oligostannanes
<b>Reaction 3</b>	Wurtz coupling of alkyl halide in the presence.....14 of sodium metal
<b>Reaction 4</b>	Wurtz coupling of group 14 metal and metalloid dichlorides.....15 using the modified reaction
<b>Reaction 5</b>	Electrochemical reaction used to synthesize linear.....16 poly(dialkyl)stannane
<b>Reaction 6</b>	Electrochemical reaction for the synthesis of network.....17 polystannanes
<b>Reaction 7</b>	Samarium Iodide reaction used in the synthesis of poly.....18 stannanes
<b>Reaction 8</b>	Dehydrocoupling of tin dihydride in the presence of a.....20 metal catalyst
<b>Reaction 9</b>	Grignard reaction for the synthesis of fluorinated tetra.....28 aryl stannanes from SnCl <sub>4</sub> and corresponding reagent
<b>Reaction 10</b>	Reaction between tetra aryl stannane and SnCl <sub>4</sub> to.....28 prepare tin chlorides
<b>Reaction 11</b>	Preparation of tin hydrides from reactions between tin.....28 chlorides and lithium aluminum hydride

## List of Abbreviation

Å	Angstrom
AsF <sub>5</sub>	Arsenic Pentafluoride
Atm	Atmospheric pressure
β	Resonance Integral
Bu	Butyl
CDCl <sub>3</sub>	Deuterated Chloroform
CF <sub>3</sub>	Trifluoromethyl
Cp	Cyclopentadiene
Da	Dalton
DCM/ CH <sub>2</sub> Cl <sub>2</sub>	Dichloromethane
Dod	Dodyl
DSC	Differential Scanning Calorimetry
ε	Molar absorptivity
eV	Electrovolt
GPC	Gel Permeation Chromatography
Hex	Hexyl
HMPA	Hexamethylphosphoramide
HOMO	Highest Occupied Molecular
Orbital	
Hz	Hertz
IR	Infrared Spectroscopy
<i>J</i>	NMR Coupling Constant (Hertz)
K	Potassium
Kcal/mol	Kilocalorie per mole
LALS	Low angle light scattering
λ	Wavelength
LUMO	Lowest Unoccupied Molecular
Orbital	
Me	Methyl
mL	Milliliter
M <sub>n</sub>	Number average molecular
weight	
M <sub>w</sub>	Weight average molecular weight
N <sub>2</sub>	Nitrogen
<i>n</i> -BuLi	Butyl Lithium
NMR	Nuclear Magnetic Resonance
Oct	Octyl
OEt	Ethoxy
PDI	Polydispersity Index
Pent	Pentyl
Ph	Phenyl
π	Pi Orbital

ppm  
RALS  
RI  
RT  
 $\delta$   
TGA  
THF  
TOF-MS  
Spectrometry  
UV/VIS

Parts Per Million  
Right angle light scattering  
Refractive Index  
Room Temperature  
NMR Chemical shift  
Thermal Gravemetric Analysis  
Tetrahydrofuran  
Time of Flight Mass  
Ultra violet/Visible Spectroscopy

# SYNTHESIS AND INVESTIGATION OF PERFLUORINATED POLYSTANNANES

Master of Science, 2010

Damion Miles

Molecular Science

Ryerson University

## Abstract

Two fluorinated tetraaryl stannanes, **1** and **2** were synthesized in good yields. X-ray crystallography revealed deviation from ideal tetrahedral geometry with C-Sn-C bond angles between 107.89°-112.7° for **1** and 104.69°-120.76° for **2**. Dichlorides **4** and **5** were synthesized using a redistribution reaction between SnCl<sub>4</sub> and **1-2**. These dichlorides also deviated from tetrahedral geometry with bond angles between 101.79°-128.44° for **4** and 99.23°-125.9° for **5**. Polymerization of **4** and **5** by Wurtz coupling produced polymers **10** and **11**. Absolute molecular weights in the range of  $1.16 \times 10^5$ - $2.92 \times 10^7$  Da was estimated for **10** and  $1.47 \times 10^5$  Da for **11**. UV/VIS spectroscopy gave values of 332 nm and 328 nm that are blue shifted to other polystannanes. The unexpected cleavage of a tin-aryl bond produced tin trihydrides **8** and **9**. Polymerization of **8-9** produced the network polymers **12** and **13** with  $\lambda_{\text{max}}$  values of 354 nm and 350 nm.

### **1.1a History of Synthetic Materials**

A good indicator of progress in any civilization is the types of materials it creates and uses.<sup>1,2</sup> The continuous growth of materials chemistry throughout the ages has given society access to a wide variety of novel synthetic products. Many of these new materials are often stronger, faster, cheaper and perform measurably better than their predecessors.<sup>2</sup> These features are some of the main drivers behind materials chemistry, all of which is aimed at making life easier via materials.

### **1.1b Organic-Carbon Based Chemistry**

Organic chemistry is based on compounds that contain the elements carbon, nitrogen, hydrogen, oxygen and to a lesser extent silicon, phosphorous and sulfur. While the majority of these elements play an important role in organic chemistry, it is the element carbon that largely defines this field of chemistry.<sup>3</sup> The abundance of carbon chemistry is largely due to the relative ease with which carbon forms bonds with itself and other heteroatoms.<sup>3</sup>

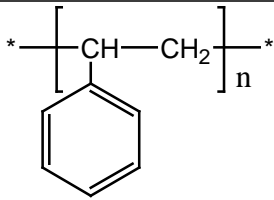
### **1.1c Application of Carbon Chemistry and Group 14 Elements**

By modifying carbon based compounds, materials with tailored properties can be obtained. This can be achieved by incorporating elements of the periodic table that possess a wide variety of properties. Some elements possess similar properties (notably those in the same group), while others differ dramatically.<sup>4</sup> The Group 14 elements Si, Ge, Sn and to a lesser extent Pb mainly due its size are expected to have similar chemistry and properties.<sup>4</sup> Overall, only a small percentage of elements in the periodic table and the compounds that they can form have been investigated for their properties.

## 1.1d Organic Based Polymers and Their Applications

Polymers are long chain, usually linear compounds that are connected by elements forming covalent bonds ( $\sigma$  or  $\pi$ ) in what is referred to as the backbone of the polymer.<sup>1,2</sup> This backbone is often highlighted by the repetition of one or more monomeric units forming a chain like structure.<sup>1,2</sup> The length of these chains along with the substituents in the backbone are often responsible for dictating the properties of polymers.<sup>1,2</sup> Many of the best studied and characterized polymers are those based upon a carbon backbone. While this continues to hold true, the polymer chemistry of elements other than carbon are now being actively investigated. These inorganic and organometallic polymers may possess improved thermal and chemical stabilities, along with novel electronic properties.<sup>1,2</sup> Synthetic polymers have found many uses ranging from everyday materials such as elastomers and thermoplastics to more technological uses in electrical, optical and biological systems.<sup>5</sup> A sampling of polymers and their applications are listed in Table 1.

**Table 1:** Some common polymers containing carbon backbone and their application

Names	Formula	Application
Polytetrafluoroethylene <sup>6</sup>	$-(CF_2-CF_2)_n-$	non-stick surfaces and electrical insulation
Polystyrene <sup>7</sup>		Styrofoam, molded objects such as tableware (forks, knives and spoons), trays, videocassette cases
Polyvinylchloride <sup>8</sup>	$-(CH_2-CHCl)_n-$	pipes, siding, flooring, automotive

## 1.2a Conducting Polymers and the Band Gap Theory

Conducting polymers are a class of polymers that have the ability to conduct an electrical charge, usually along their backbone. These type of polymers have backbones that are normally comprised of a metal, metalloid<sup>1</sup> or a fully conjugated  $\pi$  system.<sup>9-12,13,14</sup> They are generally referred to as semi-conductors because their conductivity lies between those of an insulator and a conductor (metal).<sup>10,11</sup> Conductive polymers uniquely combine the mechanical properties of modern plastic with the ability to conduct electricity like a metal or metalloid.<sup>10</sup> The electrical properties of conducting polymers can be accurately described using band gap theory.<sup>12</sup> Band gap theory is an extension of the molecular orbital theory which states that the number of molecular orbitals is equal to the number of atomic orbitals that combines to form the molecule. There is an increase in the number of atomic orbitals in the case of polymers due to the number of repeating units in their backbone and this causes the gap between these molecular orbitals to decrease.<sup>12</sup> The resulting overlapping molecular orbitals are closer in energy causing them to appear as a band on an energy diagram.<sup>12</sup> This also results in a reduction of distance between the HOMO (filled or partially filled valence band) and LUMO (empty conduction band) orbitals which is known as the band gap. This is significant because in order for conduction to occur, electrons in the valence band must absorb enough energy to be promoted to the conduction band.<sup>13</sup> The smaller the band gap, the lower the energy that is required to promote electrons and the better conductor the material will be. Figure 1 is a schematic band gap diagram describing the different types of conducting materials.<sup>12</sup>

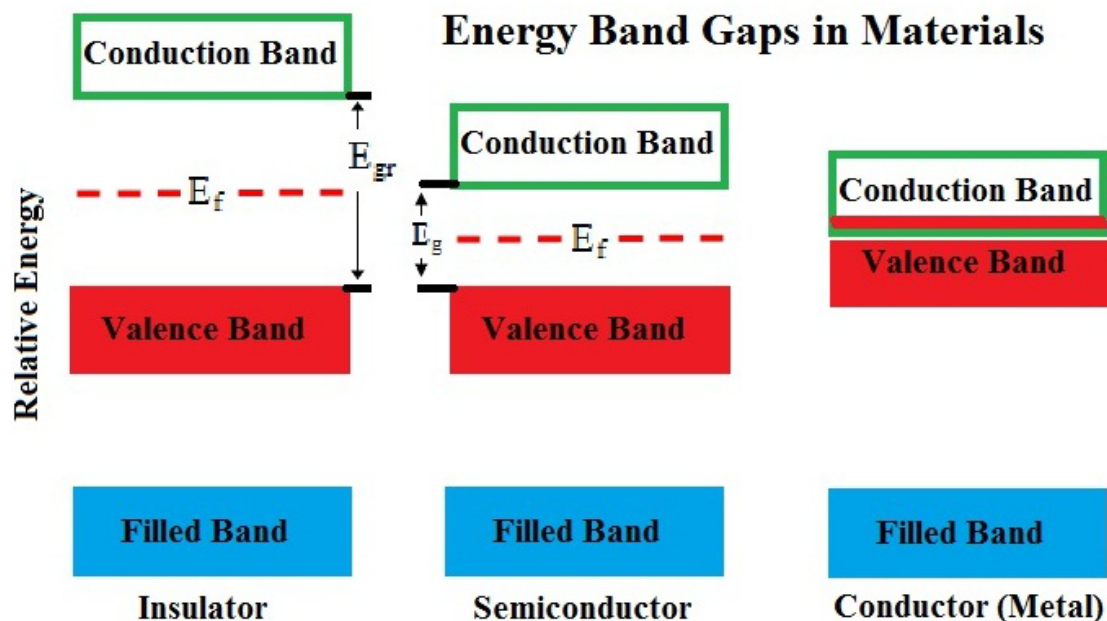


**Figure 1:** Electronic band gap of an insulator, semi-conductor, and conductor.<sup>12</sup>

Most metals characteristically have large radii when compared to other main group elements on the periodic table and as a result the outermost electrons are only weakly held.<sup>18</sup> These electrons have the ability to delocalize more freely than those in non-metallic systems.<sup>18</sup> The mobility of these electrons are also enhanced by the fact that metals intrinsically have no band gap due a overlap between the valence and conduction band as seen in Figure 1.<sup>12</sup> While conductors and semi-conductors have the ability to conduct electricity, there is a third class of material known as insulators that lack the ability to conduct charge due to a large band gap. These are often organic molecules that lack a  $\pi$  conjugated system and have saturated carbon backbones.

### 1.2b Organic $\pi$ Conjugated Conducting Polymers

Conducting polymers were first synthesized and characterized by Pohl<sup>13</sup> and Katon<sup>14</sup> who in the 1960's highlighted the electrical behaviour of some  $\pi$  conjugated polymers. While these were not the first reports of electrically conducting polymers, they represent the first in-depth study of the electrical behaviour of

polymers. Their research was instrumental, but it wasn't until 1977 that the first highly conducting polymers were reported.<sup>9</sup> Shirikawa and Heeger demonstrated the conductivity of a silvery film of the polymer *trans*-polyacetylene increased dramatically when it was doped by exposing it to halogens vapours, in particular iodine's.<sup>9,10</sup> This conductive behaviour was also evident in other  $\pi$  conjugated polymers, some of which are shown in Figure 2.

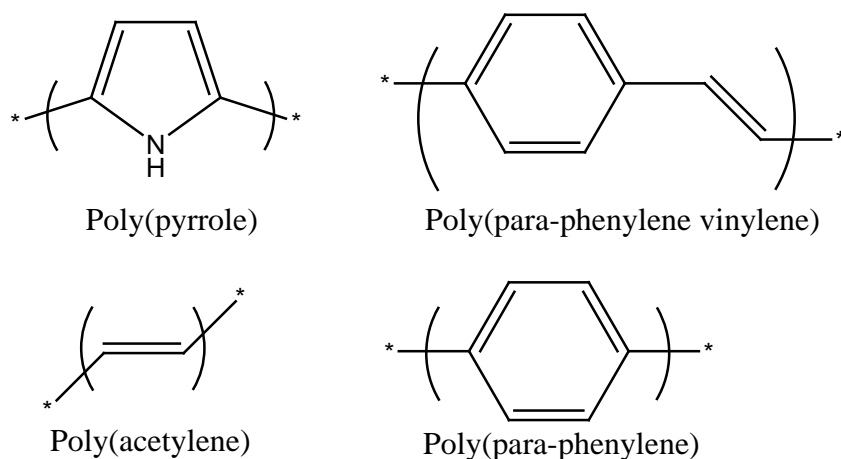


**Figure 2:** Some of the earliest well known organic conducting polymers.<sup>9</sup>

A comparison of the conductivity of a few organic polymers is illustrated in Figure 3. The diagram shows that at low doping concentrations, organic polymers such as polyacetylene are insulators or semi-conductors but can achieve the conductivities of metals upon doping.<sup>15</sup> In the example of *n*-type doping, electrons from the electron rich dopant are injected into the conduction band. Conduction is then achieved by the application of a voltage (energy) that allows these electrons to become mobile. The polymers highlighted in Figure 3 are fully conjugated, allowing electrons to delocalize along their backbone *via* their  $\pi$  system.<sup>15</sup>

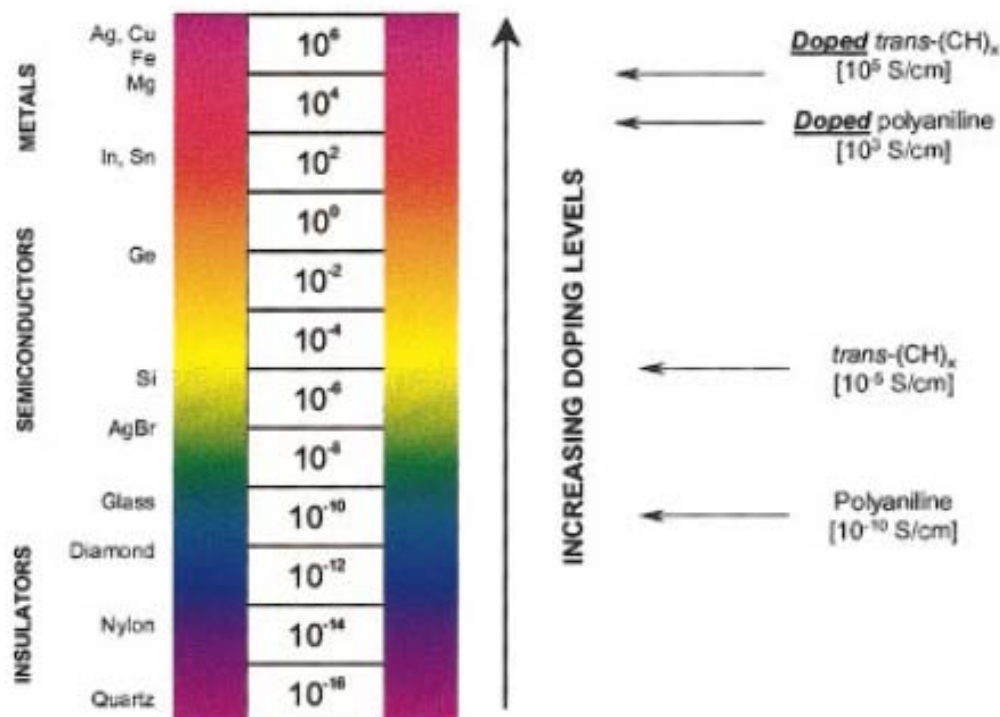


**Figure 3:** Conductivity of some organic polymer before and after doping<sup>15</sup>

This is because electrons in  $\pi$  bonds are higher in energy which brings them closer to the LUMO orbital. This feature allows these  $\pi$  electrons to achieve the mobility required for conduction upon doping.<sup>12,16</sup>

### 1.3a Group 14 Inorganic Polymers

A logical place to look for inorganic main group element based polymers is in Group 14 of the periodic table where the elements are expected to have properties that resemble those of carbon.<sup>4</sup> The similarity in chemistry should allow these heavier Group 14 elements to form polymers with similar architecture to those formed by carbon.<sup>17</sup> While organic polymers can only conduct along a conjugated  $\pi$  system along their backbone, this is not the case in organometallic polymers.<sup>1,2</sup> The electrons in a metal or metalloid  $\sigma$  bond are generally higher in energy than those in a carbon based  $\sigma$  system.<sup>18</sup> As shown in Figure 4, the band gap of the elements decrease moving downwards in the group.<sup>17</sup>

<b>B</b>	<b>C</b> 2p <sup>2</sup>	<b>N</b>
<b>Al</b>	<b>Si</b> 3p <sup>2</sup>	<b>P</b>
<b>Ga</b>	<b>Ge</b> 4p <sup>2</sup>	<b>As</b>
<b>In</b>	<b>Sn</b> 5p <sup>2</sup>	<b>Sb</b>
<b>Tl</b>	<b>Pb</b> 6p <sup>2</sup>	<b>Bi</b>

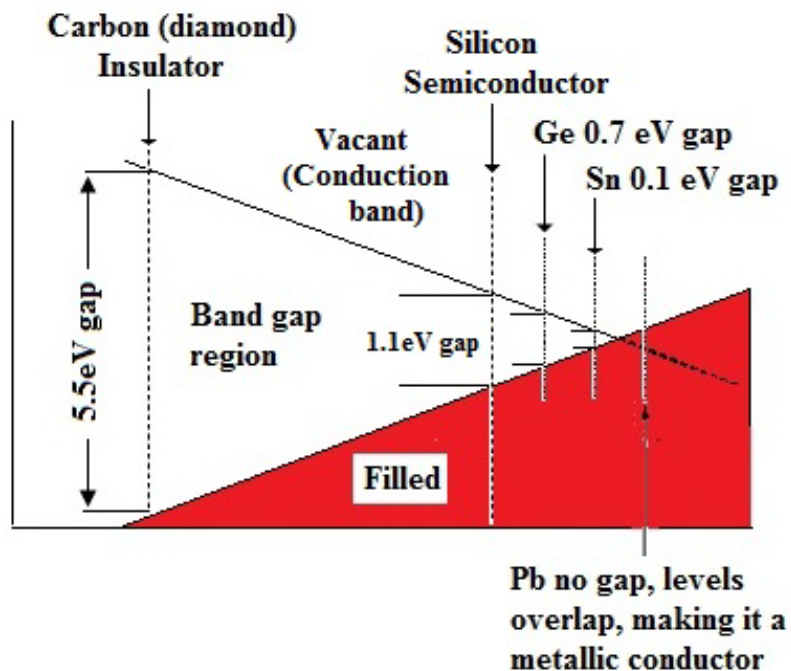


**Figure 4:** The band gap of the first 5 elements of the Group 14.

This gives metals and semi-metals the ability to conduct electricity along their sigma bond, something not observed in organic polymers.<sup>1,2,9</sup> Previous research has shown that Group 14 metal and metalloid (Si, Ge, Sn) polymers display interesting electronic properties.<sup>1,2,19</sup> Because of their intrinsic semi-conducting properties, metal containing polymers like polystannanes tend to have lower band gaps compared to their organic counterparts.<sup>19-21</sup> This is evident in that organic polymers usually require a higher degree of doping to achieve comparable conductivity to inorganic polymers.<sup>11</sup> It is also based on theoretical calculations that suggest that polystannane may be able to achieve a metallic state whereby the valence and the conduction band overlap.<sup>19</sup> Theoretically it is believed that this can be achieved by influencing the backbone conformation and bond angles. Calculations using the Sandorfy C model make the assumption that polystannanes are linear chains of Sn atoms with interacting sp<sup>3</sup> orbitals.<sup>20</sup> In this model, the ratio of the resonance integral  $\beta$  of the germinal and vicinal interaction ( $\beta_{\text{gem}}/\beta_{\text{vic}}$ ) is used to determine the degree of delocalization along the backbone of the polymers.<sup>21</sup> When this value approaches unity, the orbital

interaction between each atom and its neighbour is similar to interactions found within the atom itself which suggest that there is considerable delocalization along the backbone.<sup>21</sup> A value of 0.75 was calculated for polystannanes revealing a high degree of interaction between neighbouring orbitals.<sup>21</sup> Therefore polystannanes are expected to be fully conjugated with the ability to conduct along their sigma bond. Table 2 lists some Group 14 polymers and their corresponding conformation dependant calculated band gaps. Based on these studies, polystannanes with *trans*-planar backbones are expected to be more conjugated as compared to their non-planar counterparts. This is due to the increased orbital interactions as a result of having the correct orientation.<sup>21</sup>

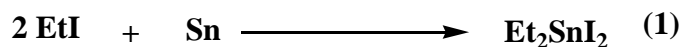
**Table 2:** Calculated band parameter for polystannane and other Group 14 elements<sup>21</sup>

Polymer	Conformation	Band gap $E_g$ (eV)	Effective hole mass at valence band edge	Effective electron mass at conduction band edge
$(CH_2)_n$	Trans-planar	-	0.21	-
$[CH=CH]_n$	Trans-planar	-	0.12	-
$[SiH_2]_n$	Trans-planar	3.89	0.14	0.10
	Gauche helical	5.94	7.84	0.88
$[GeH_2]_n$	Trans-planar	3.31	0.13	0.10
	Gauche helical	5.13	5.39	0.57
$[SnH_2]_n$	Trans-planar	2.80	0.12	0.09
	Gauche helical	4.65	9.66	2.32

### 1.3b Synthetic History of Polystannane

Tin is the only heavy metal known to form a polymer whereby the backbone is completely comprised of metal atoms.<sup>22</sup> Like carbon, tin forms four covalent bonds and a linear chain with an extended Sn-Sn backbone. These type of polymers are referred to as polystannanes. While the first examples of high

molecular weight polystannanes have only been isolated in the last two decades, organotin compounds have been known for some time. They were first discovered in the 19<sup>th</sup> century by Farkland who in 1848 was able to isolate diethyltin diiodide from a reaction between tin metal and ethyl iodide (Rxn. 1).<sup>23</sup>



He followed up this work by isolating diethyltin in 1852/53 from a reaction that involved the immersion of zinc foil into a solution of diethyltin dichloride, but this was later disputed based on the elemental analysis reported.<sup>24</sup> Oligo- and polystannanes were isolated by Löwig in 1852 from a reaction between Sn/K (or Sn/Na) alloy and iodoethane.<sup>24</sup> Löwig, using diethyl ether and ethanol as the reaction and recovery solvent, was able to isolate compounds that gave elemental analysis consistent with a structure for oligo and poly(diethyl)stannanes ( $[\text{Et}_2\text{Sn}]_n$ ). These compounds were described as viscous liquids. The liquid nature of these compounds was more consistent with smaller molecules and it was later hypothesized that this liquid was due to the presence of cyclic oligomers that resulted from the degradation of  $[\text{Et}_2\text{Sn}]_n$ .

A recent resurgence of interest in polystannanes was stimulated by work done by Dräger and coworkers on model oligostannanes in the late 1980's.<sup>25,26</sup> This critical work bridged the understanding between pure metallic and organometallic tin compounds. Dräger investigated the structure of organotin compounds as they transition from compounds with a simple  $\sigma$ - $\sigma$  bond to those with extensive delocalized character. He was able to use a variety of techniques such as X-ray crystallography and spectroscopic techniques such as IR, UV/VIS and NMR to characterize the molecular and electronic structure of oligostannanes. X-ray studies revealed that bond angles of oligostannanes deviated significantly from an ideal tetrahedral geometry. These angles were found to increase as result of the Sn-Sn bonds substantially lengthening with catenation. It was suggested that this was a clear indicator of a decreasing band gap. These two trends were further exaggerated by the introduction of bulky electron rich substituent at the Sn center<sup>25</sup> as illustrated by Figure 5.

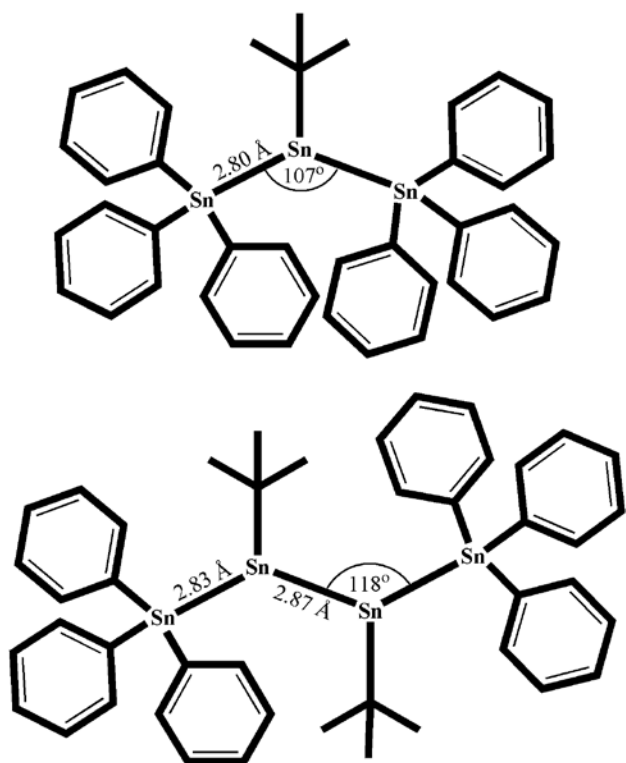


**Figure 5:** Structures and structural data showing bond angles and length of organotin compounds of different chain length.<sup>26</sup>

Dräger also investigated the electronic and structural properties of polystannanes by using  $^{119}\text{Sn}$ -NMR to study the effect of substituent and structural conformation on NMR chemical shifts. It was reported that for shorter chains an increase in the number of tin atoms resulted in a decrease in the  $^{119}\text{Sn}$ -NMR shift.<sup>25,26</sup> This trend was reversed in longer chain polystannanes whereby an increase in the number of heavy elements in the chain lead to a positive increase in NMR shift. Results of some of the electronic studies done by Dräger are illustrated in Figure 6.<sup>25</sup> He effectively demonstrated that the chemical shift of any polystannane was a combination of its structural (coordination number, steric bulk, and geometry) and electronic properties (electron withdrawing vs. electron donating groups).

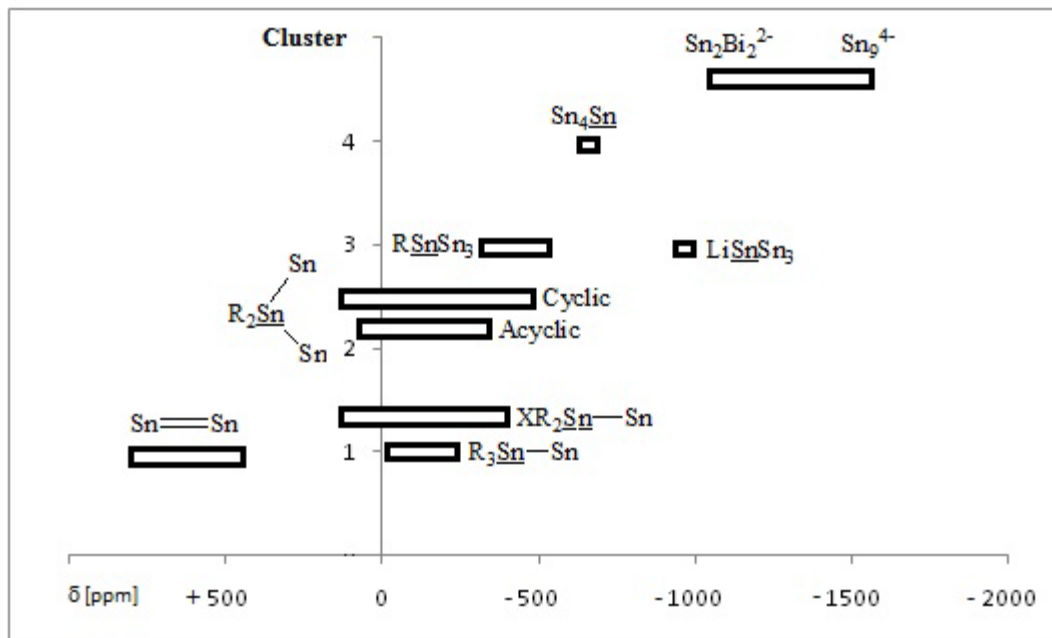


**Figure 6:** Relationship between structure and NMR shift<sup>25</sup>

Studies were also carried out using UV/VIS spectroscopy to decipher the relationship between the chromophoric behaviour and the level of catenation in polystannanes. Figure 7 identifies a direct relationship between the absorption wavelength, NMR shift and the level catenation for linear polystannanes.<sup>25</sup> Dräger also reported that five and six membered oligostannane rings were blue shifted compared to their linear counterparts. He attributed this to their geometry being less than ideal for orbital interactions; these structures deviate from planarity that is necessary for better interactions.



previously been assumed based on the yellow color of diphenyl tin from earlier studies.<sup>27</sup> These findings were in good agreement with the predicted band gap theory.

### 1.3c Current Methods for the Synthesis of Polystannanes and other Group 14 Elements

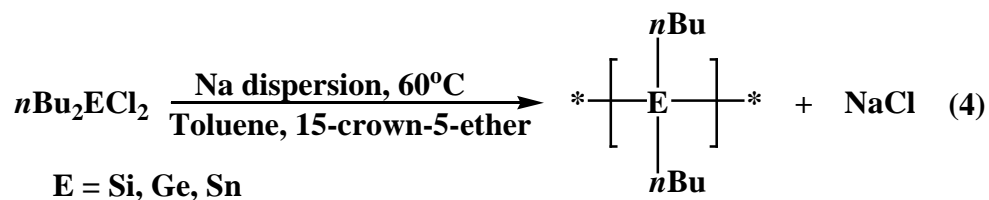
Currently there are three main reductive coupling methods that can be used to synthesize polymers of Group 14 elements, including polystannanes. These synthetic methodologies are Wurtz coupling,<sup>31,35</sup> electrochemical coupling<sup>36</sup> and dehydrocoupling reactions.<sup>21,22,24</sup>

### 1.3d Wurtz Coupling of Polystannanes

The Wurtz coupling methods are similar to the earlier reports by Löwig in his synthesis of polystannanes whereby he reacted iodoethane in the presence of Sn/Na (or Sn/K) alloy.<sup>24</sup> Wurtz coupling was first discovered as an efficient method to form carbon-carbon bonds from the reaction of alkyl halides with Na (rxn 3).<sup>28,29</sup> It was later discovered that this reaction could also be applied to other Group 14 elements.<sup>31</sup>



Kipping first investigated the Wurtz coupling of dichlorosilanes to produce silane oligomers with silicon-silicon bonds in their backbone.<sup>30</sup> This type of reaction typically involves the reaction of a dichloride species in the presence of sodium metal in a high boiling solvent such as toluene.<sup>31,35</sup> The Wurtz coupling of dichlorostannanes was modeled on work conducted using chlorogermane and chlorosilanes monomers.<sup>1</sup> The first report of the Kipping method being used to prepare a polystannane was by Zou *et al.*<sup>31</sup> in 1992. Poly(dibutylstannane),  $[(n\text{Bu})_2\text{Sn}]_n$ , was prepared from the corresponding dichlorostannane,<sup>31</sup>  $(n\text{Bu})_2\text{SnCl}_2$ , using a Wurtz type method with a reported molecular weight in the  $\sim 10^6$  Da range. This represented the first isolation of a high molecular weight polystannane.



While this reaction (Rxn 4 above) was successfully used to synthesize high molecular weight polystannanes, there are several drawbacks. The amount of undesirable cyclic oligomers produced from these types of reactions leads to a low recovery of high molecular weight fractions.<sup>32</sup> This synthetic approach results in a polymodal distribution of the molecular weights which is likely caused by end-biting and back-biting during the propagation stage of these radically initiated reactions.<sup>33</sup> More recently, a slight modification of the Wurtz coupling reaction has resulted in a dramatic reduction in the amount of cyclic oligomers produced. This modification involves lowering the reaction temperature from ~100°C to 60°C and utilizing finely dispersed sodium in toluene. Reactions were also carried out in the presence of crown ether that is known to complex sodium ions.<sup>34</sup> The introduction of crown ethers into a Wurtz type reaction was first reported by Fujino *et al.*<sup>34</sup> An increased rate of polymerization was observed when 18-crown-6-ether was used in the Wurtz coupling of silane dichloride monomers. This was attributed to an increase in the reactivity of the silyl anion due to the formation of crown-ether sodium complex.<sup>34</sup> These reactions also lead to an improvement in the polydispersity of the polymers as shown by Figure 8.<sup>34</sup> More recently reactions using a 15-crown-5-ether have resulted in polymers with average molecular weights in the 10<sup>6</sup> Da range which was estimated by GPC using an RI detector.<sup>35</sup> These reactions were also found to be highly dependent on the reaction time with longer times producing a higher fraction of cyclic due to the end and back-biting previously mentioned.<sup>35</sup>

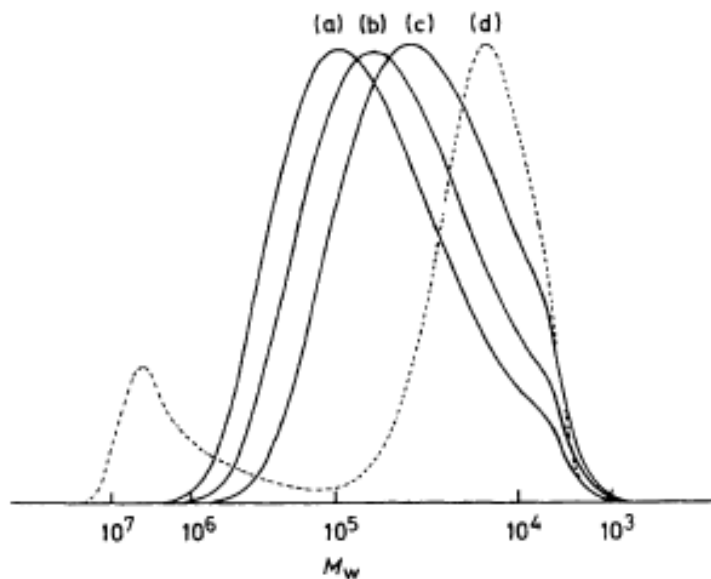


**Figure 8:** GPC chromatogram for MPrPSi in THF with different molar ratio of of 18-crown-6-ether/MePrSiCl<sub>2</sub><sup>34</sup>; (a) 0.05; (b) 0.01; (c) 0.2; (d) 0

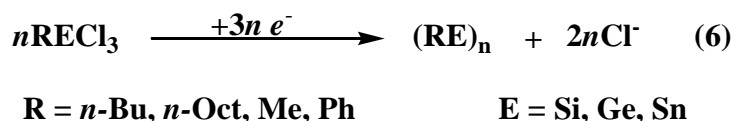
### 1.3e Electrochemical Synthesis of Polystannane

Polystannanes have also been synthesized using electrochemical methods. Okano and co-workers synthesized a series of dialkyl substituted polystannanes. This was carried out using a platinum cathode and silver anode along with constant voltage (20V) to drive the polymerization as shown below (Rxn 5).<sup>36</sup>



These polymers readily precipitated from solution and were isolated after the completion of electrolysis. The molecular weights obtained using this method were in the  $\sim 10^4$  Da range; similar to the electrochemically prepared  $(n\text{-Bu}_2\text{Ge})_n$  and  $(n\text{-Bu}_2\text{Si})_n$  polymers.<sup>36</sup> UV/VIS spectroscopy was used to investigate the properties of the electrochemically prepared polystannanes. It was observed that the absorption max ( $\lambda_{\text{max}}$ , > 378-381 nm) values were comparable to those of other poly(dialkyl)stannane prepared using alternate methods.<sup>24</sup>

Okano also investigated the moisture and air stability of polystannanes. He demonstrated that these types of polymers are stable to the presence of oxygen, contrary to previously published reports.<sup>36</sup> On the other hand, polystannanes were found to be sensitive to moisture and light as evident by their rapid depolymerisation after exposure. A similar electropolymerization technique was also used in the preparation of 3-D network polymers with silane (polysilynes), germane (polygermynes) and stannane (polystannynes) backbones.<sup>37</sup> The polymers were synthesized from trichloride monomers (Rxn 6).<sup>38</sup>

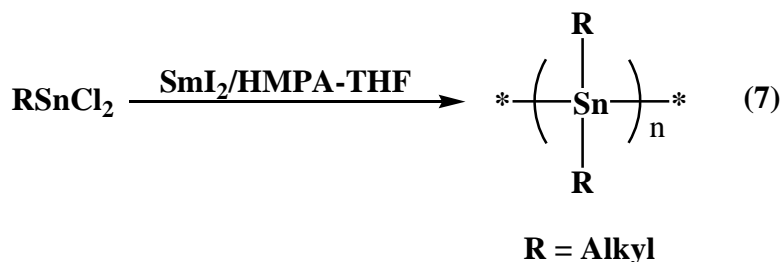


Using UV/VIS spectroscopy, Okano was able to confirm the 3-D nature of these polymers. The UV/VIS spectrum showed no obvious single absorption peak, a characteristic of network polymers.<sup>37</sup> The UV/VIS spectrum of these network polymers also possess unusually long absorption tail that extends well into the near IR (> 850 nm). This is due to their extensive 3-D  $\sigma$ -conjugated system. Compared to these network Group 14 polymers, linear poly(dialkyl)stannanes are considerably blue shifted with a distinct broad absorption between 340-500 nm.

### 1.3f One Electron Coupling of Polystannane Using Samarium Iodide

A chemical method for the synthesis of polystannane is the reductive coupling of tin dichlorides using SmI<sub>2</sub> as the coupling agent. SmI<sub>2</sub> is a strong one electron reducing agent (1.55 V vs. saturated calomel electrode)<sup>38</sup> that, unlike many inorganic reducing agents, is soluble in wide range polar of solvents. The reaction of SmI<sub>2</sub> can be placed into three different categories when it pertains to polymerization.<sup>39</sup> The first category involves inversion of a cationic growth center into one that is anionic. The second category is the polymerization of electrophilic vinyl monomers that are bisinitiated by the electron transfer from Sm and the

last category involves the extension of a carbon-carbon (or Sn-Sn) bond forming reaction into stepwise growth polymerization.<sup>39</sup> The application of SmI<sub>2</sub> to the formation of Sn-Sn bond was investigated by Mochida and co-workers in 1998 using tin dichloride monomers (Rxn 7).<sup>40</sup>



Mochida explored the synthesis of polystannanes under mild conditions using SmI<sub>2</sub> and investigated their photostability when exposed to a laser flash. The yields obtained using this method ranged from as high as 74.4% to a low of 5.8% with average molecular weight in the ~10<sup>3</sup> Da range.<sup>40</sup> In general, these values were below those obtained using other preparative methods for polystannanes.<sup>21,22,24</sup> Mochida investigated polystannanes bearing alkyl substituent (Me, Et, Hex) and found that their electronic absorption ranged from 285-368 nm. The lack of light stability of these polymers was evaluated by irradiating the samples with UV and it was determined that the chain lengths decreased due to scission by light.<sup>40</sup>

### 1.3g Dehydrocoupling of Tin Dihydrides

A more recent technique for the synthesis of polystannane is the dehydrocoupling reaction of secondary stannanes using a metal catalyzed chain growth reaction.<sup>41</sup> This involves the reaction of a tin dihydride in the presence of a metal catalyst, forming Sn-Sn bonds with the evolution of hydrogen gas. The proposed mechanism for dehydrocoupling is illustrated below.<sup>21</sup>

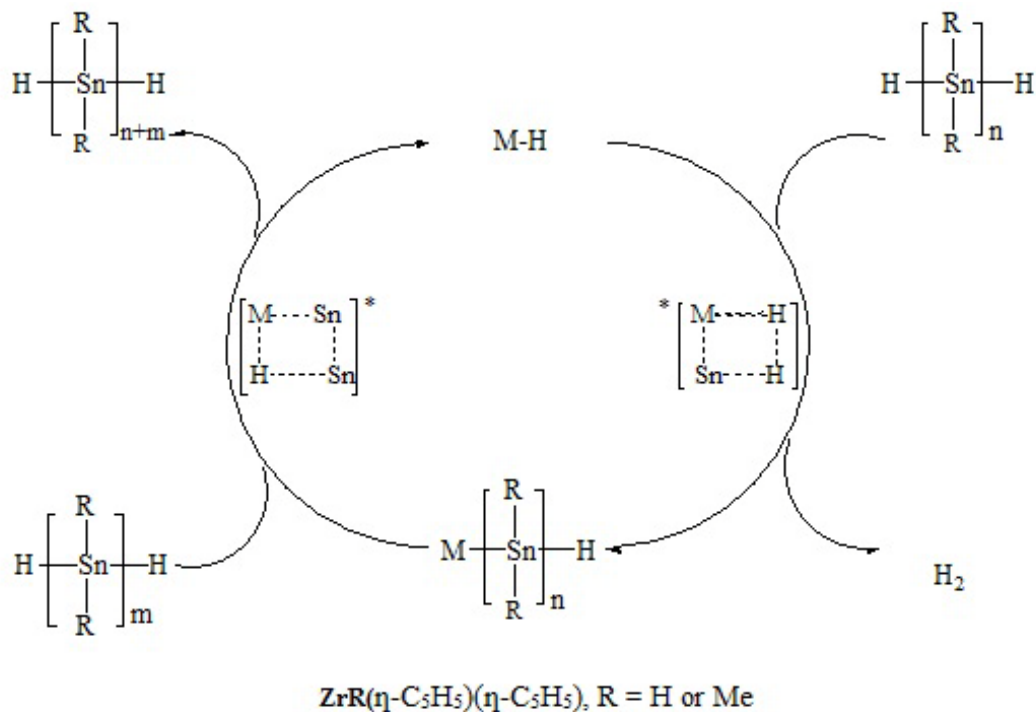
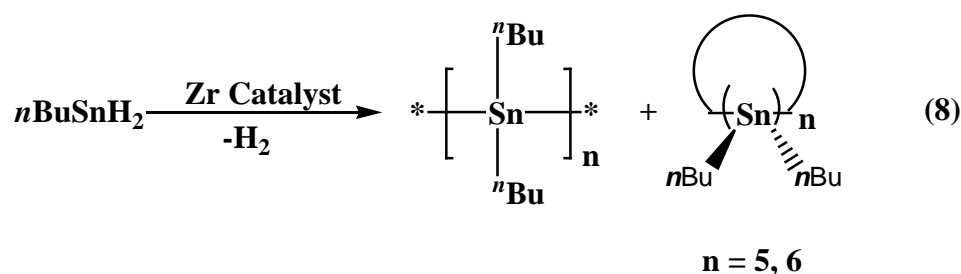


**Figure 9:** Mechanism for metal catalyzed dehydrocoupling of polystannanes<sup>21</sup>

Dehydrocoupling of Group 14 hydrides was first investigated by Harrod in the 1980's.<sup>42</sup> He successfully dehydropolymerized  $\text{PhSiH}_3$  and  $\text{PhGeH}_3$  in the presence of a titanium based catalyst to form low molecular weight oligomers. While dehydrocoupling has been successful for primary silanes and germanes, it has been less successful for the corresponding secondary systems. Currently, there has been no report of the dehydrocoupling of secondary germanes or silanes to yield high molecular weight polymer. Harrod reported that the dehydropolymerization of the germanium hydrides was easier compared to their silane counterparts.<sup>43</sup> Based on these findings, it was postulated that the ease of dehydrocoupling increases going downward in a group.<sup>43</sup> It is expected that tin hydrides should undergo dehydrocoupling more readily than their silicon and germanium counterparts.<sup>43</sup> More recent kinetic studies on the dehydrocoupling of secondary silanes to dimers or oligomers was recently investigated by Rosenberg and co-worker.<sup>44</sup> They observed that an open system was required to allow for the release of hydrogen gas in order for the reactions to progress to

completion.<sup>44</sup> In 1993 Tilley demonstrated that  $n\text{Bu}_2\text{SnH}_2$  readily undergoes dehydrocoupling in the presence of the zirconocene based catalyst,  $[\text{Zr}(\eta\text{-C}_5\text{H}_5)(\eta\text{-C}_5\text{Me}_5)\{\text{Si}(\text{SiMe}_3)_3\text{Me}]$ , to form  $[(n\text{Bu})_2\text{Sn}]_n$  and oligostannanes, along with the evolution of  $\text{H}_2$  gas (Rxn 8). This was the first report of dehydrocoupling for the synthesis of polystannanes.<sup>41</sup>



Tilley reported that these systems produced cyclic oligomers similar to those formed from the Wurtz coupling polymerization of silanes. This catalytically driven dehydrocoupling has been carried out in the presence of various transition metal catalysts including Rh, Pt, Ni and Zr.<sup>41,45,22,24</sup> Table 3 details representative molecular weights and absorption maximum ( $\lambda_{\text{max}}$ ) of polystannanes along with the catalysts used in their preparation.

**Table 3:** Molecular weight ( $M_n$ , PDI) and UV-VIS data for selected polystannanes prepared by dehydrocoupling

R substituent	Precatalyst	$\lambda_{\text{max}}$ (nm, 25°C)	$M_n$ (Da)	PDI
$n\text{Bu}^{46}$	$\text{Me}_2\text{CCp}_2\text{ZrMe}(\text{Si}(\text{SiMe}_3)_3)$	384 (THF)	$2.0 \times 10^4$	3.3
$n\text{Bu}^{46}$	$\text{CpCp}^*\text{ZrMe}_2$		$1.3 \times 10^4$	5.6
$n\text{Bu}^{46}$	$\text{CpCp}^*\text{ZrMe}(\text{Si}(\text{Si}(\text{Me}_3)_3))$		$7.8 \times 10^3$	2.2
$n\text{Bu}^{46}$	$\text{RhH}(\text{CO})(\text{PPh}_3)_3$	394 (pentane)	$3.5 \times 10^3$	1.4
$n\text{Bu}^{46}$	$\text{RhCl}(\text{PPh}_3)_3$		$1.9 \times 10^4$	-
$n\text{Bu}^{46}$	$[\text{Ni}(\text{cod})_2]$		$7.0 \times 10^3$	-
$n\text{Hex}^{47}$	$\text{CpCp}^*\text{ZrMe}(\text{Si}(\text{SiMe}_3)_3)$	384 (THF)	$1.5 \times 10^4$	2.4
$\text{P-}^t\text{BuC}_6\text{H}_4^{47}$	$\text{Cp}_2\text{ZrMe}_2$	436 (THF)	$1.5 \times 10^4$	1.4

More recent work on polystannanes has been carried out by Caseri *et al.* who also used dehydrocoupling to synthesize high molecular weight poly(dialkyl)stannanes.<sup>48</sup> Using a series of different metal catalysts Caseri demonstrated the effectiveness of Wilkinson's catalyst  $\text{RhCl}(\text{PPh}_3)_3$ , normally used in hydrogenation reactions,<sup>21,48</sup> for dehydrocoupling. Reactions utilizing this catalyst yielded high molecular weight polymers with no detectable cyclic oligomers. This catalyst was found to be sensitive to steric bulk at the tin center and was therefore less efficient for monomers with bulky or aryl groups directly attached to the tin. Caseri *et al.* reported that in order for this catalyst to be applicable for polystannanes with bulky side groups, there had to be a minimum of two methylene ( $-\text{CH}_2-$ ) units between the tin atom and the bulky substituent.<sup>21,48</sup>

### 1.3h Electronic Properties of Polystannanes

Using UV/VIS spectroscopy, Sita<sup>27</sup>, Caseri<sup>24</sup> and Tilley<sup>41</sup> were able to study the band gap trends of polystannane polymers. The visible absorption in these polymers are attributed to the  $\sigma$ - $\sigma^*$  transition of the conjugated backbone. Poly(dialkyl)stannanes were typically 40 nm red shifted compared to their silane analogs while poly(diaryl)stannanes were 70 nm redshifted to their silane analogs.<sup>46,47,41</sup> The poly(diaryl)stannanes were reported to absorb at longer wavelengths than poly(dialkyl)stannane due to the  $\sigma$ - $\pi$  mixing from the phenyl rings.<sup>47</sup> Tilley was also able to show that the bandgap of these polymers was highly influenced by the backbone conformation and the electronic properties of the substituents. Poly(diaryl)stannanes with a planar zig zag backbone and  $\pi$  donating ring substituents were found to possess the lowest band gap for any known for polystannanes ( $\lambda_{\text{max}} = 550$  nm, corresponding to a band gap of ca. 2.3 eV).<sup>48</sup> Theoretically it has been suggested that the band gap of polystannanes could approach that of metals.<sup>21</sup> By comparison band gap for most polysilanes are in the 4 eV range.<sup>50</sup> This is still considerably smaller than the band gap for polymers with saturated carbon skeletons; these typical have band gaps of  $\sim 8$  eV.<sup>51</sup>

West *et al.* reported that phenylmethylpolysilanes doped with AsF<sub>5</sub> were able to achieve conductivity of 0.5 Scm<sup>-1</sup>.<sup>52</sup> More recently Caseri *et al.* showed that [*n*-Bu<sub>2</sub>Sn]<sub>*n*</sub> are liquid crystals at room temperature, a property that may yet highlight a future use. They reported a charge mobility between 0.1 cm<sup>2</sup> V<sup>-1</sup> s<sup>-1</sup>-0.03 cm<sup>2</sup> V<sup>-1</sup> s<sup>-1</sup> for this particular polymer depending on the temperature.<sup>53</sup> Tilley described conductivities between 0.1 and 0.3 Scm<sup>-1</sup> for [*n*-Bu<sub>2</sub>Sn]<sub>*n*</sub> when oxidatively doped with SbF<sub>5</sub>.<sup>54</sup>

### 1.4a NMR spectroscopy

Techniques such as NMR spectroscopy have proven to be instrumental in the characterization of polystannanes. In particular, <sup>119</sup>Sn-NMR spectroscopy can be used to investigate the structure and chain length of these polymers. It was observed that as chain length of oligostannanes increased, it caused a substantial downfield shift in the <sup>119</sup>Sn-NMR signal. NMR can also be used to provide insight to the electronic structure of stannanes.<sup>25,26</sup> Both Caseri<sup>45</sup> and Tilley<sup>41</sup> successfully showed that <sup>119</sup>Sn-NMR spectroscopy in conjunction with other methods such as UV-VIS absorption data was instrumental in determining the structure of polystannanes synthesized in their work. They were able to differentiate between linear and cyclic species for [*n*Bu<sub>2</sub>Sn]<sub>*n*</sub> using <sup>119</sup>Sn-NMR (-189.6 ppm vs. -200.9 ppm).<sup>24</sup> Table 4 shows the NMR and *M<sub>w</sub>* of polystannanes with different substituents in their backbones.

**Table 4:** Molecular weight and <sup>119</sup>Sn-NMR chemical shift data for selected polystannanes

Polymer	<i>M<sub>w</sub></i> (PDI)	δ Sn-NMR shifts (δ = ppm)
[Et <sub>2</sub> Sn] <sub><i>n</i></sub> <sup>24</sup>	3.1 × 10 <sup>4</sup> (2.38)	-172
[ <i>n</i> Hex <sub>2</sub> Sn] <sub><i>n</i></sub> <sup>24</sup>	7.6 × 10 <sup>4</sup> (2.45)	-193
H[( <i>o</i> -Et- <i>p</i> <sup><i>n</i></sup> BO-C <sub>6</sub> H <sub>3</sub> ) <sub>2</sub> Sn] <sub><i>n</i></sub> H <sup>46</sup>	1.2 × 10 <sup>3</sup> (1.71)	-125
H[( <i>p</i> - <sup><i>t</i></sup> Bu-C <sub>6</sub> H <sub>4</sub> ) <sub>2</sub> Sn] <sub><i>n</i></sub> H <sup>46</sup>	5.6 × 10 <sup>3</sup> (3.35)	-197

### 1.4b Gel Permeation Chromatography (GPC) to determine molecular weight

Another technique often used to characterize polymers based on their size is Gel Permeation Chromatography (GPC). In GPC, polymer molecular weights are determined by comparison to a series of standards of known molecular weight and structure. Molecular weights are determined by measuring properties such as the refractive index, viscosity, UV absorption, light scattering and retention time. The absolute molecular weight of polymers can be calculated using GPC's that are equipped with light scattering, refractive index and intrinsic viscosity detectors. All polystannanes isolated to date had their molecular weights determined by GPC. This was carried out using RI detectors and referenced relative to polystyrene standards with THF as the mobile phase.<sup>47,31,24</sup> GPC was used in the molecular weight determination for polymers synthesized by Zou<sup>31</sup>, Caseri<sup>42</sup> and Okano<sup>36</sup> who all prepared polystannanes using different methods. The molecular weight determined by GPC from each method is listed in the Table 5.

**Table 5:** GPC results from the different methods for polystannane synthesis

Polymer	Method of Synthesis <sup>ref</sup>	Molecular weight (Da) and (PDI)
[ <i>n</i> Bu <sub>2</sub> Sn] <sub><i>n</i></sub>	Wurtz coupling <sup>35</sup>	1.2 × 10 <sup>6</sup> (1.3)
[ <i>n</i> Bu <sub>2</sub> Sn] <sub><i>n</i></sub>	Dehydrocoupling <sup>42</sup>	2.0 × 10 <sup>4</sup> (3.3)
[ <i>n</i> Bu <sub>2</sub> Sn] <sub><i>n</i></sub>	Electrochemistry <sup>36</sup>	1.2 × 10 <sup>4</sup> (2.1)
[Me <sub>2</sub> Sn] <sub><i>n</i></sub>	Samarium iodide <sup>40</sup>	1.1 × 10 <sup>3</sup> (1.49)

GPC has proven to be instrumental not only in the determination of molecular weights of polystannanes but also to investigate the stability of these polymers under different condition. Polystannanes have been found to breakdown to cyclic oligomers under exposure to light or solvent and this degradation can be detected using GPC.<sup>24,41</sup>

#### 1.4c Thermal Analysis: Thermal Gravimetric Analysis (TGA) and Differential Scanning Calorimetry (DSC)

The thermal stability of polymers can be accurately assessed using methods such as thermal gravimetric analysis (TGA). In this method, polymers are heated slowly and controllably to determine their stability at different temperatures by measuring the mass loss. Previous studies of polystannanes using TGA analysis revealed stability up to relatively high temperatures ( $> 300^{\circ}\text{C}$ ). The majority of polystannanes do not begin to experience mass loss until temperatures of  $250^{\circ}\text{C}$ - $310^{\circ}\text{C}$ <sup>24,46</sup> in the case of poly(diaryl)stannanes and  $180$ - $320^{\circ}\text{C}$  for poly(dialkyl)stannanes.<sup>46</sup> Table 6 shows the temperature of decomposition for selected poly(diaryl)-and poly(dialkyl)stannanes.

**Table 6:** Decomposition temperature of selected polystannanes using TGA analysis under  $\text{N}_2$  atmosphere

Polymer	Decomp. Temp. $^{\circ}\text{C}$
$\text{H}[(\text{o-Et-p}^n\text{BuO-C}_6\text{H}_3)_2\text{Sn}]_n\text{H}^{47}$	327
$\text{H}[(\text{p-}^t\text{Bu-C}_6\text{H}_4)_2\text{Sn}]_n\text{H}^{47}$	303
$\text{H}[(\text{o-Et-C}_6\text{H}_4)_2\text{Sn}]_n\text{H}^{47}$	203
$\text{H}[n\text{-Bu}_2\text{Sn}]_n\text{H}^{24}$	302
$\text{H}[\text{Pr}_2\text{Sn}]_n\text{H}^{24}$	293

These inorganic polymers are much more stable than their organic counterparts which is often highlighted as one of the possible advantages of inorganic polymers.<sup>1,2</sup>

A non-destructive thermal analysis also used to detect phase changes associated with polymers such as glass transition ( $T_g$ ), crystallization ( $T_c$ ) and melting temperature ( $T_m$ ) is DSC (differential scanning calorimetry). In DSC the polymers are heated and cooled over a wide range of temperatures while the enthalpy (heat) change in the sample is being monitored. Figure 10 shows the DSC graph for  $[(n\text{Bu})_2\text{Sn}]_n$ , which reveals its

liquid crystalline nature at room temperature.<sup>53</sup> Table 7 gives some phase transition temperatures for polystannanes from literature using DSC.

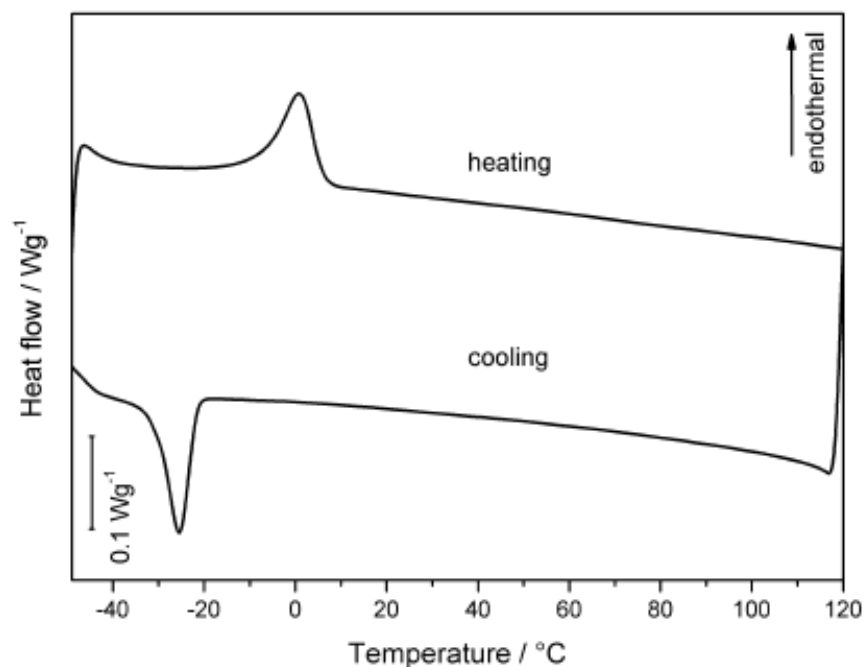


**Figure 10:** DSC chromatogram for  $[(n\text{Bu})_2\text{Sn}]_n$  after the first heating and cooling cycle<sup>53</sup>

**Table 7:** Shows the Thermal Properties of Polystannanes measured by DSC

Polymer	1 <sup>st</sup> transition Upon Heating and Cooling [ $^{\circ}\text{C}$ ]	2 <sup>nd</sup> transition upon Cooling [ $^{\circ}\text{C}$ ]
$(n\text{Pe}_2\text{Sn})_n$ <sup>24</sup>	Heating : 6 Cooling: -16	Heating : 57 Cooling: 42
$(n\text{Hex}_2\text{Sn})_n$ <sup>24</sup>	Heating : 34 Cooling: 21	Heating : 68 Cooling: 43
$(n\text{Oc}_2\text{Sn})_n$ <sup>24</sup>	Heating : 29 Cooling: 13	Heating : 74 Cooling: 58
$(n\text{Dod}_2\text{Sn})_n$ <sup>24</sup>	Heating : 55 Cooling: 39	Heating : 91 Cooling: 80
$\text{H}[n\text{Bu}_2\text{Sn}]_n\text{H}$ <sup>24</sup>	Heating : 1 Cooling: -26	

### 1.5a Properties of Fluorinated Compound

Flourine is the most electronegative atom on the periodic table and it is also one of the smallest. Because of these two properties, the fluorine carbon bond is one of the strongest known in chemistry.<sup>55</sup> The electron withdrawing capacity of flourine has also been shown to increase the strength of carbon-carbon bond. This is evident in hexafluoroethane where the C-C bonds are 7 kcal/mol stronger than those in ethane.<sup>56</sup> In this case electron density around the carbon nucleus is reduced due to the presence of the electron withdrawing fluorine. This feature allows the two atoms to come in close to each other resulting in stronger bonds. These fluorocarbons also have low polarizability which causes a lack of cohesive attractions which is normally present in their hydrocarbon counterparts such as London forces.<sup>56</sup> It is suggested that the amount of cohesive force increases with the square of the polarizability of the compound.<sup>56</sup> Table 8 shows the effect of flourine on the dipole moment of molecules.

**Table 8:** Effect of flourine on the dipole moment of molecules<sup>57</sup>

Compound	Dipole Moment (Debye)
CH <sub>3</sub> F	1.85
CH <sub>2</sub> F <sub>2</sub>	1.97
Fluorobenzene	1.70

The properties of the C-F bond can also extend to the carbon framework of fluorinated compounds which results in an overall increase in hydrophobicity.<sup>57</sup> These fluorocarbon compounds have properties that differ dramatically from their hydrocarbon counterparts such as high thermal stability, etc. Substituents with perfluorinated groups have been utilized frequently as moisture repellent due to the hydrophobic nature of perfluorinated.<sup>57</sup>

## 1.5b Fluorinated Tin Compounds

Tetraphenyl tin derivatives with fluorinated side groups were prepared from the reaction between tin (IV) chloride and the corresponding Grignard reagent by King *et al.* as shown below (Rxn 9).<sup>59</sup>



**R = Fluorinated phenyl**

They were able to characterize the structure of these compounds using <sup>13</sup>C-NMR, <sup>19</sup>F-NMR and <sup>119</sup>Sn-NMR. This was followed by the synthesis of *tris*- and *bis*-phenyl substituted tin chlorides using the redistribution reaction below. In this reaction the tetraphenyltin derivatives and tin (IV) chloride are reacted together in the neat at high temperature (Rxn 10).



The investigation of fluorinated tin compounds was also carried out by Stern *et al.* who synthesized fluorinated tin hydrides using steps similar to those employed by King *et al.*<sup>59,60</sup> They reported difficulties carrying out redistribution reactions with SnCl<sub>4</sub> when electron withdrawing groups were in the *meta* position of the phenyl ring.<sup>60</sup> This was attributed to the similarities between these reactions and electrophilic aromatic substitution reactions. Tin hydrides with fluorinated substituents were synthesized by Stern *et al.* by substitution of chlorine using the hydride nucleophile, LiAlH<sub>4</sub><sup>60</sup> (Rxn 11)



In their preparation of triaryltin hydrides, Stern and Becker encountered problems when electron-withdrawing groups were located in the *para* position.<sup>60</sup> They reported a considerable amount of the unwanted distannane being formed along with the desired product. It was argued that the presence of

electron withdrawing groups lead to cleavage of the newly formed hydride bond or even the tin-aryl bond by the various nucleophiles present in solution.<sup>60</sup> Cleavage of the tin-aryl bond was confirmed by the isolation of free phenyl substituents.<sup>60</sup> These steps have been successfully used in numerous examples in literature to synthesize dialkyl and diaryl tin dihydrides.<sup>41,46</sup>

### 1.6a Thesis Objective

While polystannanes show tremendous potential based on their electronic properties, their utility is limited by inherent instability to both moisture and light. This research will focus on stabilizing polystannanes to moisture with the hope that this work can be combined with other synthetic strategies that also addresses the need for improve light stability. The goal is to synthesize a series of fluorinated tin compounds and investigate their properties and stability. Introduction of perfluorinated groups into the backbone of polystannanes may increase their overall moisture stability. Figure 11 illustrates some of the perfluorinated groups that will be investigated.

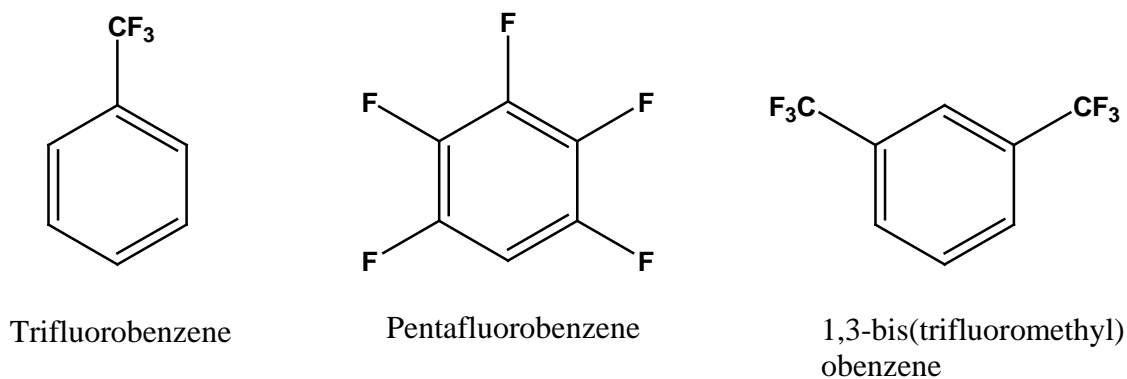


**Figure 11:** Fluorinated phenyl substituents

It is anticipated that the band gap of these polymers may also be influenced by the presence of perfluoro substituents relative to their non-fluorinated counterparts. These polymers will be synthesized using methods

already present in literature for the synthesis of high molecular weight Group 14 polymers such as Wurtz coupling and dehydrocoupling.

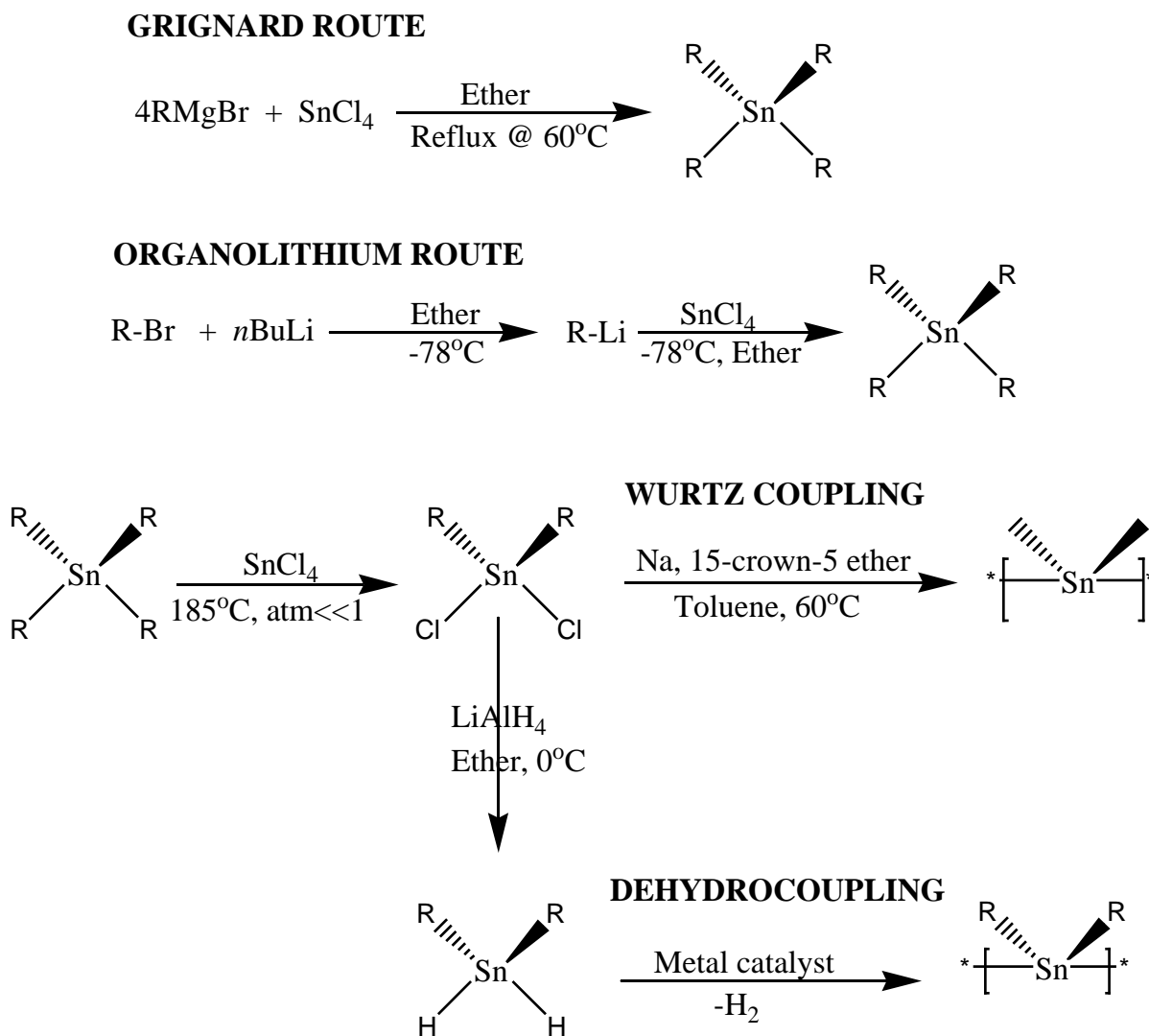


**Figure 12:** Steps for the synthesis of polymers using Wurtz coupling or dehydrocoupling reactions

Figure 12 illustrates the steps that will be used to synthesize polystannanes in this research, where R represents fluorinated side groups in Figure 11. Initially a series of tetra aryl stannanes will be synthesized using either a Grignard or organolithium route. This will be accomplished by a substitution reaction between  $\text{SnCl}_4$  and the corresponding Grignard or organolithium reagent. The next step involves the synthesis of tin

dichlorides by a redistribution reaction between  $\text{SnCl}_4$  and the tetraaryl stannanes prepared. These dichlorides will then be employed as monomers using a modified Wurtz coupling reaction. In this method, dichloride monomers are reacted in the presence of sodium metal and a crown ether. Alternatively, tin dihydrides can be synthesized from tin dichlorides by substitution of the chlorine atoms using a hydride nucleophile such as  $\text{LiAlH}_4$ . These tin dihydrides can then be used as monomers for dehydrocoupling in the presence of a suitable metal catalyst. Characterization of the polymers and products mentioned above will be carried out techniques such as X-ray crystallography, GPC, elemental analysis, and NMR and UV/VIS spectroscopy. Once characterized these fluorinated compounds will be compared to their non-fluorinated counterparts with respect to their stability and electronic properties.

## 2.1 Experimental and Method

Solvents were dried using an MBraun solvent drying system. Tin tetrachloride, 3,5-(trifluoromethyl)phenyl magnesium bromide, 3,5-(trifluoromethyl)bromobenzene and 1-bromo-4-(trifluoromethyl)benzene, diphenyltin dichloride (Compound 7), pentafluorobenzene, sodium metal, *n*-BuLi (1.6 M in hexane), 15-Crown-5, 1.0 M LiAlH<sub>4</sub> in ether and platinum(0)-1,3-divinyl-1,1-tetramethyl disiloxane complex solution in xylene (~2% pt) were purchased from Aldrich and used as received. <sup>1</sup>H NMR, <sup>13</sup>C NMR, <sup>19</sup>F and <sup>119</sup>Sn NMR spectra were recorded on a Bruker 400 MHz NMR. <sup>1</sup>H and <sup>13</sup>C spectra were collected in deuterated solvents that also served as the references. <sup>119</sup>Sn and <sup>19</sup>F resonance were referenced against the internal standards SnMe<sub>4</sub> and CFCl<sub>3</sub>. The <sup>119</sup>Sn spectra obtained using a 30° pulse with a relaxation time of 4.3 μs within the range 200 to -1000 ppm. <sup>13</sup>C, <sup>19</sup>F-NMR and <sup>119</sup>Sn spectra were acquired by decoupling of the <sup>1</sup>H to increase the signal strength. Mass spectrometry was performed at the University of Toronto AIMS Laboratory with a Waters GC TOF mass spectrometer with EI/CI sources mass spectrometer in electron impact mode. The isotopic distributions that were calculated agreed well with experimental values. Elemental Analysis was performed by Analest laboratories at the University of Toronto. Molecular weights of polymers were determined by gel permeation chromatography (GPC) using a Viscotek Triple Model 302 Detector system equipped with a Refractive Index Detector (RI), a four capillary differential viscometer (VISC), a right angle laser light scattering detector ( $\lambda_0 = 670$  nm) and a low angle laser light scattering detector. GPC columns were calibrated versus polystyrene standards (American Polymer Standards). ACS grade THF was used as the mobile phase with a constant flow rate of 1ml/min. All experiments were performed under inert atmosphere conditions (N<sub>2</sub>) using Schlenk techniques. Bruker-Nonius Kappa-CCD diffractometer was used to collect the X-ray information crystal structure obtained in this experiment. This machine is equipped with monochromated Mo-K $\alpha$  radiation source and samples were measured using a combination of  $\phi$  scans and  $\omega$  scans with  $\kappa$  offsets, in order to fill the Ewald sphere. The structure was resolved and refined using

SHELXTL V6.1 for full-matrix least-squares refinement that was based on  $F^2$ . All H atoms were included in calculated positions and allowed to refine in riding-motion approximation with U~iso~ tied to the carrier atom.

## 2.2 Synthesis of Perfluorinated Tetraarylstannanes, Diaryldichlorostannanes, Diaryltin dihydride and Diarylpolystannanes

### 2.2.1 Tetrakis[4-trifluoromethylphenyl]stannane 1

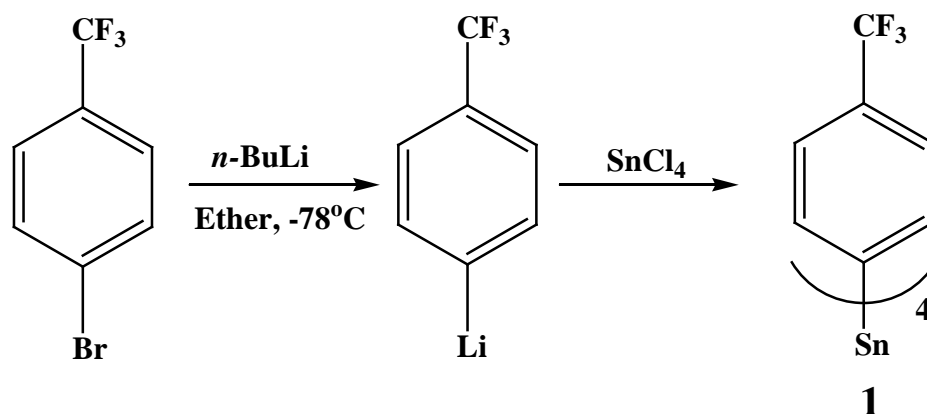


**Figure 13:** Synthesis of compound **1** using the organolithium route

5.05 g (22.4 mmol) of 1-bromo-4-(trifluoromethyl)benzene was weighed into a flamed dried 250 mL Schlenk flask equipped with a magnetic stir bar under an inert nitrogen atmosphere. The flask was charged with 70 mL of dried ether, placed in dry ice/acetone bath ( $-78^\circ\text{C}$ ) and stirred. 14.1 mL (22.6 mmol) of a 1.6M  $n\text{-BuLi}$  solution was added dropwise to the solution at  $-78^\circ\text{C}$  over a 30 min period, and allowed to stir for 2-3h at this temperature. To this light yellow solution, 0.66 mL (5.65 mmol) of  $\text{SnCl}_4$  was added dropwise, resulting in the instantaneous formation of a white precipitate. The reaction was stirred for 4h and then quenched *via* a dropwise addition of *t*-butanol. The reaction mixture was filtered to remove salts, leaving a clear solution. The ether solvent was then removed *in vacuo* to produce a yellow-white powder. The crude product was further purified by sublimation under vacuum at  $130^\circ\text{C}$  ( $5 \times 10^{-3}$  mmHg) resulting in the formation of clear white crystals. Analysis by  $^{119}\text{Sn}$  and  $^{19}\text{F}$  NMR for this compound agreed with reported literature values (2.73g, 69 % yield), mp  $148^\circ\text{C}$  (lit.  $151^\circ\text{C}$ ).<sup>59</sup>

$^1\text{H-NMR}$  ( $\text{CDCl}_3$ ):  $\delta$  7.70 (br s, 4H) ppm.  $^{13}\text{C-NMR}$  ( $\text{CDCl}_3$ ):  $\delta$  140.72 (br s, C1, C-*ipso*-Sn), 137.25 (m, C2,  $^2J_{\text{C-Sn}} = 19.88$  Hz), 132.13 (q, C4, C-*ipso*-CF<sub>3</sub>,  $^2J_{\text{C-F}} = 32.41$  Hz), 125.53, (q, C3,  $^3J_{\text{C-F}} = 3.6$  Hz), 121.18 (q, C5, CF<sub>3</sub>,  $^1J_{\text{C-F}} = 271$  Hz) ppm.  $^{119}\text{Sn-NMR}$  ( $\text{CDCl}_3$ ):  $\delta$  -131.04 (m,  $J_{\text{Sn-F}} = 5.23$  Hz) ppm.  $^{19}\text{F-NMR}$  ( $\text{CDCl}_3$ ):  $\delta$  -63.19 (s, CF<sub>3</sub>) ppm.

### 2.2.2a Tetrakis[3,5-Bis(trifluoromethyl)phenyl]stannane by the Grignard Approach 2

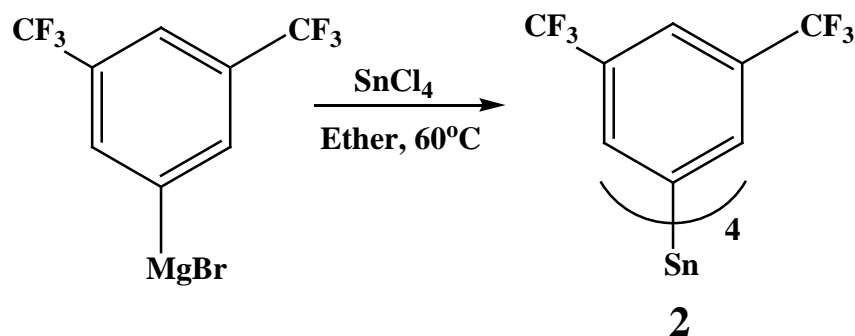


**Figure 14:** Synthesis of compound **2** using the Grignard route

The compound,  $\text{Sn}(\text{C}_8\text{H}_3\text{F}_6)_4$ , was prepared using the procedure outlined by King *et al.*<sup>59</sup> Anhydrous tin tetrachloride (3.125 mmol) was added dropwise to a solution of 3,5-trifluoromethylphenyl magnesium bromide (12.5 mmol) in ether cooled in an ice bath. The reaction mixture was refluxed overnight, cooled and filtered to remove salts. The crude compound was purified first by sublimation, and then recrystallized from ether to yield long large needle crystals. Analysis by  $^{119}\text{Sn}$  and  $^{19}\text{F}$  NMR for this compound agreed with reported literature values. (1.33g, 44% yield), mp 157°C (lit. 163°C).<sup>59</sup>

### 2.2.2b Tetrakis[3,5-Bis(trifluoromethyl)phenyl]stannane by the organolithium Approach

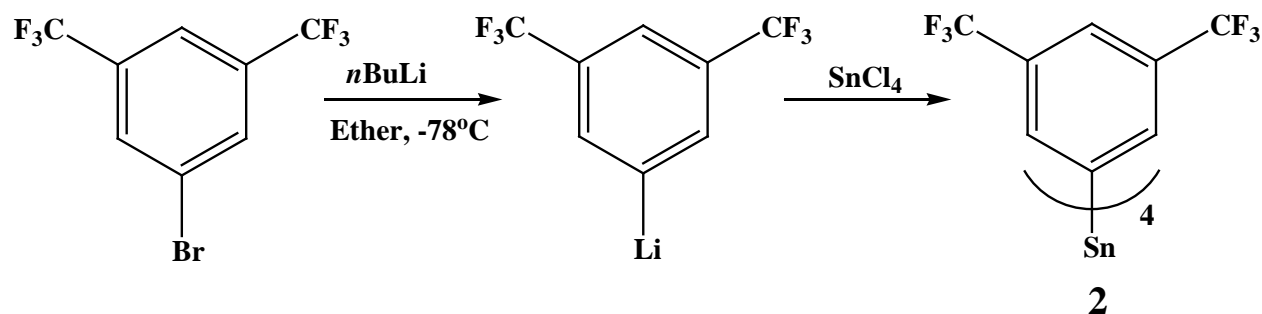


**Figure 15:** Synthesis of compound 2 using the organolithium route

5.00 g (17.1 mmol) of 3,5 bis (trifluoromethyl) bromobenzene was weighed into a flame dried 250mL Schlenk flask equipped with a magnetic stir bar under an inert nitrogen atmosphere. The flask was charged with 70mL of dried ether, placed in dry ice/acetone bath ( $-78^\circ\text{C}$ ) and stirred. 10.70 mL (17.1 mmol) of a 1.6M  $n\text{-BuLi}$  solution was added dropwise to the solution at  $-78^\circ\text{C}$  over a 30 min period, and allowed to stir for 2-3h at this temperature. To the light yellow solution, 0.50 mL of  $\text{SnCl}_4$  (4.28 mmol) was added dropwise, resulting in the instantaneous formation of a white precipitate. The reaction was stirred for 4h and then quenched *via* a dropwise addition of *t*-butanol. The reaction mixture was filtered to remove salts, leaving a clear solution. The ether solvent was then removed *in vacuo* to produce a yellow-white powder. The crude product was further purified by sublimation under vacuum at  $135^\circ\text{C}$  ( $5 \times 10^{-3}$  mmHg) resulting in the formation of clear white crystals. (3.53g, 85% yield), mp  $157^\circ\text{C}$ .

$^1\text{H-NMR}$  ( $\text{CDCl}_3$ ):  $\delta$  8.07(br s, 1H), 7.97 (br s, 2H,  $J_{\text{Sn-H}} = 24.64$  Hz) ppm.  $^{13}\text{C-NMR}$  ( $\text{CDCl}_3$ ):  $\delta$  138.30 (br s, C1, C-*ipso*-Sn), 136.34 (s, C2), 132.72 (q, C3,  $C_{\text{ipso-CF}_3}$ ,  $J_{\text{C-F}} = 33.5$  Hz), 125.41 (s, C4), 122.69 (q,  $\text{CF}_3$ ,  $J_{\text{C-F}} = 270$  Hz) ppm.  $^{119}\text{Sn-NMR}$  ( $\text{CDCl}_3$ ):  $\delta$  -126.1 ppm.  $^{19}\text{F-NMR}$  ( $\text{CDCl}_3$ ):  $\delta$  -63.10 (s,  $\text{CF}_3$ ,  $J_{\text{Sn-F}} = 9.5$  Hz) ppm.

### 2.2.3 Tetrakis[pentafluorophenyl]stannane **3**

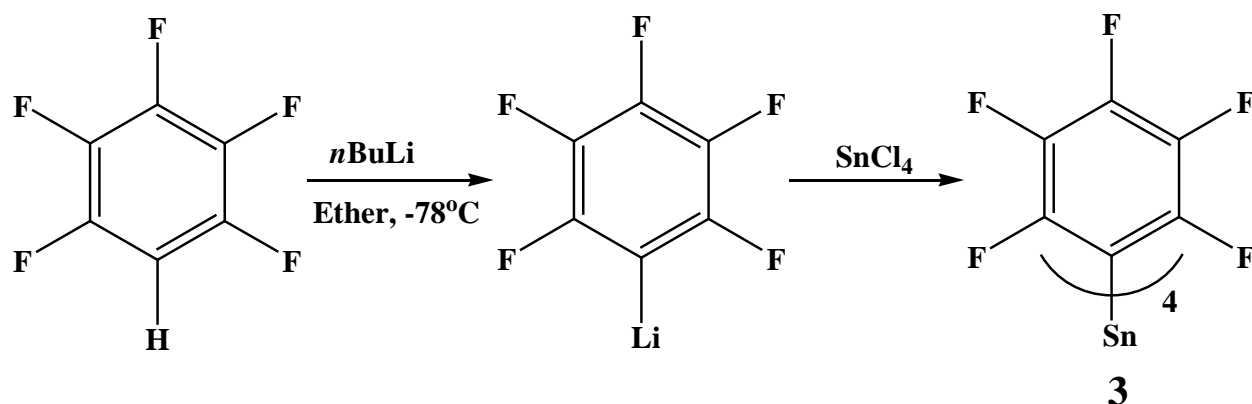


**Figure 16:** Synthesis of compound **3** using the organolithium route

To a 100 mL Schlenk flask equipped with a magnetic stir bar and rubber septa under an  $\text{N}_2$  environment was added 25 mL of dry ether and 3.28 mL (29.8 mmol) of pentafluorobenzene. The mixture was cooled, with stirring to  $-78^\circ\text{C}$  in a dry/ice acetone bath. 18.8 mL (30.1 mmol) of 1.6 M  $n\text{-BuLi}$  was added via syringe. After 30 minutes, 4.32 mL of  $\text{SnCl}_4$  (7.4 mmol) was added. The solution was stirred at this temperature for 5h and left to warm up overnight, whereupon the solution colour changed from dark purple to a clear solution containing a white precipitate. The solution was filtered to remove solids, and the ether removed. The crude material was redissolved in toluene, filtered through celite and brought to dryness. The sample was further purified by sublimation ( $250^\circ\text{C}$ ,  $1 \times 10^{-4}$  mmHg) onto a cold finger. Compound **3** was recovered as a white powder. Analysis by  $^{19}\text{F}$  NMR for this compound agreed with reported literature values [42]. Recrystallization from ether afforded long, transparent crystals (4.4 g, 75%) m.p.  $219^\circ\text{C}$  (lit.  $221^\circ\text{C}$ ).<sup>61</sup>

$^{13}\text{C}$ -NMR{ $^{19}\text{F}$ }:  $\delta$  148.49 (br m, C1, *C-ipso-Sn*), 143.75 (s, C2, *o-C<sub>6</sub>F<sub>5</sub>*), 137.56 (s, C3, *m-C<sub>6</sub>F<sub>5</sub>*), 105.04 (s, C4, *p-C<sub>6</sub>F<sub>5</sub>*) ppm.  $^{119}\text{Sn}$ -NMR ( $\text{CDCl}_3$ ):  $\delta$  -218.77 (s) ppm.  $^{19}\text{F}$ -NMR ( $\text{CDCl}_3$ ):  $\delta$  -157.1 (s, *m-C<sub>6</sub>F<sub>5</sub>*), -146.0 (s, *p-C<sub>6</sub>F<sub>5</sub>*), -121.2 (d, *o-C<sub>6</sub>F<sub>5</sub>*,  $^2J_{\text{F}} = 15$  Hz,  $^2J_{\text{Sn-F}} = 102$  Hz) ppm.

#### 2.2.4 Di-[4-(trifluoromethyl)phenyl]dichlorostannane **4**

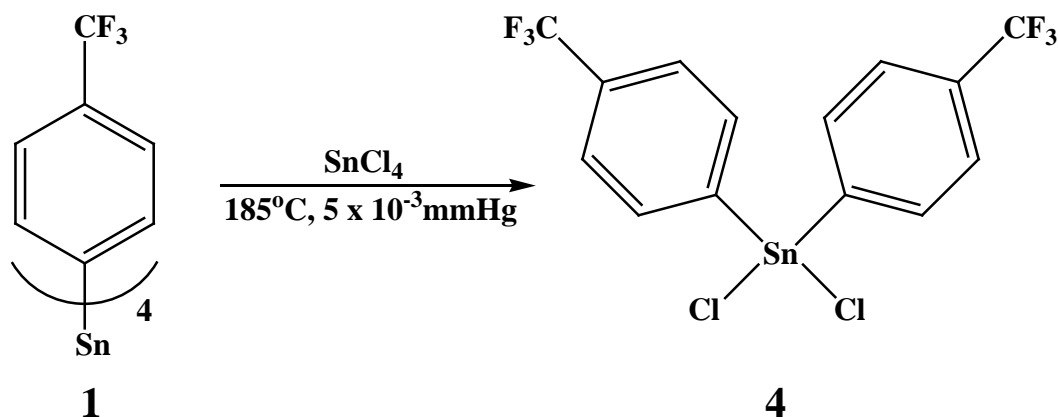


**Figure 17:** Synthesis of compound **4** by the redistribution reaction between **1** and SnCl<sub>4</sub>

Compound **1** (2.73 g, 3.99 mmol) was added to a flame dried 100 mL Schlenk flask under nitrogen. Using a syringe, 0.47 mL (3.99 mmol) of SnCl<sub>4</sub> was slowly added to the flask. The flask was equipped with a glass stopper, placed under static vacuum, and heated at 180°C for 3d. After completion of the reaction a black mixture was obtained. The dark black solution was dissolved in 5 mL of CH<sub>2</sub>Cl<sub>2</sub>, filtered through a sintered frit, and brought to dryness under vacuum. Crude compound **4** was further purified by sublimation under vacuum at 65°C to afford clear white crystals (2.41 g, 64% yield), mp 143°C.

<sup>1</sup>H-NMR (CDCl<sub>3</sub>): δ 7.85 (d, 2H, <sup>3</sup>J<sub>Sn-H</sub> = 8.5 Hz), 7.83 (d, 2H, <sup>4</sup>J<sub>Sn-H</sub> = 8.5 Hz) ppm. <sup>13</sup>C-NMR: δ 140.61 (br m, C1, C-*ipso*-Sn), 135.43 (s, C2, J<sub>C-Sn</sub> = 31.43 Hz), 133.08 (q, C4, C-*ipso*-CF<sub>3</sub>, <sup>2</sup>J<sub>C-F</sub> = 33.3 Hz), 126.34 (q, C3, <sup>3</sup>J<sub>C-F</sub> = 3.7 Hz), 126.10 (q, C5, CF<sub>3</sub>, J<sub>C-F</sub> = 273 Hz) ppm. <sup>119</sup>Sn-NMR (CDCl<sub>3</sub>): δ -32.14 ppm. <sup>19</sup>F-NMR (CDCl<sub>3</sub>): δ -63.40 (s, CF<sub>3</sub>, <sup>5</sup>J<sub>Sn-F</sub> = 9.5 Hz) ppm. Calc: C 35.04, H 1.68; Found: C 34.36, H 1.63.

### 2.2.5 Di-[3,5-(trifluoromethyl)phenyl]dichlorostannane **5**

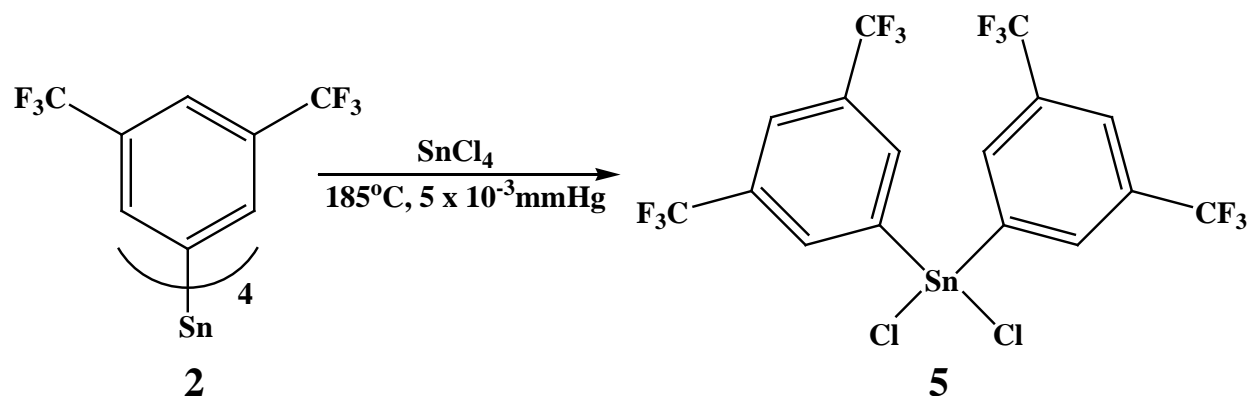


**Figure 18:** Synthesis of compound **5** by the redistribution reaction between **2** and  $\text{SnCl}_4$

Compound **2** (3.00 g, 3.09 mmol) was added to a flame dried 100 mL Schlenk flask under nitrogen. Via syringe, 0.43 mL (3.71 mmol) of  $\text{SnCl}_4$  was slowly added to the flask. The flask was equipped with a glass stopper, placed under static vacuum, and heated at  $180^\circ\text{C}$  for 3d. After completion of the reaction, a black mixture was obtained. The dark black solution was dissolved in 5 mL of  $\text{CH}_2\text{Cl}_2$ , filtered through a sintered frit, and brought to dryness under vacuum. Crude compound **5** was further purified by sublimation under vacuum at  $80^\circ\text{C}$  to afford clear white crystals (2.81 g, 74% yield), mp  $108^\circ\text{C}$ .

$^1\text{H-NMR}$  ( $\text{CDCl}_3$ ):  $\delta$  8.16 (br s, 2H,  $^2J_{\text{Sn-H}} = 40$  Hz), 8.12 (br s, 1H) ppm.  $^{13}\text{C-NMR}$  ( $\text{CDCl}_3$ ):  $\delta$  138.03 (s, C2), 134.86 (m, C1, C-*ipso*-Sn), 133.08 (q, C3, C-*ipso*- $\text{CF}_3$ ,  $J_{\text{C-F}} = 33.3$  Hz), 126.20 (m, C4,  $^2J_{\text{C-F}} = 13.7$  Hz), 125.46 (q, C5,  $\text{CF}_3$ ,  $J_{\text{C-F}} = 273$  Hz) ppm.  $^{119}\text{Sn-NMR}$  ( $\text{CDCl}_3$ ):  $\delta$  -36.83 (s) ppm.  $^{19}\text{F-NMR}$  ( $\text{CDCl}_3$ ):  $\delta$  -62.94 (s,  $\text{CF}_3$ ,  $^4J_{\text{Sn-F}} = 2.9$  Hz) ppm. HR-MS  $\text{EI}^+$ : calcd for  $\text{C}_{16}\text{H}_6\text{Cl}_2\text{F}_{12}\text{Sn}$ : 615.8713, No molecular ion present. calcd  $\text{M}^+ - \text{F}$ , 596.8693, found 596.8697  $\text{g}\cdot\text{mol}^{-1}$ . Calc: C 31.21, H 0.98; Found: C 32.50, H 1.11.

### 2.2.6 Attempted Preparation of Di-[Pentafluorophenyl]dichlorostannane **6**

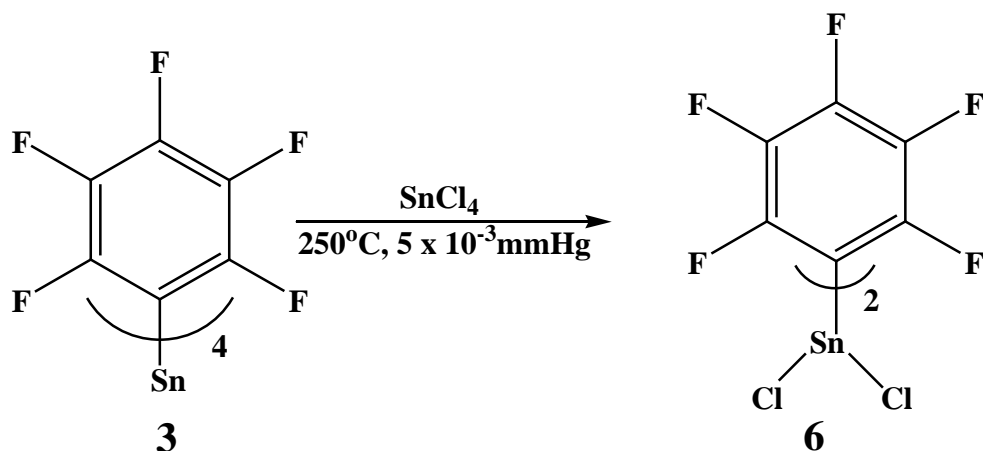


**Figure 19:** Synthesis of compound **6** via redistribution reaction between **3** and  $\text{SnCl}_4$

Compound **3** (3.00 g, 3.81 mmol) was added to a flame dried 100 mL Schlenk flask under nitrogen. Using a syringe, 0.46 mL (3.91 mmol) of  $\text{SnCl}_4$  was slowly added to the flask. The flask was equipped with a glass stopper, placed under static vacuum, and immersed in an oil bath heated to  $250^\circ\text{C}$  for 7d. The dark brown mixture was dissolved in 5 mL of dichloromethane, filtered through a sintered frit, and brought to dryness under vacuum. Analysis of the reaction by  $^{19}\text{F}$  NMR indicated only partial conversion to the desired dichlorostannane **6**. In an attempt to drive the reaction to completion, an additional quantity of  $\text{SnCl}_4$  (0.23 mL, 1.96 mmol) was added to the crude material and left at  $250^\circ\text{C}$  for an additional 3d. No further improvement in the distribution of products was observed. The percent conversion, estimated by  $^{19}\text{F}$  NMR integration, revealed that the mixture contained 57% of compound **6** and 43% of the starting material **3**. No further characterization of these products was carried out.

$^{19}\text{F}$ -NMR ( $\text{CDCl}_3$ ):  $\delta$  -157.5 (*o*- $\text{C}_6\text{F}_5$ ), -144.7 (*p*- $\text{C}_6\text{F}_5$ ), -121.0 (*m*- $\text{C}_6\text{F}_5$ ), ppm.

### 2.2.7 Synthesis of [(trifluoromethyl) phenyl] tin Trihydride 7

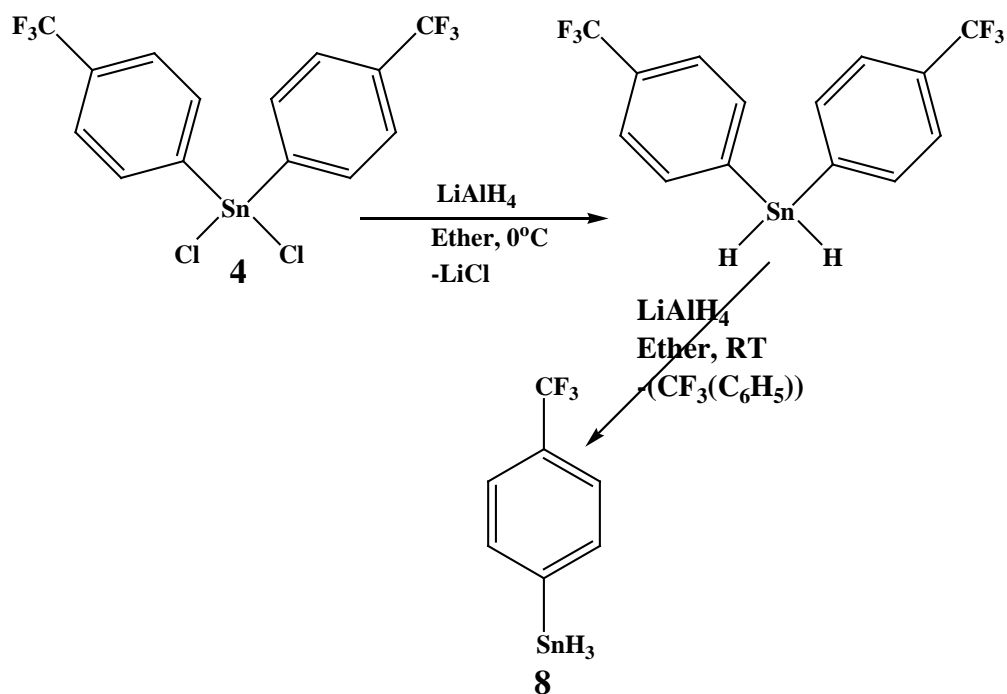


**Figure 20:** Synthesis of tin trihydride **8** by the substitution reaction between **4** and  $\text{LiAlH}_4$

0.5 g (1.04 mmol) of compound **4** was dissolved in 50 mL of ether in a 100 mL schlenk flask and placed in an ice bath at  $0^\circ\text{C}$ . In a separate 250 mL schlenk flask, 4.2 mL (4.2 mmol) of 1M  $\text{LiAlH}_4$  was added to a 50 mL ether solution and allowed to cool to  $0^\circ\text{C}$  in an ice bath. Using a double tipped canula, the solution containing the dichloride monomer **4** was added dropwise to the  $\text{LiAlH}_4$  solution over a 30 minute period resulting in the formation of a white precipitate. The reaction was then removed from the ice bath and stirred at room temperature for an additional 2h. The reaction was quenched by the slow addition of cold degassed water until the liberation of hydrogen gas was no longer evident. Addition of water also resulted in the formation of a slight yellow color. The mixture was poured into a 250 mL separatory funnel followed by extraction to separate the aqueous layer from the slightly yellow organic layer. The aqueous layer was discarded and the ether layer placed over a drying agent ( $\text{CaCl}_2$ ) for 2 h to remove any remaining moisture.

The ether solution was filtered with a glass schlenk frit and placed under vacuum to remove the solvent. A white waxy product with a slight yellow ting was recovered (0.27g, 63% crude yield).

$^1\text{H-NMR}$  ( $\text{CDCl}_3$ ):  $\delta$  7.6 (dd,  $J = 7.64$  Hz aryl) ppm.  $^{19}\text{F-NMR}$ ( $\text{CDCl}_3$ ):  $\delta$  -63.20 (s) ppm.  $^{119}\text{Sn-NMR}$  ( $\text{CDCl}_3$ ): $\delta$  -145.73 (s) ppm.  $^{13}\text{C-NMR}$  ( $\text{CDCl}_3$ ): $\delta$  141.62 (br, m), 137.28 (m,  $J = 4.4$  Hz) 132.06 (q,  $^2J = 32.8$  Hz), 126.71 (m,  $^3J = 3.62$  Hz), 123.80 (q,  $^1J = 270$  Hz) ppm.

### 2.2.8 Synthesis of bis(3,5(trifluoromethyl) phenyl tin dihydride 9

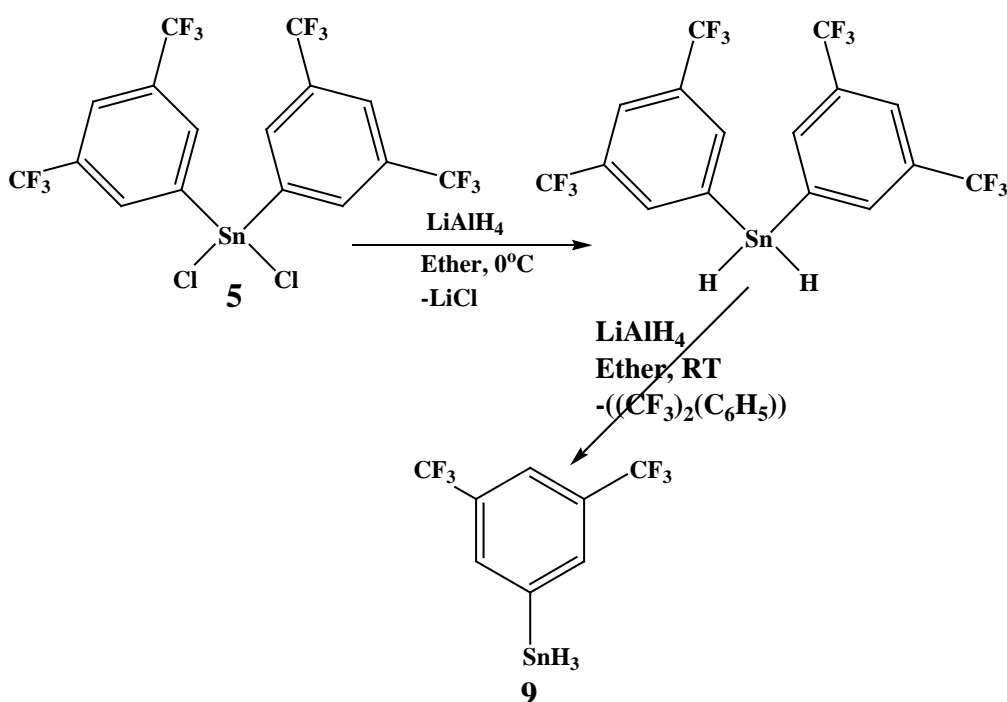


**Figure 21:** Synthesis of tin trihydride **9** by the substitution reaction between **5** and  $\text{LiAlH}_4$

Compound **5** (0.7 g 1.14 mmol) was dissolved in 50 mL of ether in a 100 mL schlenk flask and placed on a ice bath at  $0^\circ\text{C}$ . In a separate 250 mL schlenk flask 4.6 mL (4.6 mmol) of 1M  $\text{LiAlH}_4$  was added to a 50 mL ether solution and allowed to cool to  $0^\circ\text{C}$  on an ice bath. Using a double tipped canula, the solution containing **5** was added dropwise to the  $\text{LiAlH}_4$  solution over a 30 min period resulting in the formation of a

white precipitate. The solution was stirred for at 0°C for an addition 30 min then removed from the ice bath and stirred at room temperature for an additional 2h. The reaction was quenched by the slow addition of cold degassed water until the liberation of hydrogen gas was no longer evident. The mixture was poured into a 250 mL separatory funnel followed by extraction to separate the aqueous layer from the organic layer. The aqueous layer was discarded and the ether layer placed over a drying agent for 2 h to remove any remaining moisture. The ether solution was filtered and placed under vacuum to remove the solvent, leaving a white waxy crude product (0.3g, 48% yield).

$^1\text{H-NMR}$  ( $\text{CDCl}_3$ ):  $\delta$  (m, 8.04-7.55 aryl), 6.72 ( $J_{\text{sn-H}} = 55.3$  Hz) ppm.  $^{19}\text{F-NMR}$  ( $\text{CDCl}_3$ ):  $\delta$  63.04 (s,  $\text{CF}_3$ ) ppm.  $^{119}\text{Sn-NMR}$ ( $\text{CDCl}_3$ ):  $\delta$  -142.34 (s) ppm.  $^{13}\text{C-NMR}$  ( $\text{CDCl}_3$ ):  $\delta$  136.49 (br) ppm. 136.11 (br m), 132.17 (q,  $^2J_{\text{C-F}} = 33.47$  Hz), 127.96, 124.09 (m,  $^3J_{\text{C-F}} = 3.68$ ), 122.53 (q,  $^1J_{\text{C-F}} = 271$  Hz) ppm.

### 2.2.9 Poly[di[4-(trifluoromethyl)phenyl]stannane 10

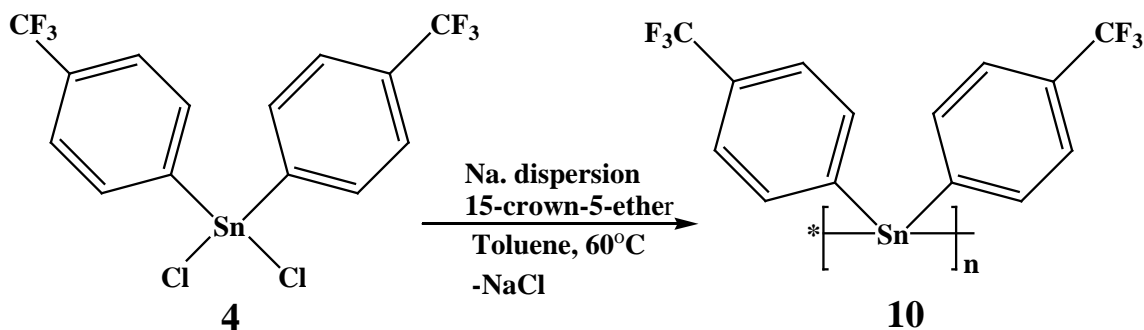


**Figure 22:** Synthesis of **10** *via*. Wurtz coupling of **4** in the presence of sodium metal

To a 50 mL Schlenk flask equipped with a magnetic stirring bar under  $\text{N}_2$  was added 5 mL of toluene, **4** (1.00 g, 2.1 mmol), and 15-crown-5-ether (11 mg, 0.05mmol). In a separate 25 mL 3-neck flask equipped with a reflux condenser, of frit filtered sodium (0.079g, 3.43 mmol) was added to 5 mL of toluene. Sodium dispersion was prepared by refluxing the sodium-toluene solution at a temperature of 110°C under  $\text{N}_2$  for 1h

and allowed to cool to room temperature. The flask was then carefully wrapped in aluminum foil to shield the reaction products from light. Using a syringe, the solution of **4** was added dropwise to the stirring sodium dispersion at room-temperature. The reaction was then heated to 60°C for 4h. The reaction mixture was then filtered and transferred into an aluminum foil wrapped Schlenk flask. The toluene was then removed by vacuum to produce a yellow-tinged powder of **9** (0.46 g, 54% yield).

$^1\text{H-NMR}$  ( $\text{CDCl}_3$ ):  $\delta$  7.82 (d, 2H, *o*-,  $^3J_{\text{HF}} = 8.3$  Hz), 7.87 (d, 2H,  $^2J_{\text{HF}} = 8.3$  Hz) ppm.  $^{13}\text{C-NMR}$ :  $\delta$  135.56 (s, C1, C-*ipso*-Sn,  $^1J_{\text{C-Sn}} = 33.2$  Hz), 133.7 (q, C2,  $^3J_{\text{C-F}} = 32.9$  Hz), 133.7 (q, C4, C-*ipso*-CF<sub>3</sub>,  $^2J_{\text{C-F}} = 33.3$  Hz), 126.88 (q, C3,  $^3J_{\text{C-F}} = 3.7$  Hz), 123.50 (q, C5, CF<sub>3</sub>,  $^1J_{\text{C-F}} = 273$  Hz) ppm.  $^{119}\text{Sn-NMR}$  ( $\text{CDCl}_3$ ):  $\delta$  -56.7 (br s) ppm.  $^{19}\text{F-NMR}$  ( $\text{CDCl}_3$ ):  $\delta$  -63.36 (s. CF<sub>3</sub>) ppm. UV-Vis  $\lambda_{\text{max}} = 332$  nm,  $\epsilon = 32$  L mol cm<sup>-1</sup>. Calc: C43.78, H 3.21; Found: C42.58, H 2.85.

#### 2.2.10 Poly(di[3,5-(trifluoromethyl)phenyl]stannane **11**)

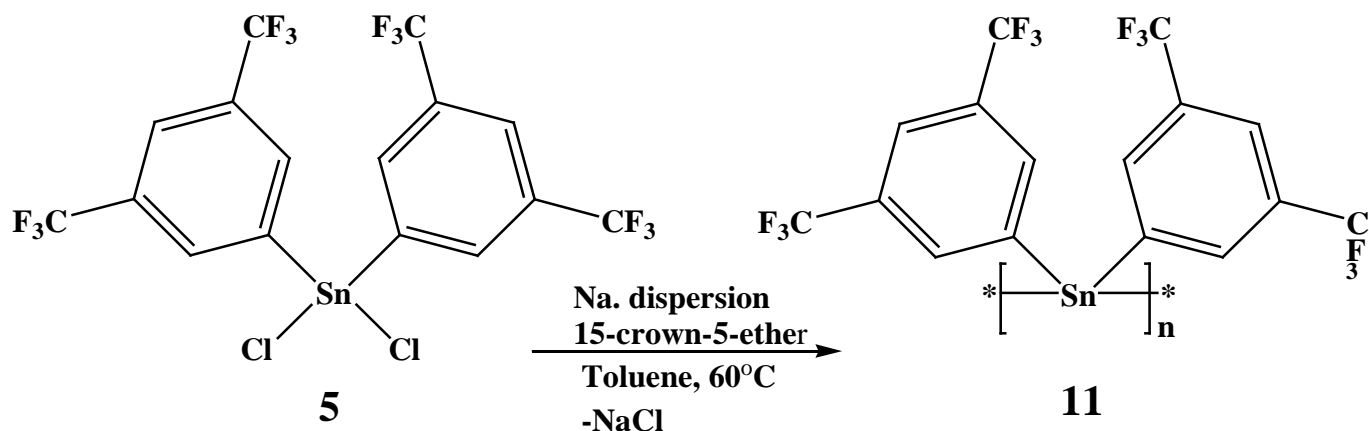


**Figure 23:** Synthesis of **11** *via*. Wurtz coupling of **5** in the presence of sodium metal

To 50 mL Schlenk flask equipped with a magnetic stirring bar under N<sub>2</sub> was added, 5 mL of toluene, **5** (1.18 g, 1.91 mmol), and 15-crown-5-ether (16.7 mg, 0.076 mmol). In a separate 25mL 3-neck flask equipped with a reflux condenser, frit filtered sodium (0.07 g, 3.0 mmol) was added to 5mL of toluene. A sodium dispersion was prepared by refluxing the sodium-toluene solution at a temperature of 110°C under N<sub>2</sub> for 1h

and allowed to cool to room temperature. The flask was then carefully wrapped in aluminum foil to shield light from the reaction. Using a syringe the solution containing **5** in dry toluene was added dropwise to the stirring sodium dispersion at room-temperature. The reaction was then heated to 60°C for 4h. The reaction mixture was then filtered and transferred into an aluminum foil wrapped Schlenk flask. The toluene was then removed by vacuum to produce a yellow white oil of **11**. (0.56 g, 54% yield).

<sup>1</sup>H-NMR (CDCl<sub>3</sub>): δ 8.59 (br s, 2H,  $J_{\text{Sn-H}} = 40.1$  Hz), 8.59 (br s, H4, 1H) ppm. <sup>13</sup>C-NMR(CDCl<sub>3</sub>): δ 140.3 (br s, C4), 135.82 (q, C1, C-*ipso*-Sn,  $^4J_{\text{CF}} = 1.34$  Hz,  $^1J_{\text{Sn-C}} = 27.2$  Hz), 132.21 (q, C3, C-*ipso*-CF<sub>3</sub>,  $^2J_{\text{C-F}} = 33.5$  Hz), 124.72 (q, C2,  $^3J_{\text{C-F}} = 3.7$  Hz), 123.09 (q, C5, CF<sub>3</sub>,  $^1J_{\text{C-F}} = 274$  Hz). <sup>119</sup>Sn-NMR (CDCl<sub>3</sub>): δ -48.90 (s) ppm. <sup>19</sup>F-NMR (CDCl<sub>3</sub>): δ -63.02 (s. CF<sub>3</sub>) ppm. UV-Vis  $\lambda_{\text{max}} = 328$  nm,  $\epsilon = 48$  Lmolcm<sup>-1</sup>. Calc: C 35.27, H 1.10; Found: C 36.02, H 1.03.

#### 2.2.11 Poly[(trifluoromethyl)phenyl]stannane using dehydrocoupling **12**

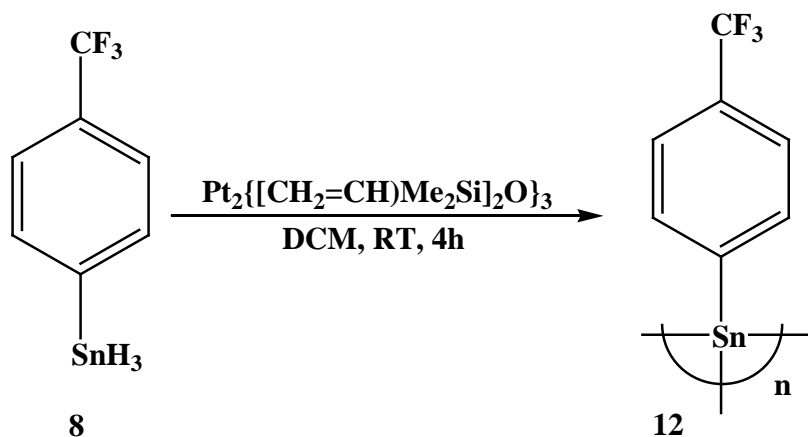


**Figure 24:** Synthesis of **12** by the dehydrocoupling of tin hydride **8** using Kardstedt catalyst

The crude dihydride **8** was dissolved in 60 mL of CH<sub>2</sub>Cl<sub>2</sub> in a 250 mL flask equipped with a magnetic stir bar, carefully wrapped in aluminum foil and placed under a inert N<sub>2</sub> atmosphere. To the solution containing **8**, 6 drops of Kardstedt catalyst (Pt<sub>2</sub>{[(CH<sub>2</sub>=CH)Me<sub>2</sub>Si]<sub>2</sub>O<sub>3</sub>}) was slowly added dropwise. The reaction was



$^1\text{H-NMR}$  ( $\text{CDCl}_3$ ):  $\delta$  8.08 (s, 1H), 7.96 (s, 2H) ppm.  $^{19}\text{F-NMR}$ ( $\text{CDCl}_3$ ):  $\delta$  -63.11 (s,  $\text{CF}_3$ ) ppm.  $^{119}\text{Sn-NMR}$  -127.09 (s) ppm.  $^{13}\text{C-NMR}$  ( $\text{CDCl}_3$ )  $\delta$  140.4 (s), 136.31 (br, m), 132.84 (q,  $^2J_{\text{C-F}} = 33.52$ ), 127.48 (m,  $^3J = 3.76$ ), 122.9 (q,  $^1J_{\text{C-F}} = 272$ ) ppm. UV-VIS,  $\lambda_{\text{max}} = 354$  nm.

### 3.0 Results and Discussion

#### 3.1 Fluorinated Tetraaryl Tin Compounds

The preparation of *tetrakis* fluorinated phenyl tin precursors (**4** and **5**) was successfully carried using both the Grignard and organolithium routes. The Grignard reaction was more time consuming as this reaction required overnight refluxing while the two step lithium route required only 4 h to reach completion. The organolithium route is also superior in terms of the percent yield (> 70%) when compared to the Grignard route (< 44%) for compound **2**. The organolithium route was therefore chosen for all subsequent reactions. The clear white product obtained after sublimation was investigated using NMR spectroscopy ( $^{19}\text{F}$ -NMR,  $^{119}\text{Sn}$ -NMR,  $^{13}\text{C}$ -NMR and  $^1\text{H}$ -NMR). The  $^{119}\text{Sn}$ -NMR shift observed for **1** and **2** are comparable to those reported by King *et al.*<sup>59</sup> for the same compounds as shown by Table 9.

**Table 9:** Comparison of experimental and literature  $^{119}\text{Sn}$ -NMR shift for **1** and **2**

Compound	Experimental $^{119}\text{Sn}$ -NMR $\delta$ (ppm)	Literature <sup>59</sup> $^{119}\text{Sn}$ -NMR $\delta$ (ppm)
<b>1</b>	131.0	132.3
<b>2</b>	126.1	128.1

The para disubstituted ring substituents of compound **1** are expected to give rise to a AA'BB'  $^1\text{H}$ -NMR pattern.<sup>62</sup> However this was not the case as only a singlet at 7.7 ppm was observed (Figure 26). The two proton environments found in the structure of **1** are considered to be chemically different but magnetically equivalent therefore giving rise to a single peak. Compound **2** gave the expected ABA pattern with a 2/1 ratio for a 1,3,5 trisubstituted phenyl ring (Figure 26).

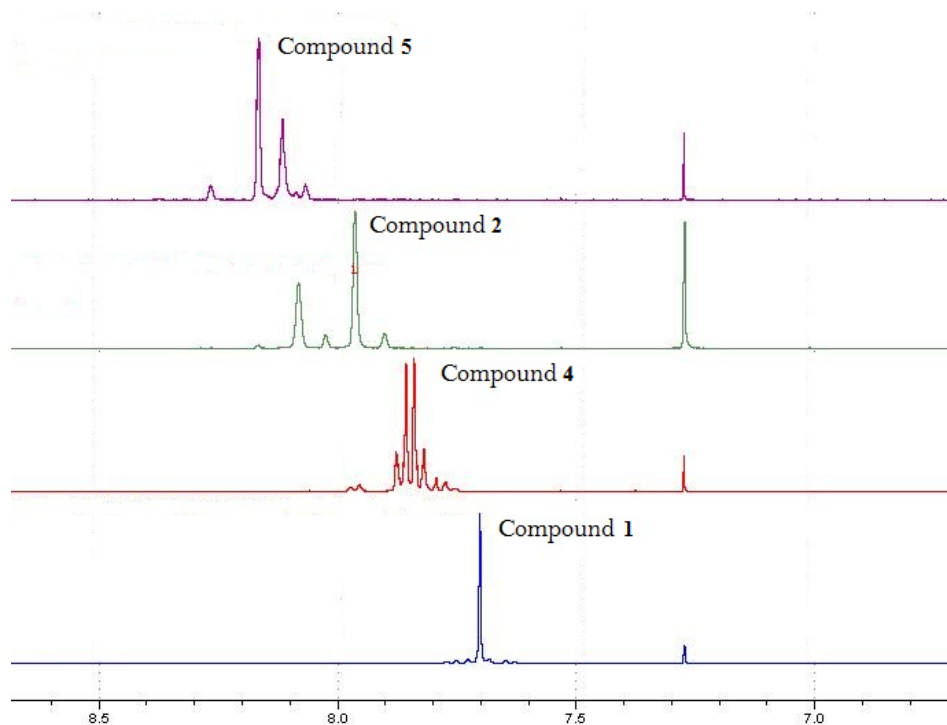


**Figure 26:** A plot of the  $^1\text{H}$ -NMR spectra for compounds **1-2** and **4-5**

X-ray analysis was also used to characterize the structure of one of the fluorinated tetraaryl stannanes. Compound **2** showed Sn-C bond lengths of (2.149 Å) that were very similar to those of tetraphenyl tin<sup>63</sup> (2.144 Å) and other similar compounds. However, **2** deviates dramatically from ideal tetrahedral compared tetraphenyl tin where all angles at the central tin atom are nearly ideal ( $109.5^\circ \pm 1^\circ$ ). With C-Sn-C bond angles between  $104.69^\circ$ - $120.76^\circ$  compound **2** can best be described as having a distorted tetrahedral geometry. Such deviations indicate that the introduction of the  $\text{CF}_3$  groups is having steric and/or electronic effect on the structure of these compounds.

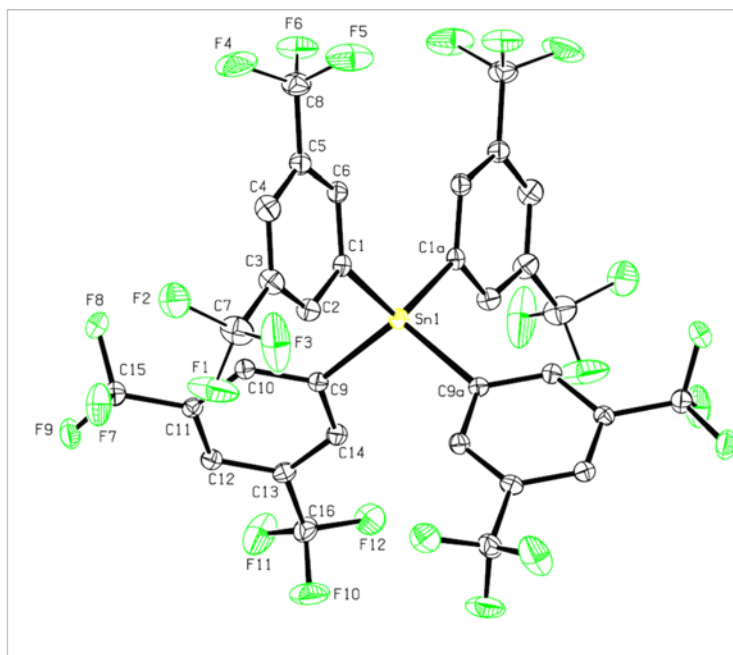


**Figure 27:** Crystal structure for compound **2**<sup>64</sup>

The X-ray structure for **2** is shown in Figure 27.<sup>64</sup> Based on the close proximity of the CF<sub>3</sub> groups, it is evident that steric crowding impacts the geometry of this compound. These electron rich CF<sub>3</sub> groups also lead to extensive electronic repulsion with neighbouring CF<sub>3</sub> groups. While distortion of the bond angles is evident in the analogous non fluorinated compounds (3,5(CH<sub>3</sub>)C<sub>6</sub>H<sub>3</sub>)<sub>4</sub>Sn<sup>65</sup> and (3,5(Cl)C<sub>6</sub>H<sub>3</sub>)<sub>4</sub>Sn,<sup>66</sup> it is much less compared to **2**. In the case of **1**, the literature shows that bond angles around the central tin atom are between 107.89°-112.9°.<sup>67</sup> The *para* position of the single CF<sub>3</sub> group in **1** allows this structure to have less hindrance between substituents unlike **2** where the CF<sub>3</sub> groups are in close proximity. The lone CF<sub>3</sub> on each ring in **1** is also expected have a lesser electronic effect compared to compound **2**. These compounds were also characterized using time of flight mass spectroscopy (TOF-MS) as way to determine the structures. The data is summarized in Table 10.

**Table 10:** MS fragmentation patterns for **2** after TOF-MS

M/z	Fragment peak	Fragment lost
758.9	$[(3,5(\text{CF}_3)_2\text{C}_6\text{H}_3)_3\text{Sn}]^+$	$[(3,5((\text{CF}_3)_2(\text{C}_6\text{H}_3)))]$
332.9	$[(3,5(\text{CF}_3)_2\text{C}_6\text{H}_3)\text{Sn}]^+$	$[(3,5((\text{CF}_3)_2(\text{C}_6\text{H}_3))_3]$
213	$[(3,5(\text{CF}_3)_2\text{C}_6\text{H}_3)]^+$	$[(3,5(\text{CF}_3)_2\text{C}_6\text{H}_3)_3\text{Sn}]$
194	$[(\text{CF}_3(\text{C}_6\text{H}_3))]^+$	$[\text{CF}_3], [(3,5(\text{CF}_3)_2\text{C}_6\text{H}_3)_3\text{Sn}]$

There was no molecular ion observed for **2** and this is likely due to the instability of the quaternary ion  $[\text{SnR}_4]^+$ . The more stable tertiary ion ( $m/z = 758.9$ ) which resulted from the loss of one perfluorinated ring  $[\text{SnR}_3]^+$  is observed instead. The most abundant ion peak was observed at  $m/z = 194$  which represents a phenyl ring with a single  $\text{CF}_3$  group attached.

### 3.2 Synthesis of Fluorinated Tin Dichlorides

Tin dichloride derivatives (**4** and **5**) were synthesized using a redistribution reaction between their parent compounds (**1** and **2**) and  $\text{SnCl}_4$  in the neat. The reaction was carried out under a static vacuum condition using high temperatures (150-185°C). These conditions were similar to those used in literature for the synthesis of other tin dichlorides with aryl substituents.<sup>46,47</sup> Initially, equimolar amounts of the tetraaryl tin compounds (**1-2**) and  $\text{SnCl}_4$  were used. Investigation by  $^{119}\text{Sn}$ -NMR spectroscopy showed that complete conversion to dichloride did not occur under these conditions and instead a mixture of the mono and dichloro species was being formed. This is likely attributed to the decomposition of  $\text{SnCl}_4$  and formation of tin metal indicated by the appearance of a black colour. Using Le Châtelier's principle,<sup>16</sup> a slight excess of  $\text{SnCl}_4$  was added to favor the right side of the reaction while keeping other variables constant (temp., reaction time). It was observed that a higher fraction of the dichlorides were obtained with these changes. Therefore better results were obtained when the loss of  $\text{SnCl}_4$  by decomposition was compensated.

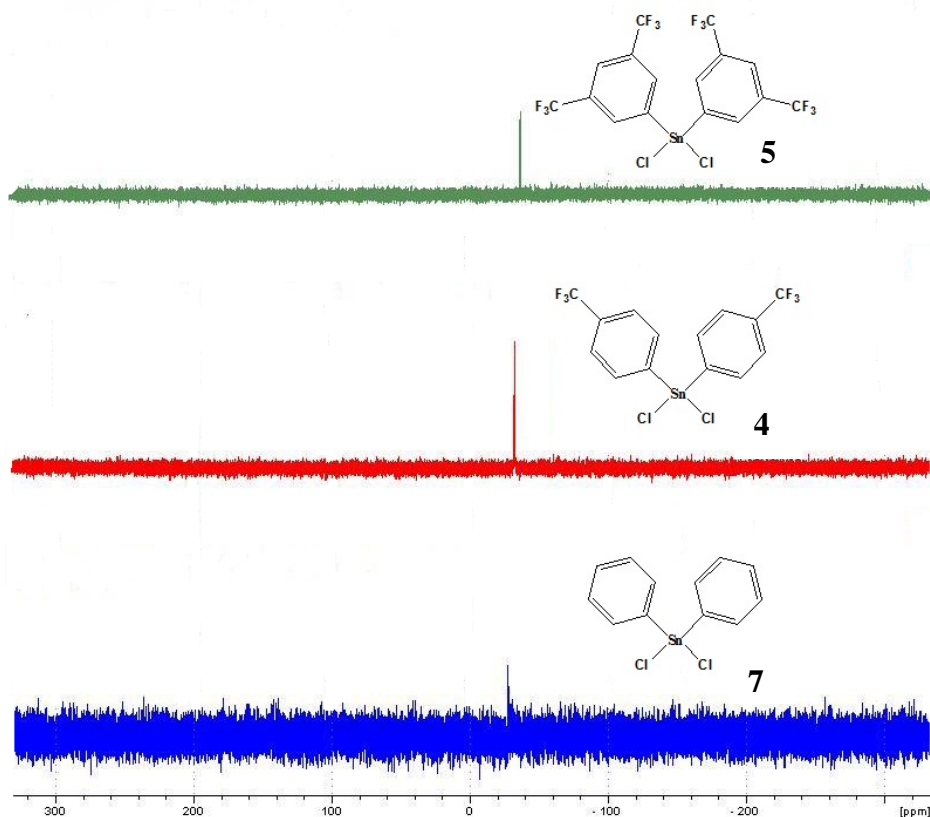


**Figure 28:** Stack plot of the  $^{119}\text{Sn}$ -NMR for aryl tin dichlorides

These compounds were then compared to the non-fluorinated diphenyltin dichloride (compound **7**). Figure 28 shows that **4** ( $\delta$ , -32.14 ppm), **5** ( $\delta$ , -36.83 ppm) and **7** (-28.9 ppm) have very similar  $^{119}\text{Sn}$ -NMR chemical resonances. Since NMR spectroscopy reflects both molecular and electronic structure it was expected that these compounds would have similar  $^{119}\text{Sn}$ -NMR chemical shift based on the similarities between their structures. Therefore  $^{119}\text{Sn}$ -NMR was used as an indication that the correct products were being synthesized. The effect of the  $\text{CF}_3$  group on the electronic structure was also investigated using  $^{119}\text{Sn}$ -NMR spectroscopy and the results are illustrated in the graph below.

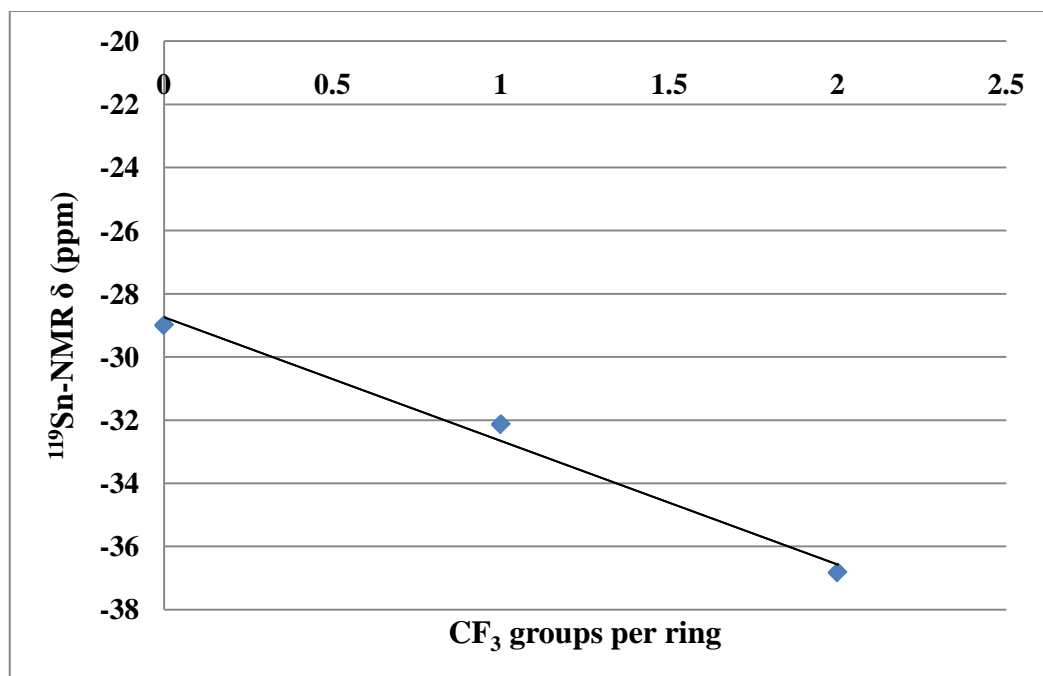


**Figure 29:** A plot of the relationship between the <sup>119</sup>Sn-NMR shift and number of CF<sub>3</sub> for aryltin dichlorides

Figure 29 shows that a linear relationship exists between the number of CF<sub>3</sub> per ring and the <sup>119</sup>Sn-NMR chemical resonance observed. This was also deemed to be an inverse relationship as evident by the negative slope (upfield shift) of the graph. The electron withdrawing behavior of the CF<sub>3</sub> group was expected to have a deshielding effect on the tin nucleus resulting in a downfield field shift (higher δ) but the opposite was observed. This indicate that the trend observe in figure 29 is most likely due geometric influence on the electronic structure of these tin dichlorides as a result of the various positions of the CF<sub>3</sub> groups. Similar finding were reported by Dräger *et al.* who demonstrated the influence of geometry on the electronic structure of oligostannanes using <sup>119</sup>Sn-NMR spectroscopy.<sup>25,26</sup> The <sup>119</sup>Sn-NMR shifts for **4** and **5** are found downfield from tetraaryl tin compounds (**1,2**) due to the presence of two electron withdrawing Cl atoms. The chlorines directly attached to tin cause a considerable amount of deshielding of the tin nuclei, resulting in a large downfield shift (+50 ppm). Figure 26 shows that **5** gave the expected 2/1 ratio in the aromatic region with an ABA substitution pattern while the spectrum for **4** is indicative of an aromatic ring with an AA'BB'

substitution. This pattern was expected for a para disubstituted ring but was not evident in **1** where both protons were magnetically equivalent. As expected the  $^1\text{H-NMR}$  shifts of **4** and **5** are also downfield from their parent compounds (**1** and **2**) due to the deshielding effect of the chlorine atoms (Figure 26). Sublimation proved to be a suitable method for the purification of both **4** and **5** which resulted in the formation of powdered semi-crystalline products. Similar to their parent compounds, **4** and **5** were also recrystallized by first dissolving in ether followed by slow evaporation. The X-ray crystallographic data for compounds<sup>57,58</sup> **1-7** are summarized in Table 11 while the crystal structure for **4** and **5** is shown below.

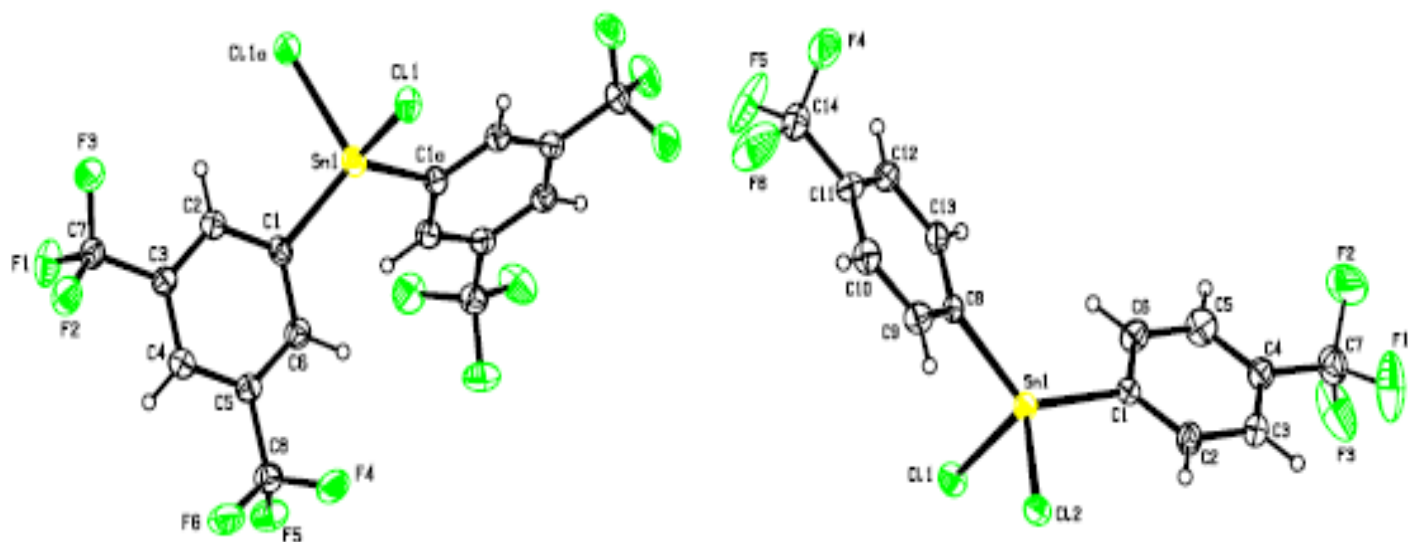


**Figure 30:** A unit cell molecule defined by the X-ray crystal structure for compounds **4** (right) and **5** (left)

Analysis of their crystallographic data showed that compared to their tetraaryl parent compounds **4** and **5** have slightly shorter average Sn-C bond length. This may be due to the presence of the two chlorine atoms. The chlorine atoms are electron withdrawing and are therefore expected to pull electron density away from the tin atom. Removal of electron density from the tin center by the chlorine atoms allows the phenyl rings

to increase their participation in the bond with tin. This result in the Sn-C bonds having a higher s-character causing them to be stronger and shorter for the dichlorides.

**Table 11:** X-ray crystallographic data for compounds **1-2, 4- 5** and **7**

Compound <sup>ref</sup>	C-Sn-C Bond length Å	C-Sn-C Bond angle °	Cl-Sn-Cl Bond length Å	Cl-Sn-Cl Bond angles°
<b>1</b> <sup>67</sup>	2.149(4)	107.89(19), 112.7 (4)	N/A	N/A
<b>2</b> <sup>64</sup>	2.147(3) 2.150(3)	120.76(17), 104.69(11),	N/A	N/A
<b>4</b> <sup>68</sup>	2.116(4), 2.119(4)	128.44(15)	2.3369(9) 2.3478(10)	101.76(3)
<b>5</b> <sup>68</sup>	2.119(4)	125.9(2)	2.3399(11)	99.23(6)
<b>7</b> <sup>69</sup>	2.119(5), 2.105(5)	123.9(2)	2.353(2) 2.336(2)	101.7(1)
<b>7</b> <sup>69</sup>	2.118(5), 2.112(6)	127.0(2)	2.357(2) 2.336(2)	97.8(1)

Table 11 also reveals that when compared to **7** the average Sn-C bond length for **4** and **5** are slightly longer. This is likely a consequence of the CF<sub>3</sub> groups removing electron density from the Sn-C bond. This decrease in electron density will result in longer bonds since stronger bonds usually require a higher electron density. Bond angles for **4** and **5** also deviate from the ideal tetrahedral geometry, even more so than **1** and **2**. Bond angles of 125.9° for the C-Sn-C and 99.23° for Cl-Sn-Cl were observed compound **5** while **4** had C-Sn-C angles of 128.44° and Cl-Sn-Cl angles of 101.76°. The structures for **4** and **5** seem to parallel the two discreet crystal structures found to exist for **7** (**a** and **b**).<sup>69</sup> This is evident even though the bond angles for **3** and **4** are slightly larger than those of **7a** and **7b** respectively. Angles that dramatically deviate from tetrahedral geometry were also reported for other dichlorides of Group 14 elements with the level of deviation increase going down the group as result of the increase polarization of the bonds.<sup>75</sup> These deviations can be described using Bent's rule which states that the atomic s-character is concentrated in orbitals directed towards electropositive substituents while the atomic p-character is concentrated in orbitals

that are directed towards the electronegative substituent.<sup>75</sup> Those orbitals with the greater *s*-character are expected to have bond angles greater than 109.5° while those with the greater *p*-character will have angles less than 109.5°. In the case of **4** and **5** the orbitals with more *s*-character are directed towards the aryl substituent which results in C-Sn-C bonds > 109.5° while those with higher *p*-character are directed towards the chlorine atom causing bond angles to be < 109.5°. MS analysis was also carried out on **5** and the data is listed in the Table 12.

**Table 12:** Fragmentation of **5** after TOF-MS

M/z	Fragment ion	Fragment loss
596.9	$[(\text{CF}_3)_3(\text{CF}_2)(\text{C}_6\text{H}_3)_2\text{SnCl}_2]^+$	[F]
580.8	$[(\text{CF}_3)_4(\text{C}_6\text{H}_3)_2\text{SnCl}]^+$	[Cl]
402.9	$[(\text{CF}_3)_2(\text{C}_6\text{H}_3)\text{SnCl}_2]^+$	$[(\text{CF}_3)_2(\text{C}_6\text{H}_3)]$
194	$[(\text{CF}_3)(\text{C}_6\text{H}_3)]^+$	$[\text{CF}_3, (\text{CF}_3(\text{C}_6\text{H}_3)\text{SnCl}_2)]$

Similar to **2**, there was no molecular ion observed for **5**. However, unlike **2** a quaternary stannane ion peak was observed for **5** at 596.9 m/z due to the loss of fluorine from a CF<sub>3</sub> group. C-F bonds are some of the strongest bonds in chemistry therefore cleavage of this bond is most likely driven by the stability of the ion formed. This explains the observation of the quaternary stannane ion. These ions are typically not observed in mass spectrometry due to the instability when the charge site is located at the tin center. A tertiary ion was also observed for **5** at 580.8 m/z due to the loss of a chlorine atom. The most abundant peak was observed at 194 m/z and this was attributed to a phenyl fragment with a single CF<sub>3</sub> attached. This was also the most abundant peak in **2** and suggests that this fragment is very stable likely due to resonance stabilization. The isotopic ratios of the molecular ion peaks also agree with a molecule that contains two chlorine atoms.

### 3.3 Synthesis of Tin Dihydrides

Synthesis of the tin dihydrides derivatives (**8,9**) from the substitution reaction between tin dichlorides (**4, 5**) and  $\text{LiAlH}_4$  are based on similar reactions carried out by Stern *et al.*<sup>60</sup> and Tilley *et al.*<sup>46,47</sup> A 4-fold excess of  $\text{LiAlH}_4$  was used to ensure complete substitution of chlorides by hydrides. It is known from previous studies that the order in which the reactants were added to the reaction is crucial in obtaining the right products. Following the method used by Tilley *et al.*,<sup>46,47</sup> an ether solution containing the tin dichlorides was cooled to  $0^\circ\text{C}$  then added dropwise to another solution at  $0^\circ\text{C}$  containing the  $\text{LiAlH}_4$ . The addition of **5** to  $\text{LiAlH}_4$  resulted in the formation of a white precipitate assumed to be  $\text{LiCl}$ . The solution remained colorless during the entirety of the reaction. However, the solution unexpectedly turned slightly yellow after the addition of water during quenching. The slightly yellow ether layer was separated from the aqueous layer and then dried over  $\text{CaCl}_2$  which resulted in the disappearance of the yellow color. Removal of the solvent gave a white solid product which was consistent with other diaryl tin dihydrides from literature.<sup>46,47</sup> A  $^{119}\text{Sn}$ -NMR analysis of the reaction product revealed a resonance signal at  $-142.3$  ppm, which initially was attributed to the tin dihydride, but based on further investigation was determined to be the tin trihydride **9**. A resonance at  $6.72$  ppm was observed in the  $^1\text{H}$ -NMR spectrum for **9** and was assigned to the protons attached to the tin atom (inset Figure 31). The  $^{19}\text{F}$ -NMR spectrum showed that other products were also being formed, probably due to unwanted side reactions. Research in the 1960's showed that cleavage of tin-carbon bond was likely when this bond was sufficiently polar.<sup>70</sup> The cleavage of tin-carbon bond in fluorinated compounds in the presence of a base was first reported by Holmes *et al.*<sup>71</sup> Later work by Stern *et al.*<sup>60</sup> showed that substitution of chlorine using hydride nucleophiles were prone to side reactions when a fluorinated substituent was bound to the tin. In an attempted synthesis of tris(*p*-chlorophenyl) tin hydride from the corresponding chloride and  $\text{LiAlH}_4$  Stern and Becker were able to isolate chlorobenzene as a byproduct which suggested there was a cleavage of the tin-aryl bond.<sup>60</sup> It was argued that the tin center was more electrophilic due to the presence

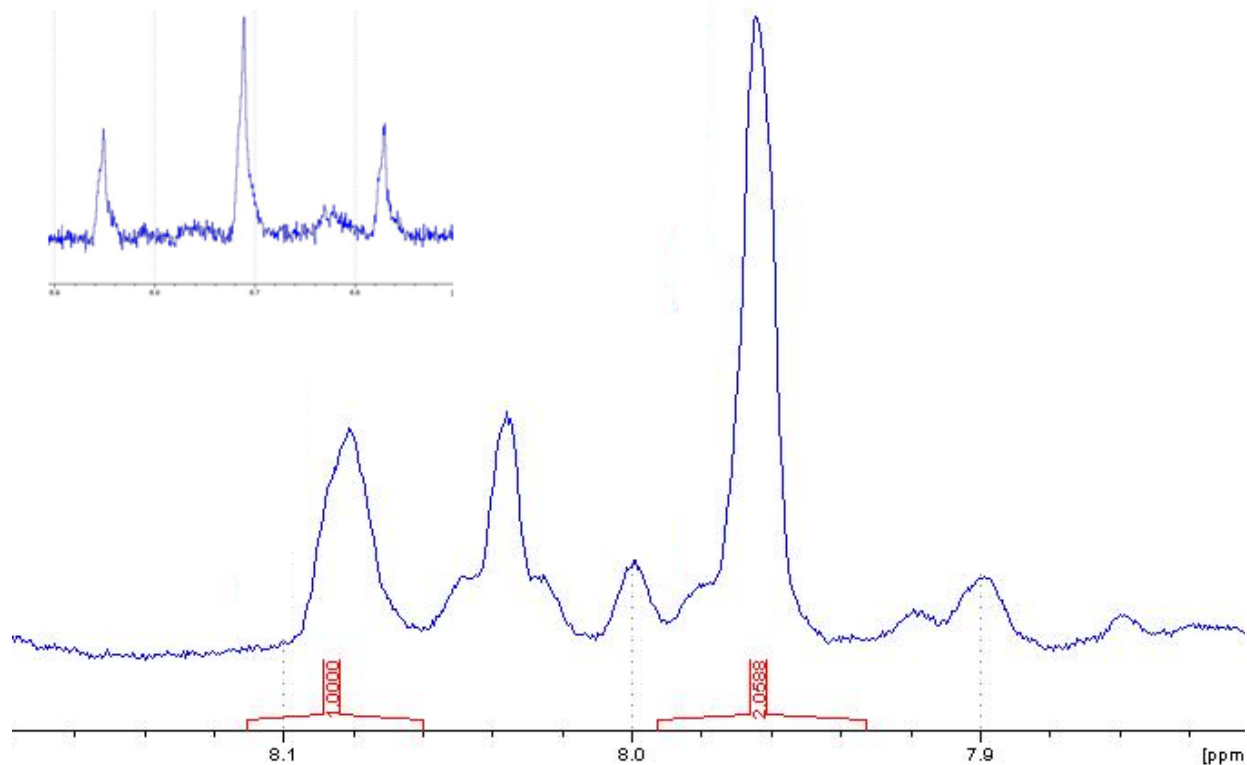


**Figure 31:** <sup>1</sup>H-NMR spectrum for the tin trihydride **9** showing the phenyl and hydride region (inset)

of the electron withdrawing chloro group on the phenyl ring. This resulted in the tin being more susceptible to attack from strong nucleophiles such as LiAlH<sub>4</sub>. A similar finding was also reported by Bregadze *et al.*<sup>70</sup> when di(phenylborenyl)tin dichloride was treated with a strong base/nucleophile such as KOH. In this work they reported that 30% of the tin-carbon was cleaved as evident by the isolation of phenylbarene from the reaction.<sup>70</sup> It is suspected that a similar reaction is taking place in this work, where the presence of the CF<sub>3</sub> groups result in an increase polarization of the tin-aryl bond. Therefore, while the goal is substitution of the chlorine atoms it likely that the phenyl-tin bonds are also being cleaved by LiAlH<sub>4</sub>. This can lead to a substitution reaction whereby two chlorine atoms and a fluorinated phenyl are replaced with three hydride atoms. In the case of **8**, a slight yellow color appeared before the addition of water and the final product was isolated as a yellowish-white solid which gave a major <sup>119</sup>Sn-NMR resonance at -145 ppm (Figure 32).

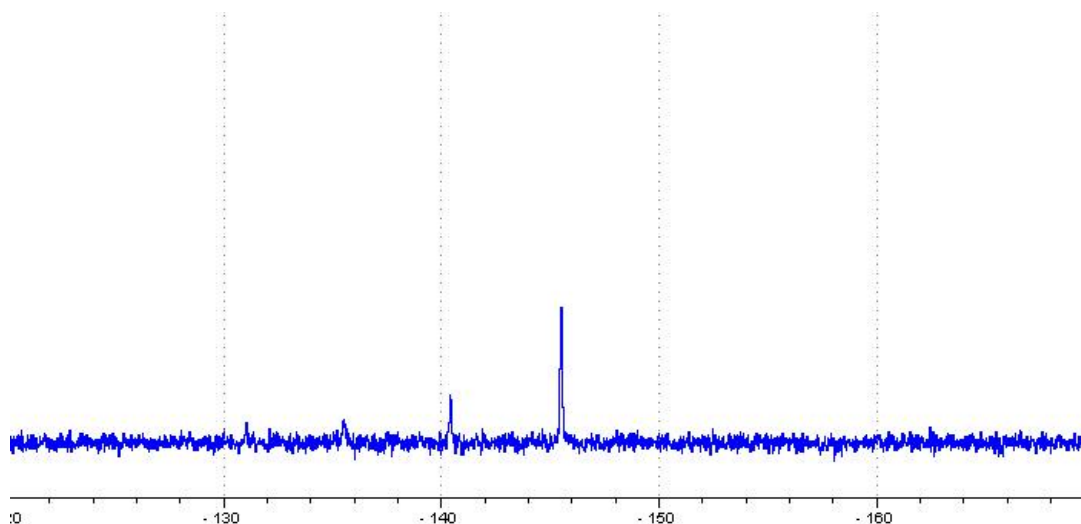


**Figure 32:**  $^{119}\text{Sn}$ -NMR spectrum for the tin hydride **8**

This shift is very similar to that of **9** and was therefore attributed to the tin trihydride. In the case of **4**, the fluorinated group is in the para position which Stern *et al.* suggest may lead to the formation of hexakis(4-trifluoromethylphenyl) ditin compound or other unwanted side products.<sup>60</sup> It may be possible to limit these side reactions by lowering the reaction temperature, varying the  $\text{LiAlH}_4$ /monomer ratio or reducing the reaction time. For both **8** and **9**, interpretation of the  $^1\text{H}$ -NMR and  $^{19}\text{F}$ -NMR spectra proved to be difficult due to the number of peaks, but the major peaks were attributed to the tin trihydrides. The polymerization behavior of these crude materials in the presence of metal catalyst was also used as an indirect indication that these crude materials were indeed tin trihydrides.

#### 3.4a Synthesis of Polymers using Wurtz Coupling

At the moment there are only a few examples of Wurtz coupling being used for the synthesis of high molecular weight polystannanes.<sup>31,35</sup> The two previous examples were carried out using a modified version of these reaction. This modification involves introduction of 15-crown-5-ether and lowering of the reaction time and temperature (Figure 33).<sup>35</sup>

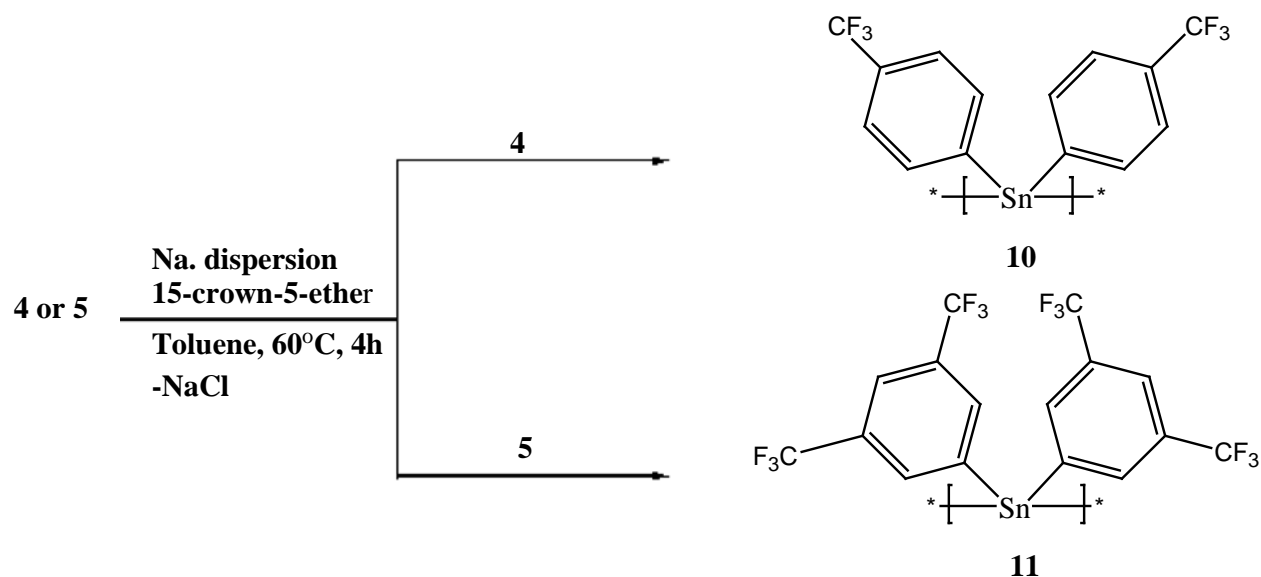


**Figure 33:** Schematic diagram for the Wurtz coupling of compounds **4** and **5**

In this research it was also observed that the best results were obtained when dispersions from purified sodium metal were used along with the modifications mentioned. Unpurified sodium resulted in the formation of a yellow solution with poor dispersion of the remaining sodium metal; this maybe due to oxidation at the sodium surface. Using the reaction condition outlined by Price *et al.*<sup>35</sup>, the monomer **4** and **5** were Wurtz coupled using reaction times of 4h to prevent the formation of cyclic oligomers. These compounds were isolated as a yellow tinged powder in the case of **10** and yellow waxy solid for **11**. Based on previous studies carried out in our group it was known that polystannanes were dark yellow to orange in color. A chromophoric shift for these fluorinated polystannanes was suspected based on their color which remained a pale yellow. The product was further purified by precipitation from cold hexanes (-48°C).

#### 3.4b Synthesis of polystannynes using dehydrocoupling

Polystannynes were prepared by dehydrocoupling using Kardstedt catalyst,  $(\text{Pt}_2\{[(\text{CH}_2=\text{CH})\text{Me}_2\text{Si}]_2\text{O}\}_3)$ , which was previously known to carry out hydrosilylation reactions. This catalyst was shown to be useful for

the dehydrocoupling of bifunctional Group 14 monomers by Baumgartner *et al.*<sup>72</sup> With the exception of the catalyst, all other conditions were similar to those used by Caseri *et al.*<sup>22,48</sup> in their synthesis of polystannanes. Their catalyst of choice  $\text{RhCl}(\text{PPh}_3)_3$ , was shown to be ineffective to monomers with bulky substituents that were directly attached to the tin atom and therefore a Pt catalyst was explored in this work (Figure 34).

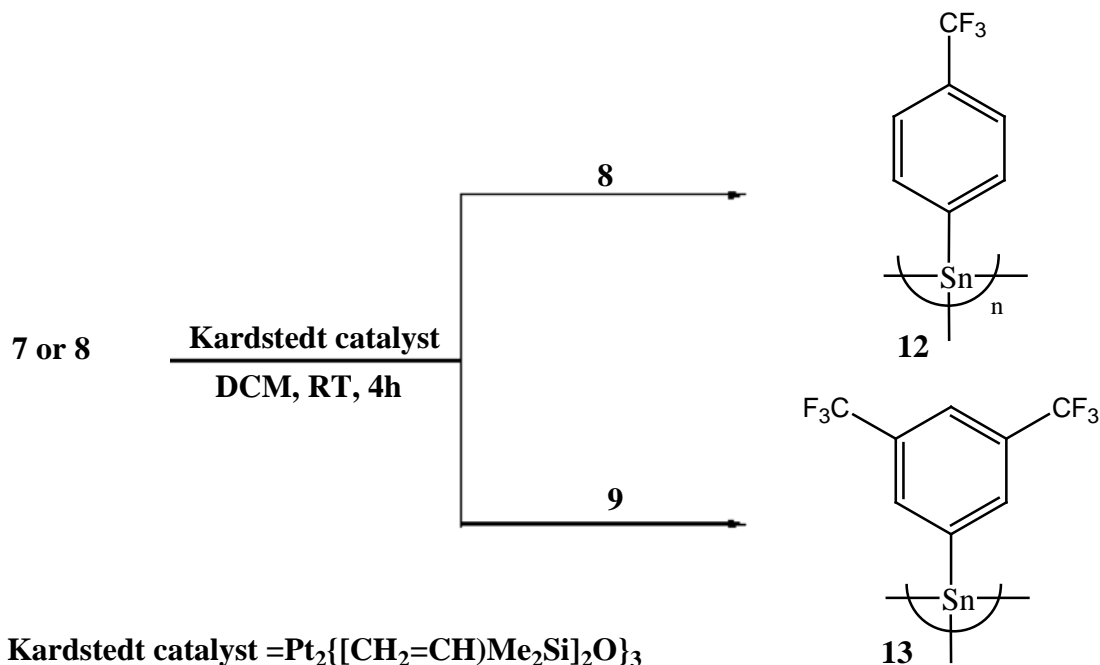


**Figure 34:** Schematic diagram for the dehydrocoupling of tin trihydride monomer **8** and **9** to yield polymers **12** and **13**

The polystannynes prepared from the dehydrocoupling of **8** and **9** had brownish-yellow colors that were consistent with other polystannanes from literature. The products synthesized by Wurtz coupling (**10**, **11**) and dehydrocoupling (**12** and **13**) were characterized using GPC, NMR, UV/VIS and elemental analysis.

### 3.5 UV/VIS Spectroscopy

Polystannanes are known to have UV-VIS absorbance values  $> 380 \text{ nm}$ .<sup>21</sup> As the data in Table 13 shows, the polystannanes synthesized by Wurtz coupling are drastically blue-shifted compared to other linear

polystannanes from the literature.<sup>24,41</sup> This is especially true for polystannanes with aryl substituents which are known to have absorbance values  $> 440$  nm.<sup>46,47</sup> Tilley suggested aryl substituted polystannanes were red-shifted compared to those with alkyl substituents due to their  $\sigma - \pi$  mixing.<sup>46,47</sup> In his review of polysilanes, Miller showed that the  $\pi^*$  of the aryl interacts with the antibonding MO of the polysilanes while the  $\pi$  orbitals interact with the bonding orbitals.<sup>51</sup> These two effects lead to a stabilization of the LUMO and destabilization of the HOMO resulting in a smaller band gap. This effect was amplified by the addition of  $\pi$  donating groups such as alkoxy moieties onto the phenyl substituent.<sup>47,50</sup> In this work, the opposite is observed since the  $\text{CF}_3$  groups are highly withdrawing and therefore are expected to lower the amount of  $\sigma - \pi$  mixing, resulting in blue-shift of the absorption wavelength. The introduction of the bulky fluorinated group may also affect the conformation of the polymer backbone. This would agree with previous literature where perfluoro groups have been shown to “harden” the backbone structure of molecules.<sup>56</sup> These conformational changes may result in a decrease of the orbital overlap required for maximum conjugation. It was previously shown that a planar zig-zag conformation is most ideal for lower band gap polystannanes.<sup>47,50</sup> The suspected reduction of the  $\sigma - \pi$  and the change in backbone conformation by the introduction of the fluorinated groups may have resulted in the drastic blue-shift observed in these linear polystannanes. On the other hand, investigation by UV/VIS spectroscopy showed that the polystanylenes obtained by dehydrocoupling are redshifted compared to those synthesized via Wurtz coupling and this is due to the difference between their structures (Table 13).

**Table 13:** UV/VIS data for polymers synthesized by Wurtz and Dehydrocoupling

Compound	Synthesis Method	UV/VIS data
<b>10</b>	Wurtz Coupling	332 nm
<b>11</b>	Wurtz Coupling	328 nm
<b>12</b>	Dehydrocoupling	350 nm
<b>13</b>	Dehydrocoupling	354 nm

The shape of the spectrum observed for the polystannynes synthesized by dehydrocoupling is indicative of network structure. Group 14 network polymers were first synthesized by the Bianconi group who prepared germanium and silicon 3-dimensional (3-D) polymers from their respective trichloride monomers.<sup>73</sup> Polystannynes analogs were later synthesized by the Okano group using electrochemistry.<sup>37</sup> Both groups observed that Group 14 network polymers showed significant tailing into the visible region. A similar behaviour is observed for the polystannynes synthesized using dehydrocoupling in this work (see Figures 36 and 37). These polymers show tailing into the visible region at wavelength > 700 nm. The red-shift compared to the linear polystannanes can be explained by the increased conjugation as a result of the additional Sn-Sn bonds present in these network structures (Figure 35).<sup>34</sup>

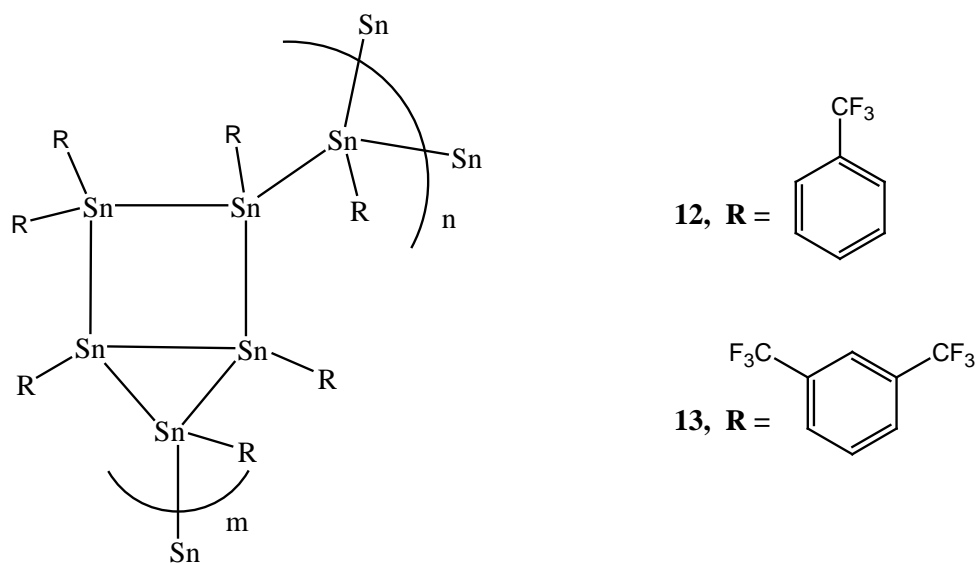


**Figure 35:** Structure for network polymers (**12** and **13**) synthesized in this work

As previously mentioned, an increase in the number of molecular orbital decreases the separation between the valence and conduction band causing a bathochromic shift. A similar finding was reported for polysilanes and polygermanes when moving from the linear to network 3-D polymers.<sup>34,73</sup> The isolation of

network polymer in this work is due to the polymerization of the tin trihydrides that were inadvertently synthesized. This resulted from the unexpected cleavage of a tin-aryl bond by the nucleophile  $\text{LiAlH}_4$ .

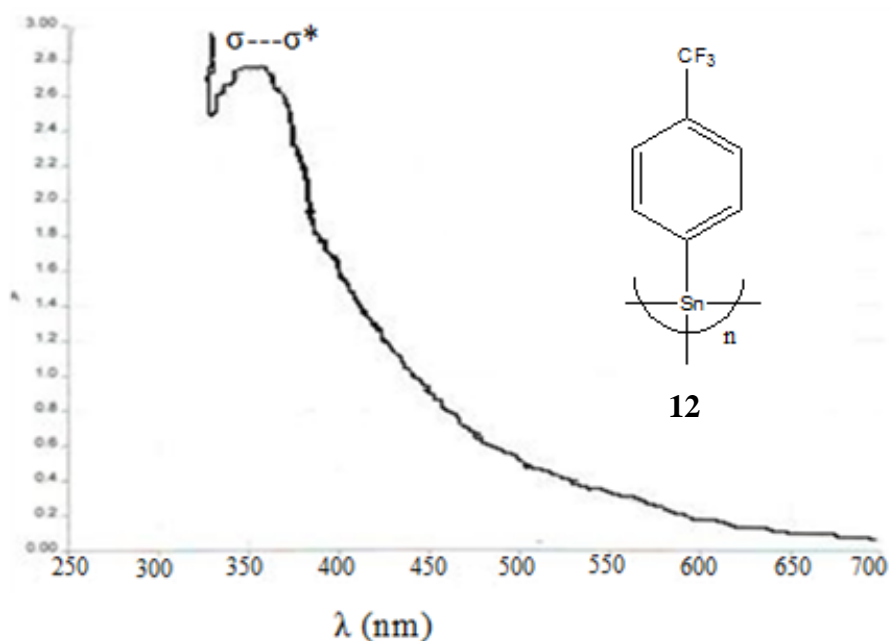


**Figure 36:** UV/VIS spectrum for **12** after dehydrocoupling

These polymers are expected to be more unstable than the linear counterparts due to 3-D tin-tin bond being longer than those in linear polystannanes.<sup>36</sup> Evidence of instability is shown when compound **13** was irradiated by successive scans in UV/VIS region (Figure 37). Initially, the spectrum shows a  $\lambda_{\text{max}}$  of 350 nm with the extensive tailing that is indicative of network polymers. However, there is an obvious change in the absorption spectrum for **13** when the sample was irradiated a second time with light in the UV-VIS region (Figure 37).

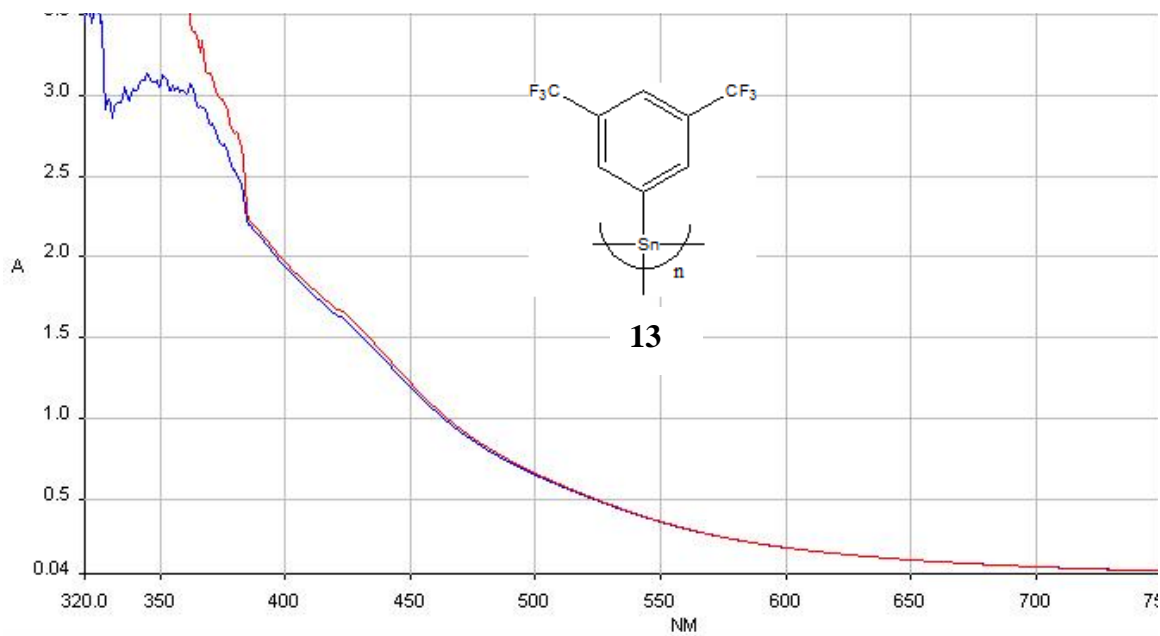


**Figure 37:** UV/VIS spectrum for **13** after 1 and 2 scans of UV/VIS

The UV-VIS scans are identical at wavelengths greater than  $\sim 375$  nm but deviate below this point. The most obvious change is the disappearance of the peak due to the  $\sigma-\sigma^*$  transition at 350 nm. Disappearance of this peak after only two scans suggests that the polymers, potentially due to the loss of linear segments from dihydride monomers, are being degraded at a fairly rapid rate when exposed to the light in the UV/VIS region. Similar studies were carried by Okano *et al.* who showed that these network polymers are more sensitive to light than their linear counterparts.<sup>37</sup>

### 3.6 GPC analysis

GPC was used in this work for the molecular weight determination of the polymers synthesized by both Wurtz and dehydrocoupling. A GPC equipped with a triple detector array was employed and calibrated against broad and narrow molecular weight polystyrene standards. The molecular weights obtained by triple detection provided absolute molecular weights which represents a first for polystannanes. While dehydrocoupling and electrochemical coupling have yielded only moderate molecular weight polymer in the  $\sim 10^4$  Da range,<sup>22,24,38,47</sup> Wurtz coupling was shown by Zou *et al.*<sup>31</sup> as a suitable method for the synthesis of

high molecular weight polystannanes ( $\sim 10^6$  Da range). Polystannanes are sensitive to both light and moisture and therefore samples for GPC were prepared using dried THF and wrapped in aluminum foil to shield from light. The molecular weight obtained by the Wurtz coupling in this work are between  $1.73 \times 10^4$ -  $2.92 \times 10^7$  Da for **10** which at the moment represents the highest reported molecular weight achieved for polystannane.<sup>68</sup> Compound **10** gave a polymodal GPC curve indicating polymers of varying molecular weights were synthesized. This also suggests that the problems synonymous with Wurtz coupling, although reduced, have not completely disappeared. In the case of **11**, molecular weight acquisition proved to be more challenging due to the instability of these polymers to the laser light source of the RI and light scattering detector. Initial calculated molecular weights suggest that these polymers had broken down into oligomers. An absolute molecular weight of  $1.47 \times 10^5$  Da was finally obtained for **11** using a UV absorbing molecule (UVA) that slowed the rate of depolymerization in the presence of radiation. Figure 38 shows the GPC chromatogram for compound **10** in the presence of a UV absorbing molecule. Previous work by Caseri *et al.* investigated the stability of polystannanes when irradiated with light in the presence of different light absorbers and radical scavengers.<sup>74</sup> The formation of oligostannanes by the chain scission of polystannanes was dramatically reduced in the presence of these absorbing molecules. The goal of the light absorbing molecule was to prevent depolymerisation of the polystannane without interfering with the molecular weight determination. Therefore a sample containing only the light absorbing molecule dissolved in THF was investigated by GPC. Based on the elution time of these molecules interference with the molecular weight determination was unlikely. A control was also employed in this method using  $[\text{nBu}_2\text{Sn}]_n$ . Molecular weight obtained for  $[\text{nBu}_2\text{Sn}]_n$  in the absence and presence of the UVA were comparable which is seen as a validation of this method. Therefore the molecular weights obtained using this method can be deemed accurate.

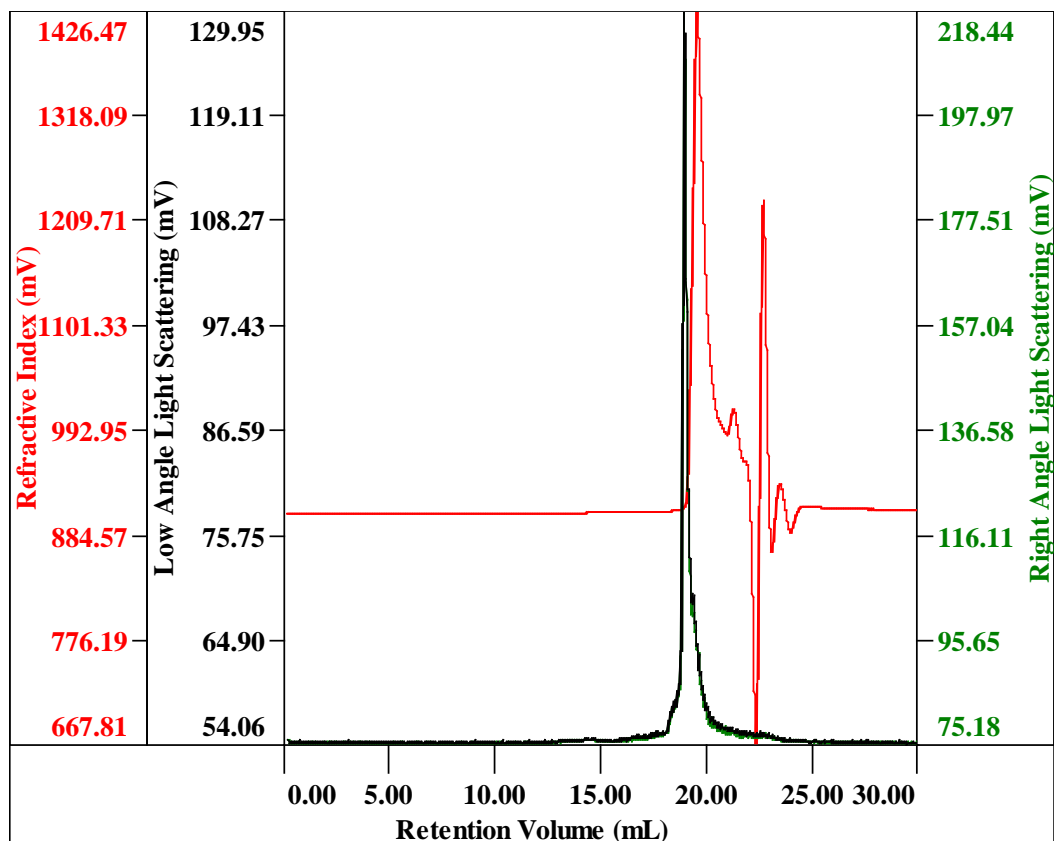


**Figure 38:** Chromatogram of refractive index (red), low angle light scattering (black) and right angle light scattering detectors after GPC analysis of **11**

The GPC chromatogram for compound **11** indicated that this polymer is monomodal. Isolation of a monomodal polystannane in the case of **11** highlights the superiority of the modified Wurtz coupling used in this work to earlier version of this reaction. Earlier versions of the Wurtz coupling reaction used for the polymerization of Group 14 compounds often resulted in low molecular weights with poor polydispersity. A similar method was attempted for polymer **12** and **13** but proved to be unsuccessful. The failure to analyze these network polymers using GPC even in the presence of a light absorbing molecule highlights their increased sensitivity towards light in THF. It may be necessary to investigate other UVA molecules in order to find more suitable candidates for these systems.

### 3.7 NMR Analysis

The polymers synthesized by the Wurtz coupling showed similar upfield  $^{119}\text{Sn}$ -NMR chemical shifts of -48 ppm for **11** and -53 ppm for **10** when compared to the dichloride monomers **4** and **5**.

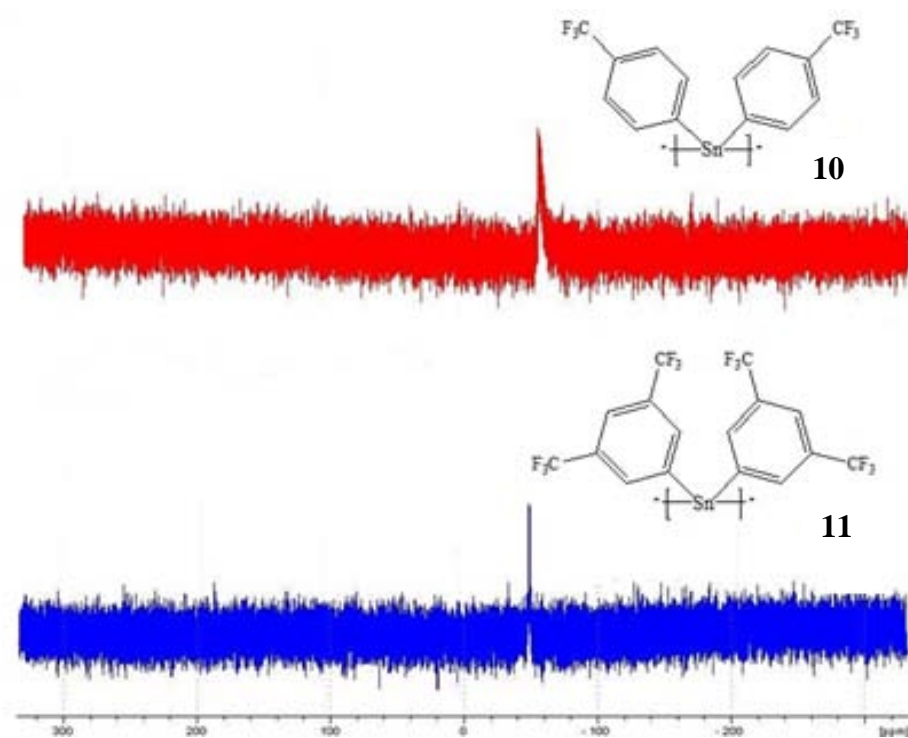


**Figure 39:** A plot of the  $^{119}\text{Sn}$ -NMR signals for polymers **10** and **11**

Such a shift was expected as two Sn-Cl bonds are replaced two Sn-Sn bonds. With the chlorine substituents being more electronegative, a deshielding of the tin nucleus and resultant downfield shift is expected. Figure 39 shows that the  $^{119}\text{Sn}$ -NMR chemical shifts for polymers **10** and **11** are very similar to each other. This follows a trend that saw the  $^{119}\text{Sn}$ -NMR chemical shifts of the corresponding tetraaryl and dichloride compounds also being similar. These  $^{119}\text{Sn}$ -NMR shifts are downfield from other poly(diaryl)stannanes. This is likely due to the presence of the  $\text{CF}_3$  groups and/or the geometric influence on the electronic structure by the bulky fluorinated substituents. Similar to chlorine, these groups are strongly electron withdrawing and can cause a deshielding of the tin nucleus. It is also possible that the geometric effect of the fluorinated ring

is influencing these  $^{119}\text{Sn}$ -NMR chemical resonance values. More investigation is required at this moment to prove this hypothesis.

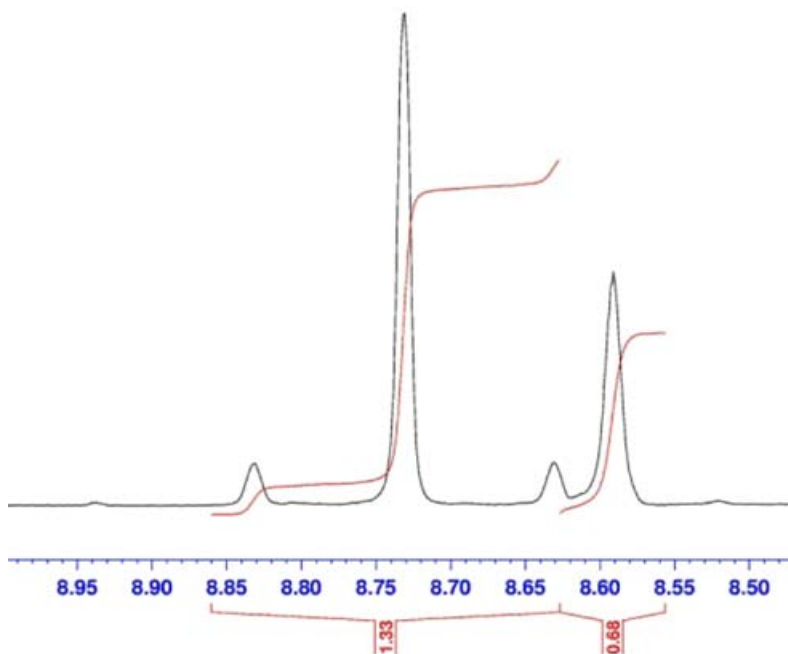


**Figure 40:**  $^1\text{H}$ -NMR spectrum for compound **11** after Wurtz coupling

The NMR spectra from Wurtz coupling are surprisingly clean considering that these reactions are known to give numerous unidentified products.<sup>32</sup> The  $^1\text{H}$ -NMR spectrum for compound **11** shows that only one product is isolated (Figure 40) which is also agrees with the monomodal curves observed in the GPC chromatogram for this compound. This also suggests that the problems associated with Wurtz couplings have been reduced in this work. The NMR spectra of the compounds prepared by dehydrocoupling compounds **8** and **9** showed evidence of more than one product but there are major products. The major peaks in the NMR spectra ( $^{19}\text{F}$ -NMR,  $^{119}\text{Sn}$ -NMR,  $^{13}\text{C}$ -NMR and  $^1\text{H}$ -NMR) were assigned to the network polymers (**12** and **13**) (Figure 41).

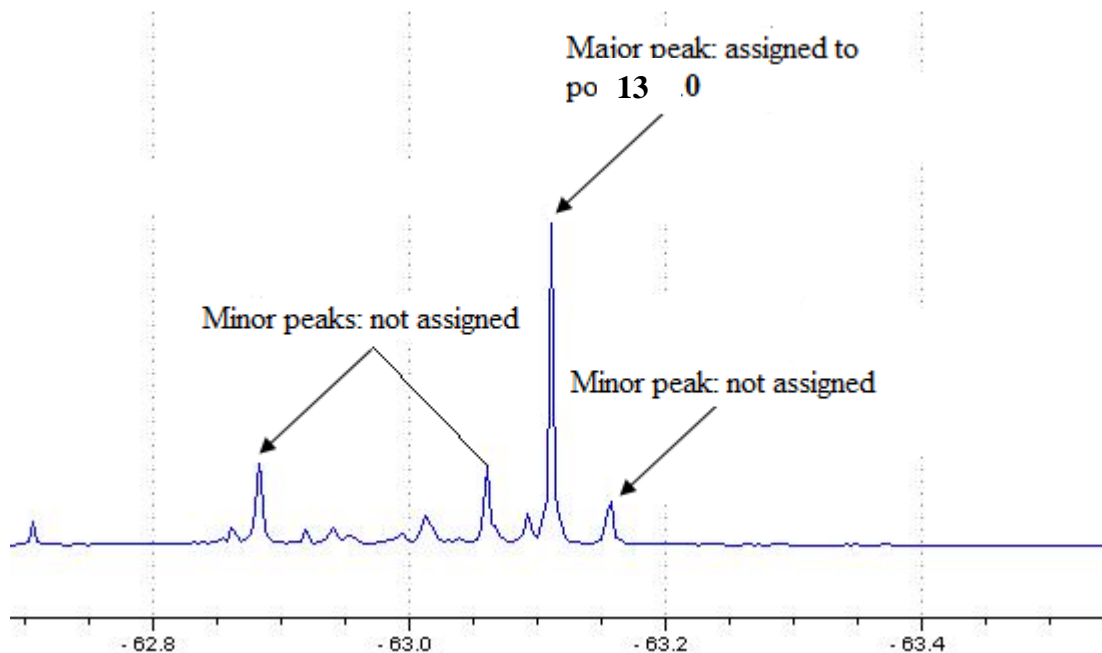


**Figure 41:**  $^{19}\text{F}$ -NMR spectrum after the dehydrocoupling of **9** to yield polymer **13**

There was a characteristic downfield shift in the  $^{119}\text{Sn}$ -NMR chemical shift from the hydrides to polymers in the case of both **12** and **13**. In the case of **12** there is downfield shift of approximately 10 ppm from the corresponding hydride **8**. Compound **13** on the other hand shows a downfield shift of approximately 15 ppm from the hydride **9**. This is in agreement with other polystannanes from literature synthesized by dehydrocoupling where the polymers are known to be 10-15 ppm downfield from the dihydride.<sup>22</sup>

## Conclusion

Polystannanes represent a new growing class of inorganic materials that are being exploited for their novel properties. The elements of the Group 14 have displayed electronic properties that have spurred interest in these compounds. The chemistry of polystannanes has grown dramatically in the last 20 years. Earlier investigation of polystannanes focused largely on synthetic methods that are ideal for the production of linear polymers such as temperature, length of reaction and catalyst of choice. This was followed by work that focused on the influence of the substituent on the band gap of polystannanes. More recent investigation have focused on the stability of these compounds under different conditions such temperature, solvent and the presence of dyes and/or radical scavengers. This work represents the first investigation of the stability of polystannanes by the incorporation of a stabilizing factor onto the backbone of the molecule.

The research indentified that the organolithium route is superior to the Grignard route in the preparation of fluorinated systems with respect to overall yield, length of reaction and ease purification. This work also demonstrated that the harsh conditions required for the preparation of tin dichlorides resulted in some decomposition of  $\text{SnCl}_4$ . Complete conversion to dichlorides were only successful when the loss of  $\text{SnCl}_4$  was compensated for. X-ray analysis of the crystals obtained by recrystallization from ether show dramatic deviation from tetrahedral geometry. It is believed that the electronic and structural influence of the bulky fluorinated phenyl ring is partially responsible for these deviations. Bent's rule was also used to explain these deviations whereby an increase in the *s* and *p*-character of some orbital resulted in the deviation of the bond angles from ideal tetrahedral geometry.

The polarization of the Sn-aryl bond due to the presence of the  $\text{CF}_3$  groups is blamed for the inadvertent synthesis of tin trihydride monomers by cleavage of the tin-aryl bond by  $\text{LiAlH}_4$ . The increase in reactivity of this bond suggests these compounds may warrant their own unique parameters instead of using those

based non-fluorinated systems. Dehydrocoupling of these trihydrides produced network polymers polystannanes with  $\lambda_{\text{max}}$  values of 350 and 354 nm that were blueshifted compared to poly(diaryl)stannanes. These were, however, red shifted when compared to their linear analogs prepared by Wurtz coupling as a result of the increase conjugation from the additional Sn-Sn bond. The  $\sigma$ — $\pi$  mixing normally observed in poly(diaryl)stannanes are absent or even reversed by the electron withdrawing nature of the  $\text{CF}_3$  groups. Molecular weight acquisition was investigated in the presence of a light absorbing molecule. However, GPC analysis for the network polymers was unsuccessful due to the increase instability as a result of the three dimensional tin-tin bonds. Stronger light absorbing molecules maybe required if absolute molecular weights are to be determined for these network polymers. These molecules are necessary to slow chain scission by the light source of the GPC detectors.

Polymerization of the dichlorides using Wurtz coupling proved once again to be suitable for the synthesis of high molecular weight polystannanes. The molecular weights obtained here are the highest reported for polystannanes, on the order of  $10^2$  larger than those obtained by other methods. It was initially believed that incorporation of fluorinated groups into the backbone of these polymers would increase their stability particularly to moisture. Surprisingly the perfluorinated polymers prepared are more sensitive than other non-fluorinated polystannanes. It is suspected that an increase in the electrophilicity of the tin centers is making these compounds more sensitive. GPC analysis was only made possible by the use of a UV absorbing dye. The GPC values obtained in this work represents the first absolute molecular weights reported for polystannanes. The polymer **11** gave a monomodal GPC curve shows that the problems normally associated with Wurtz coupling such as formation of cyclic oligomers is greatly reduced using the modified Wurtz reaction. However, the polymodal curve obtained for **10** suggested that these problems have not altogether disappeared. The polymers isolated from Wurtz coupling were blue shifted compared to poly(diaryl)stannanes from literature with absorption max values of 328 and 332 nm. This dramatic blue

shift is attributed to the electronic and conformational influence of the fluorinated groups. If higher  $\lambda_{\max}$  are to be obtained for fluorinated compound it is likely that methylene bridges will have to be used to minimize the effect of the fluorine on the central tin atom. In doing not only will these molecules absorb at a longer wavelength but they may also have the desired hydrophobic effect from the fluorinated groups.

It was anticipated that the incorporation of perfluoro groups into the backbone of polystannanes would increase their moisture stability. However, because of their severe sensitivity towards light no moisture stability tests were carried out on these polymers. The work done here was instrument in further characterizing the structural and electronic behaviour of fluorinated tin compounds. This work can therefore be used a stepping stone in the march towards light and moisture stable polystannanes.

### **Future Work**

At the moment there are no known polystannane polymers that are stable in the presence of moisture or light. In order for polystannanes to become useful materials, stabilizing their structure in presence of light and moisture is paramount. This research shows that there is adverse effect when the fluorinated groups are too close to the tin atom. Therefore future work could investigate substituent with fluorinated groups that are separated by methylene bridges. A series of these compounds will be synthesized by varying the length of the methylene bridge in order to find the optimum distance for the perfluoro groups. The optimum distance would be a distance that reduces the electronic effect of the perfluoro group on the tin center while still providing moisture stability. GPC investigations showed that it was possible to stabilize polystannanes in the presence of light by utilizing an external factor such as a UV absorbing (UVA) molecule. Ultimately, future work will also include insertion of UVA moieties into the backbone of polystannanes with hope that this will stabilize the chain to light. The final goal will be the combination of the light and moisture stabilizing work.

This will involve insertion of the groups that provides both moisture and light stabilization. This group will be chosen based on information gathered from the individual work done in moisture and light stabilization.

## REFERENCES

1. Chandrasekhar, V. Inorganic Polymers: Problems and Prospects. In *Inorganic and Organometallic Polymers*. Berlin: Springer Berlin Heidelberg, 2005. 1-26
2. Chandrasekhar, V. Organometallic Polymer. In *Inorganic and Organometallic Polymers*. Berlin: Springer Berlin Heidelberg, 2005. 296-335.
3. Setton, R., Bernier, P; Lefrant, S. *Carbon Molecules and Material*. Paris: CRC Press, 2002.
4. Sceri, E.R. *American Scientist* **2008**, 96, 52-59
5. Rezwan, K.; Chen, Q.Z.; Blaker, JJ.; Roberto, A. *Biomaterials* **2006**, 3413-3431.
6. Fox, H.W.; Zisman, W.A. *J. Colloid Interface Sci.* **1950**, 5(6), 514-531.
7. Spertus, M. *Packaging Materials*. Chicago: Highland Park, 1968.
8. Sorenson, W.R. *Encyclopedia of Materials Science and Engineering*, **1986**, 3810-3813.
9. Chiang, C.K.; Fincher, C.R.; Park, Y.W.; Heeger, A.J.; Shirakawa, H.; Louis, E.H.; Gau, S.C.; MacDiarmid, A.G. *Phy. Rev. Lett.*, **1977**, 39 (17), 1098-1101.
10. Roth, S. *Festkorperprobleme* **1984**, 24, 119-132.
11. Kotz, J.C.; Treichel, P.; Townsend, J.R. *Chemistry and chemical reactivity volume 2*. Belmont: Thomson Brooks/Cole. 2009
12. Leadley, David. Electronic band structure.  
<http://www2.warwick.ac.uk/fac/sci/physics/postgraduate/current/regs/mpags/ex5/bandstructure>  
(accessed June 19, 2010)
13. Pohl, H.A.; Gogos, C.G.; Cappas, C. *J. Polym. Sci., Part A: Polym. Chem.* **1963**, 1, 2207-2212.
14. Katon, J.E.; Wildi, B.S. *J. Chem. Phys.* **1964**, 40(10), 2977-2982.
15. MacDiarmid, A.G. *Mod. Phys. Lett.* **2001**, 73, 701-712.
16. Hornback, J.M. *Organic Chemistry 2<sup>ed</sup>*; Thomson Nelson: Toronto. 2006
17. Jones, R. *Electronic Devices and Circuits Engineering Sciences 154*. Harvard University  
[http://people.seas.harvard.edu/~jones/es154/lectures/lecture\\_2/energy\\_gap/energy\\_gap.html](http://people.seas.harvard.edu/~jones/es154/lectures/lecture_2/energy_gap/energy_gap.html).  
(Accessed 06 21, 2010)
18. Sondheimer, E.H. *Adv. Chem. Phys.* **2001**, 50(6), 499-537

19. Takeda, K.; Shiraishi, K. *Chemical Physical Letters* **1992**, 195 (2-3), 121-126.
20. Sita, L.; Terry, K.W.; Shibata, K. *J. Am. Chem. Soc.* **1995**, 117, 8049-8050.
21. Manners, Ian. *Synthetic Metal Containing Polymers*. London: Wiley-VCH, 2004.
22. Caseri, W.; Choffat, F.; Smith, P. *Adv. Mater.* **2008**, 2225-2229.
23. Jousseume. *Mikrochim. Acta*, **1992**, 190, 5-12.
24. Choffat, F.; Kaser, S.; Wolfer, P.; Schmid, D.; Mezzanga, R.; Smith, P.; & Caseri, W. *Macromolecules* **2007**, 40, 7878-7889.
25. Adams, S.; Drager, M. *Organomet. Chem.* **1988**, 11 (3), 151-180.
26. Adams, S.; Drager, M. *Organomet. Chem.* **1987**, 323 (1), 11-20.
27. Sita, L.R. *Organometallics* **1992**, 11(4), 1442-1444.
28. Weygand, C.; Hilgetag, G. *Preparative Organic Chemistry*; John Wiley & Sons, New York, **1972**. pp 903-910.
29. Billington, D. C. *Coupling Reactions Between sp<sup>3</sup> Carbon Centers, in Comprehensive Organic Synthesis*. Ed. Trost, B. M.; Fleming, I.; Chapter 2.1, Vol. 3; Pergamon Press, Oxford, 1991.
30. Kipping, F.S. *J. Amer. Chem. Soc.* **1924**, 2291-2297
31. Zou, W.; Yang, N., *Polym. Prepr. (Am. Chem. Soc. Div. Polym. Chem.)* **1992**, 33(2), 188
32. Jones, R.G.; Benfield, R.E.; Cragg, R.H.; Swain, A.C.; Webb, S.J. *Macromolecules* **1993**, 26, 4878-4887
33. Jones, R.G.; Holder, S.J. *Polym. Int.* **2006**, 55, 711-718.
34. Fujino, M; Isaka, H. *J. Chem. Soc. Chem. Comm.* **1989**, 466-467.
35. Devylder, N.; Hill, M.; Molloy, K.; Price, G. *J. Chem. Soc., Chem. Commun.* **1996**, 711.
36. Okano, M.; Matsumoto, N.; Arakawa, M.; Tsuruta, T.; Hamano, H. *Chem. Comm.* **1998**, 1799-1800.
37. Okano, M.; Watanabe, K., & Totsuka, S. *Chem. Comm.* **2003**, 71 (4), 257-259.
38. Azemi, T.; Yokoyama, Y. & Mochida, K. *J. Organomet. Chem.* **2005**, 1588-1593.
39. Nomura, R.; Endo, T. *Chem. Eur. J.* **1998**, 4 (9), 1605-16010.

40. Mochida, K.; Hayakawa, M.; Tsuchikawa, T.; Yokoyama, Y.; Wakasa, M.; Hayashi, H. *Chem. Lett.* **1998**, 91-92.
41. Imori, T.; Tilley, T.D. *J. Chem. Soc. Chem. Comm.* **1993**, 1607-1609
42. Aitken, C. H. . *J. Organomet. Chem.* **1985**, C11, 279.
43. Aitken, C.H.; Harrod, J.F.; Malek, A.; Samuel, E. . *J. Organomet. Chem.* **1988**, 349(3), 285-291
44. Rosenberg, L. *Exploiting Catalytic Dehydrogenative Coupling in the Synthesis and Study of Polysilane*. Abd-El-Aziz, A.S. *Macromolecule Symposia: Metal-and Metalloid- Containing Macromolecules*. Ottawa: Wiley-VCH, **2003**. 347-353
45. Thompson, S.M. *Inorg. Chim. Acta*, **2004**, 357, 1959-1964
46. Lu, V.; Tilley, T.D. *Macromolecules* **1996**, 29, 5763, 5764.
47. Lu, V.Y.; Tilley, T.D. *Macromolecules* **2000**, 33, 2403-2412.
48. Choffat, F.; Smith, P.; Caseri, W. *J. Mater. Chem.* **2005**, 15, 1789-1792.
49. Osborn, J.A.; Jardine, F.H.; Young, J.F.; Wilkinson, G. *J. Chem. Soc.* **1966**, 1711-1732.
50. Miller, R.D.; Michl, J. *Chem. Rev.* **1989**, 89, 1359-1410.
51. Takeda, K.; Shiraishi, K. *Phys. Rev. B: Condens. Matter* **1989**, 11 028-11 037.
52. Manner, I. *Angew. Chem. Int. Ed.* **1996**, 35 (15), 1602-1621
53. de Haas, M.P.; Choffat, F.; Caseri, W.; Smith, P.; Warman, J.M. *J. Adv. Mater.* **2006**, 18, 44-47.
54. Imori, T.; Lu, V.; Cai, H.; Tilley, T.D. *J. Am. Chem. Soc.* **1995**, 117 (40), 9931-9940.
55. O'Hagan, D. *Chem. Soc. Rev.* **2008**, 37, 308-319.
56. Lemal, D.M. *J. Org. Chem.* **2004**, 69, 1-11.
57. Biffinger, J.C., Kim, H.W.; DiMagno, S.G. *Chembiochem* **2004**, 5, 622-627.
58. Imae, T. *Adv. Colloid Interface Sci.* **2003**, 8, 307-314.
59. King, B.; Eckert, H.; Denny, D.; & Herber, R.H. *Inorg. Chim. Acta* **1986**, 122,45-53.
60. Stern, A.; Becker, E.I. *J. Org. Chem.* **1964**, 29 (11), 3221-3225.
61. Zanger, M. *Organic Magnetic Resonance* **1972**, 4, 1-25.

62. Chieh, P.C.; Trotter, J. *J. Chem. Soc.* **1970**, 911-914.
63. Foucher, D.; Miles, D.; Lough, A.J. *Acta Crystallogr. Sect. E.* **2009**, E65, m704
64. Wharf, I.; Belanger-Gariepy, F. *Acta Crystallogr. Sect. E.* **2003**, E59, m661-m663
65. Wharf, I.; Lebius, A.M. *Acta Crystallogr. Sect. E.* **2003**, E59, m794-m796.
66. Young, D.J.; Manuaba, P.; Healy, P.C.; & Tiekink, E.R.T. *Acta Crystallogr. Sect. E.* **2005**, E61, m956-m957.
67. Miles, D.; Burrow, T.; Lough, A.; Foucher, D. *J. Inorg. Organomet. Polym.* 2010 (in press)
68. Green, P.T.; Bryan, R.F. *Inorganic, Physical, Theoretical* **1971**, 2549-2554.
69. Bregadze, V.I. & Okhlobystin. *Izvestiya Akademii Nauk SSSR, Seriya Khimicheskaya* **1967**, 9, 2084-2086.
70. Holmes, J.M.; Peacock, R.D.; Tatlow, J.C. *Proc. Chem. Soc.* **1963**, 108
71. Baumgarter, T.; Wilk, W. *Org. Lett.* **2006**, 8 (3), 503-506.
72. Szymanski, W.J.; Visscher, G.T.; & Bianconi, P.A. *Macromolecules* **1993**, 26, 869-871.
73. Choffat, F., Wolfer, P., & Caseri, W. *Macromol. Matl and Eng.* **2010**, 210-221.
74. Rohwer, H; Dillen, J. *Inorg. Chem.* **2002**, 41, 4167-4172
75. R. D. Chambers; T. Chivers, *J. Chem. Soc.* **1964**, 4782

## APPENDICES

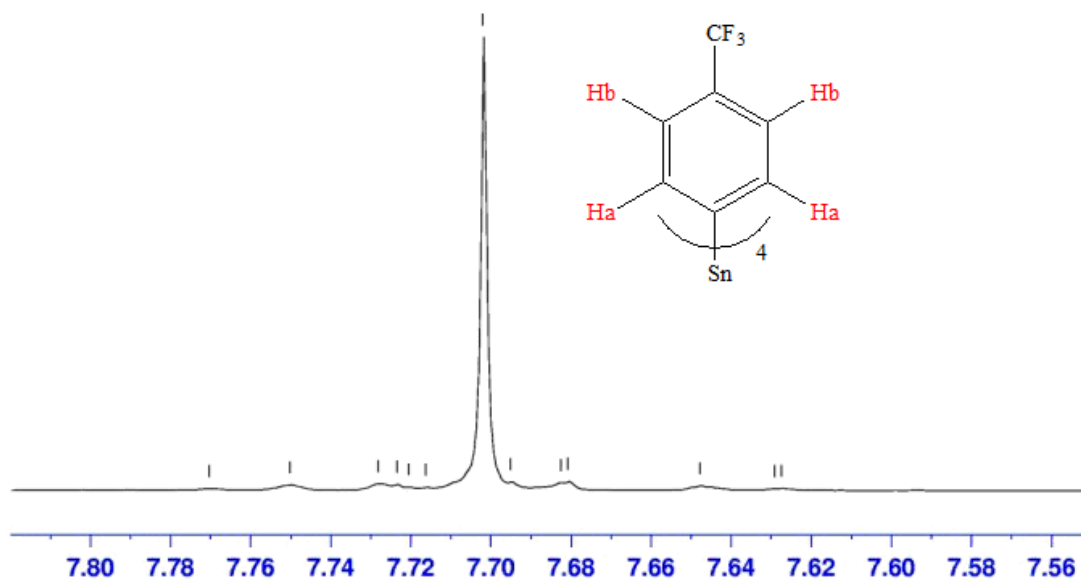


Figure 42:  $^1\text{H}$ -NMR spectrum of compound 1 ( $\text{CDCl}_3$ , 400MHz)

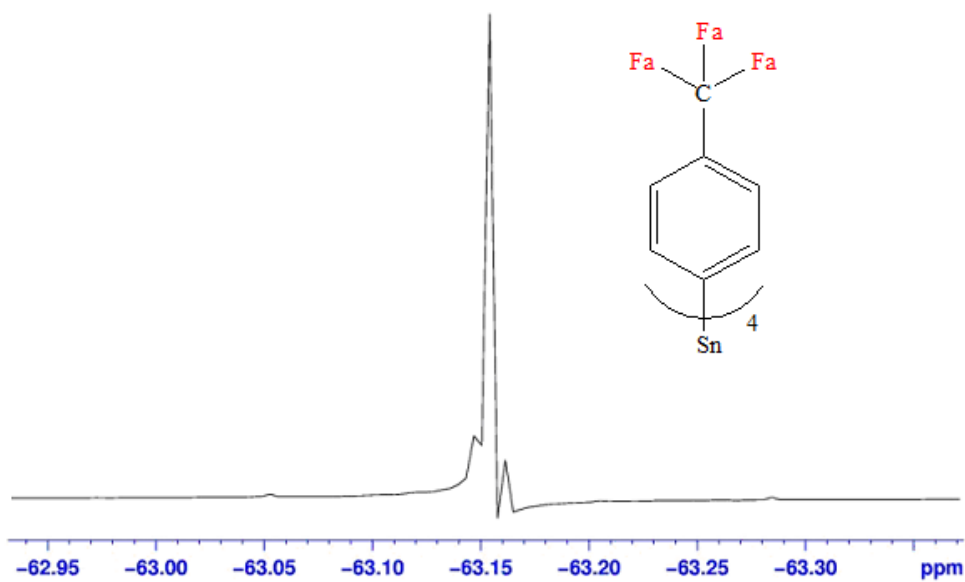


Figure 43:  $^{19}\text{F}$ -NMR spectrum for compound 1 ( $\text{CDCl}_3$ , 376MHz)

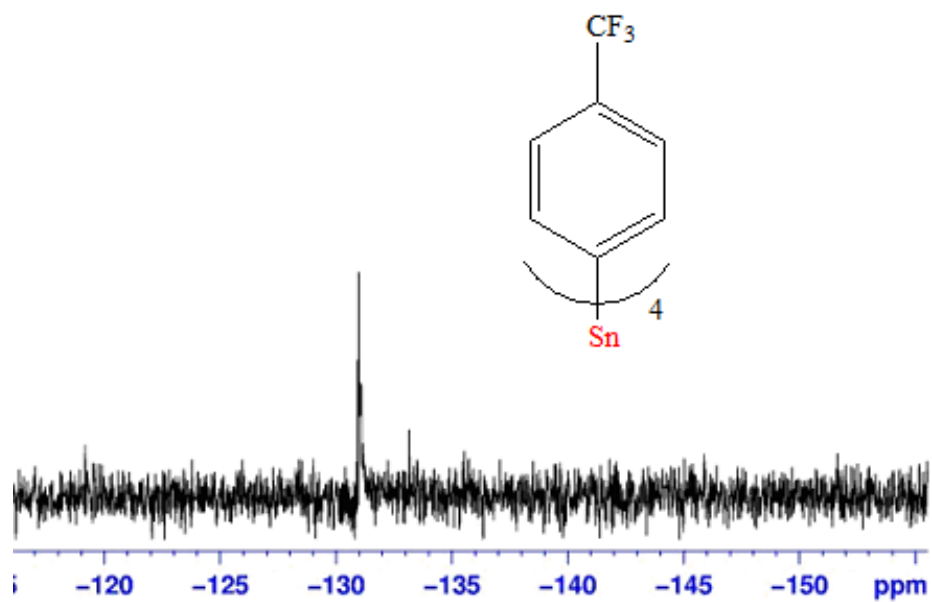


Figure 44:  $^{119}\text{Sn}$ -NMR spectrum of compound 1 ( $\text{CDCl}_3$ , 149MHz)

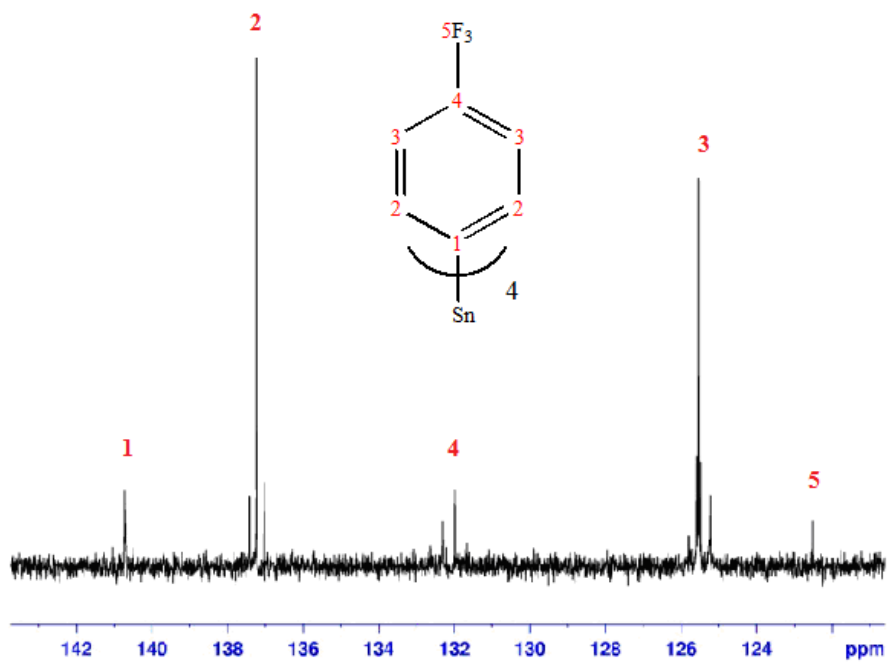


Figure 45:  $^{13}\text{C}$ -NMR spectrum for compound 1 ( $\text{CDCl}_3$ , 100MHz)

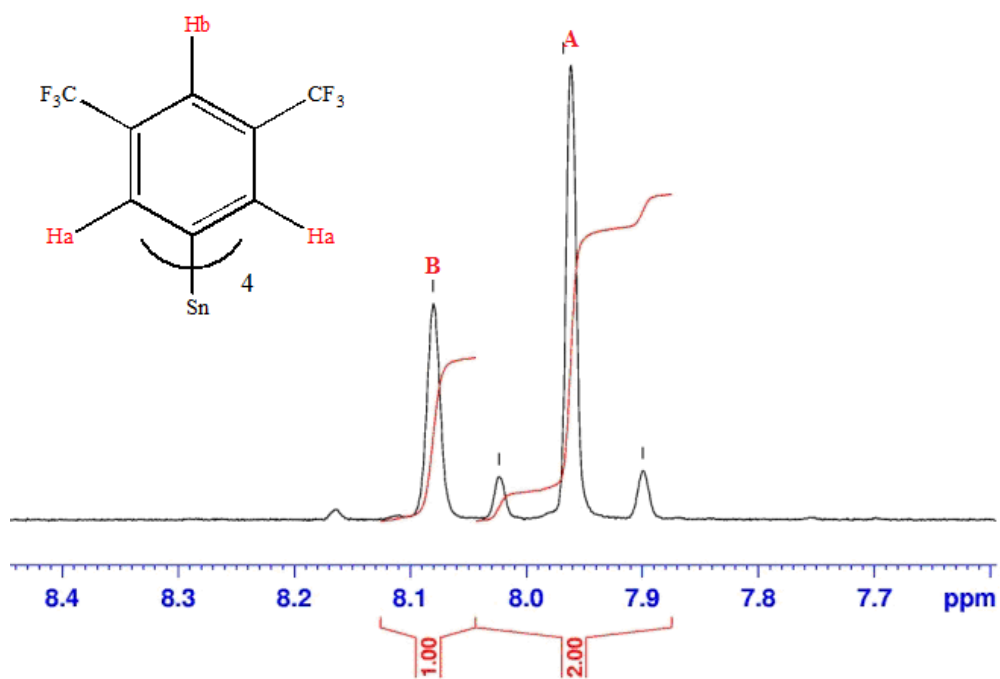


Figure 46:  $^1\text{H-NMR}$  spectrum for 2 ( $\text{CDCl}_3$ , 400MHz)

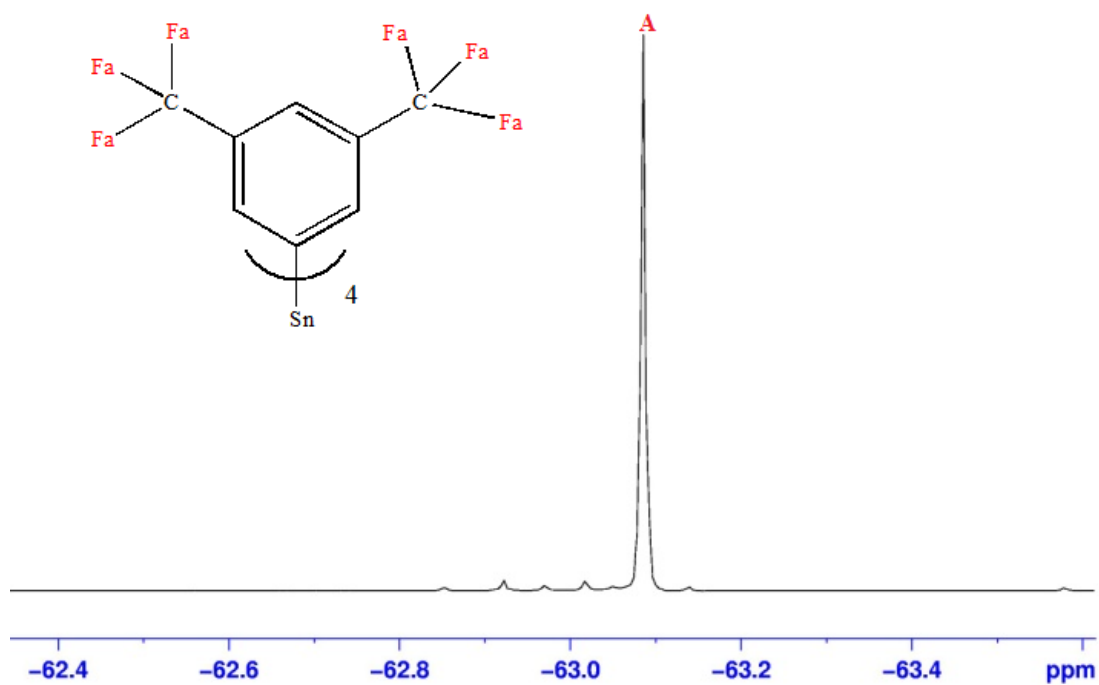


Figure 47:  $^{19}\text{F-NMR}$  spectrum for compound 2 ( $\text{CDCl}_3$ , 376MHz)

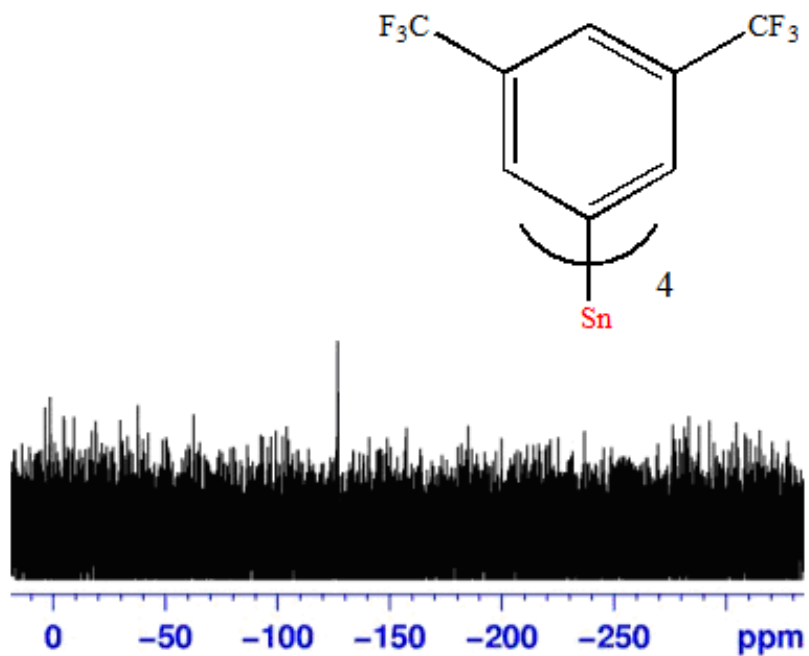


Figure 48:  $^{119}\text{Sn}$ -NMR spectrum of 2 in ( $\text{CDCl}_3$ , 149MHz)

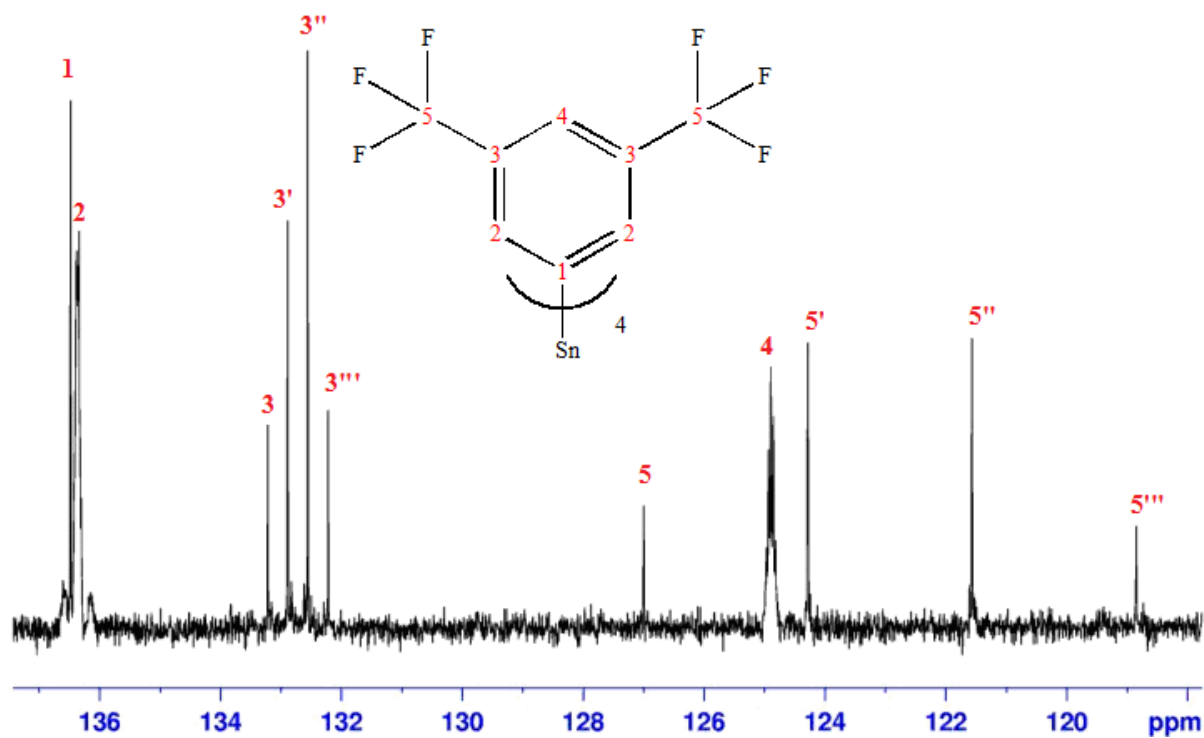


Figure 49:  $^{13}\text{C}$ -NMR spectrum for 2 ( $\text{CDCl}_3$  100MHz)

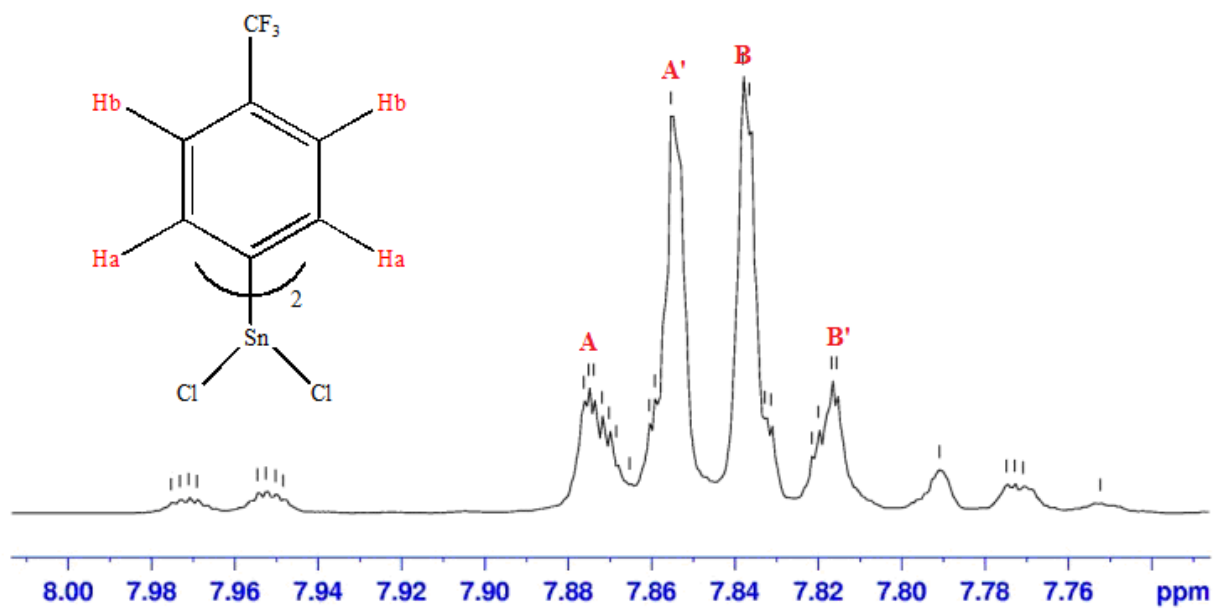


Figure 50:  $^1\text{H}$ -NMR spectrum for compound 4 ( $\text{CDCl}_3$ , 400MHz)

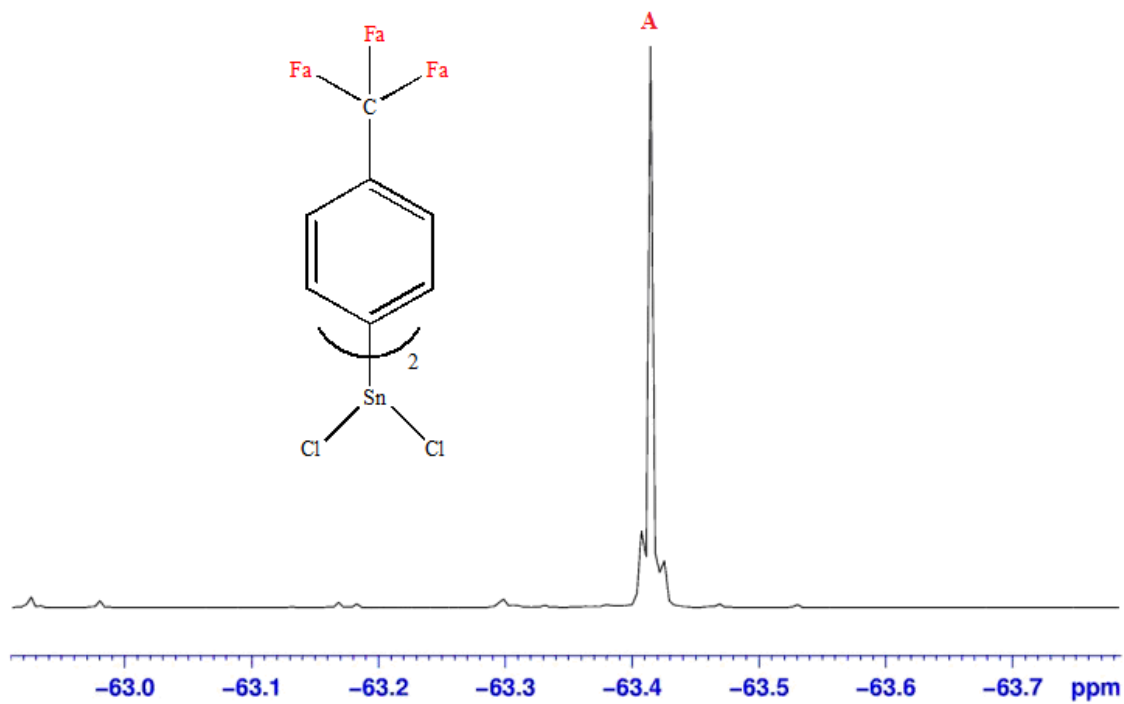


Figure 51:  $^{19}\text{F}$ -NMR spectrum for compound 4 ( $\text{CDCl}_3$ , 376 MHz)

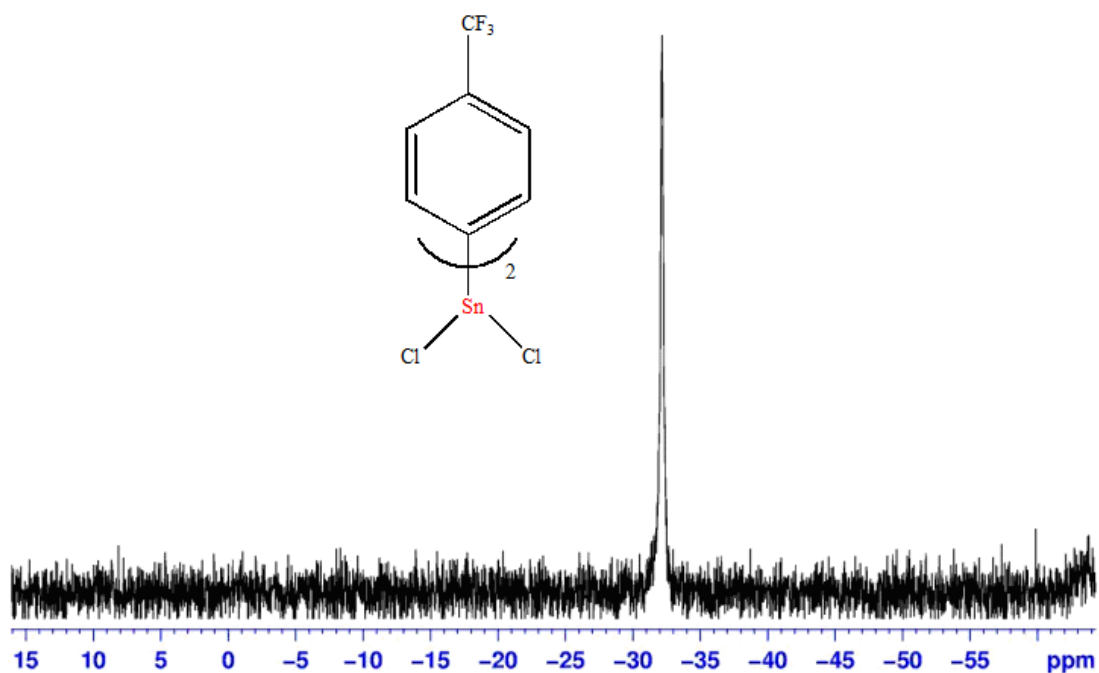


Figure 52:  $^{119}\text{Sn}$ -NMR spectrum for compound 4 ( $\text{CDCl}_3$ , 149MHz)

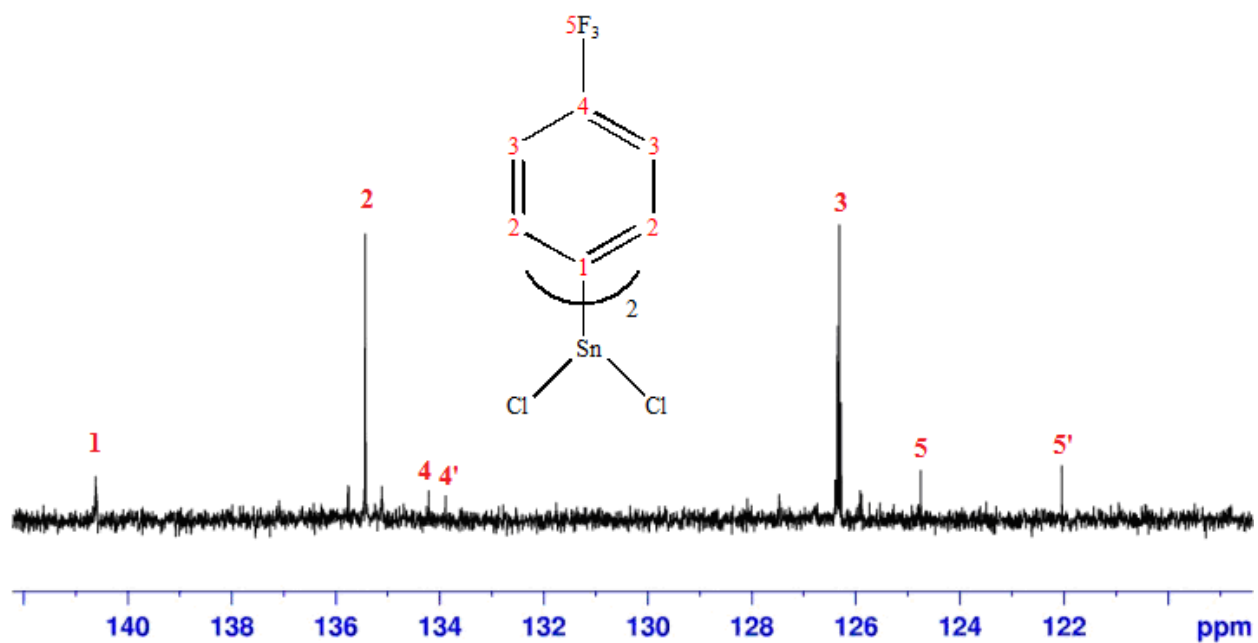


Figure 53:  $^{13}\text{C}$ -NMR spectrum for compound 4 ( $\text{CDCl}_3$ , 100 MHz)

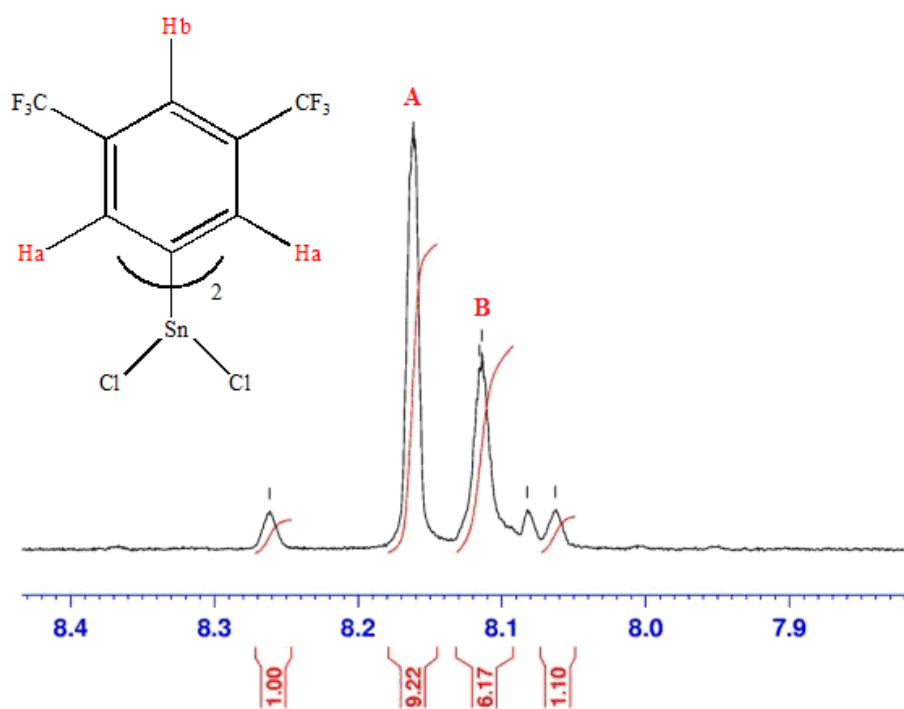


Figure 54:  $^1\text{H-NMR}$  spectrum for compound 5 ( $\text{CDCl}_3$ , 400MHz)

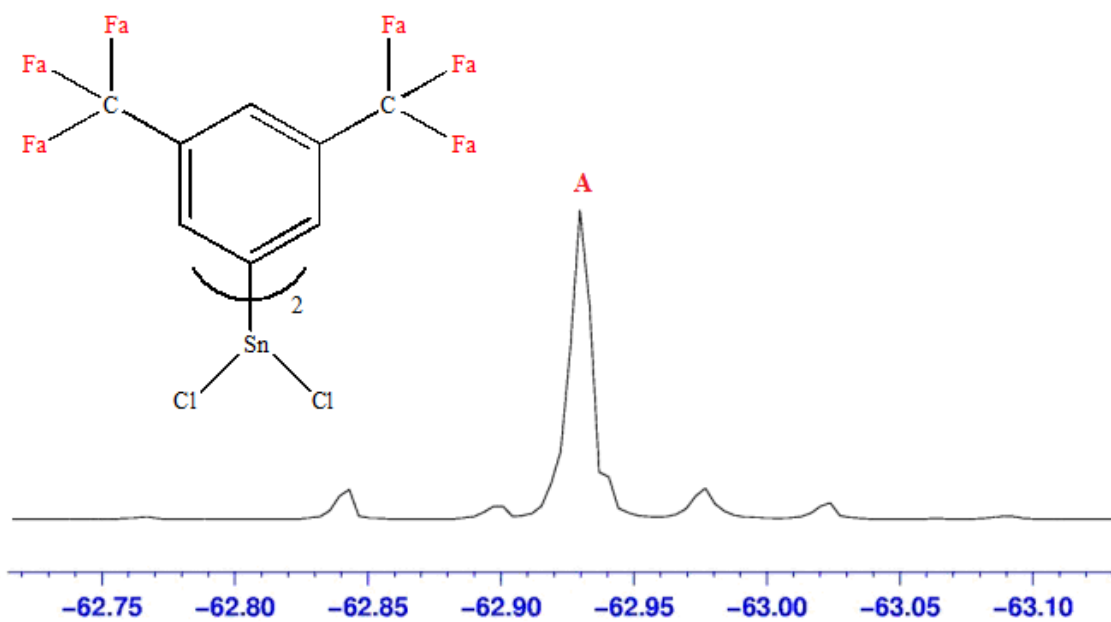


Figure 55:  $^{19}\text{F-NMR}$  spectrum for compound 5 ( $\text{CDCl}_3$ , 376MHz)

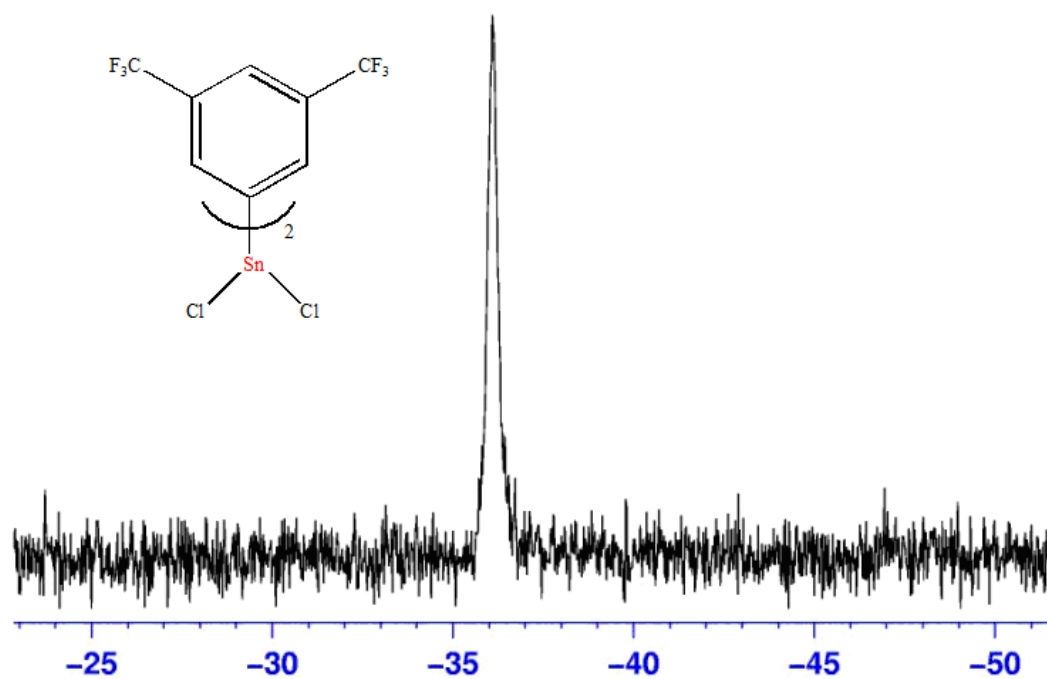


Figure 56:  $^{119}\text{Sn}$ -NMR spectrum for compound 5 ( $\text{CDCl}_3$ , 149MHz)

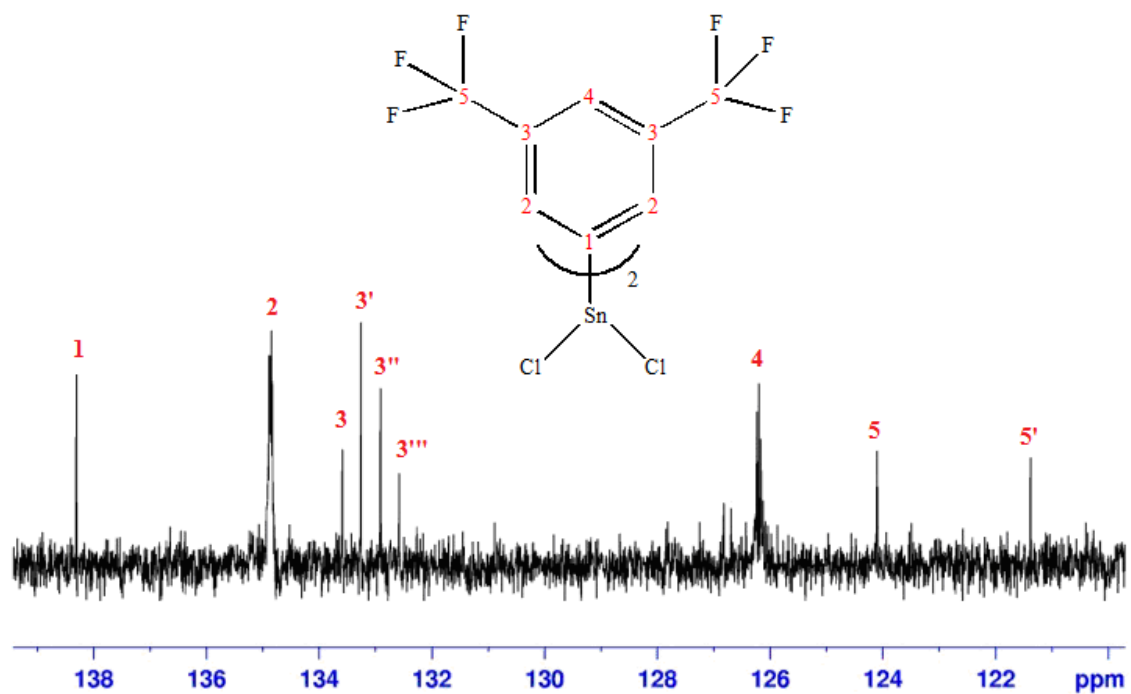


Figure 57:  $^{13}\text{C}$ -NMR spectrum for compound 5 ( $\text{CDCl}_3$ , 100MHz)

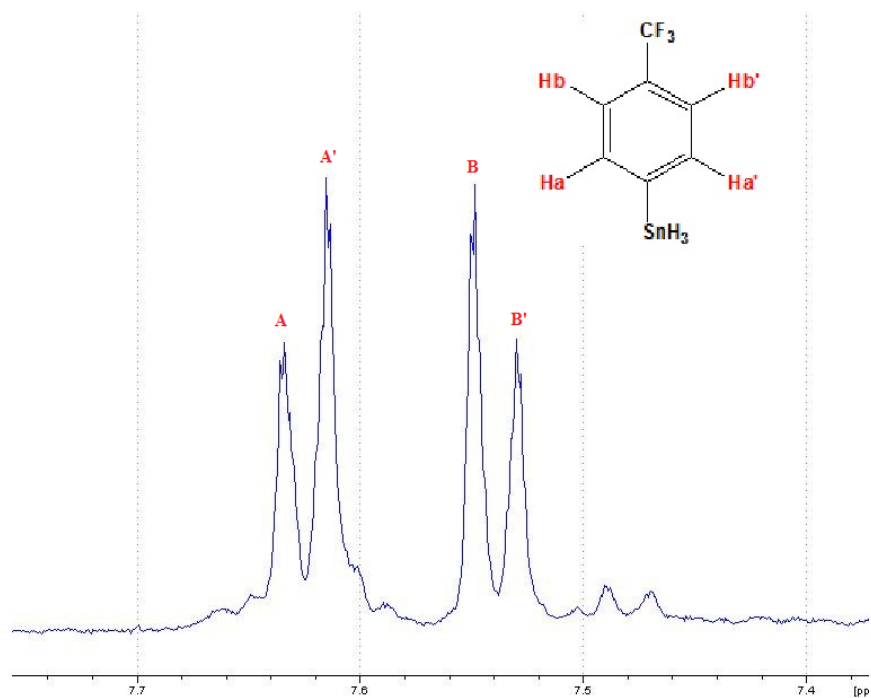


Figure 58:  $^1\text{H}$ -NMR spectrum for compound 8 ( $\text{CDCl}_3$ , 400 MHz)

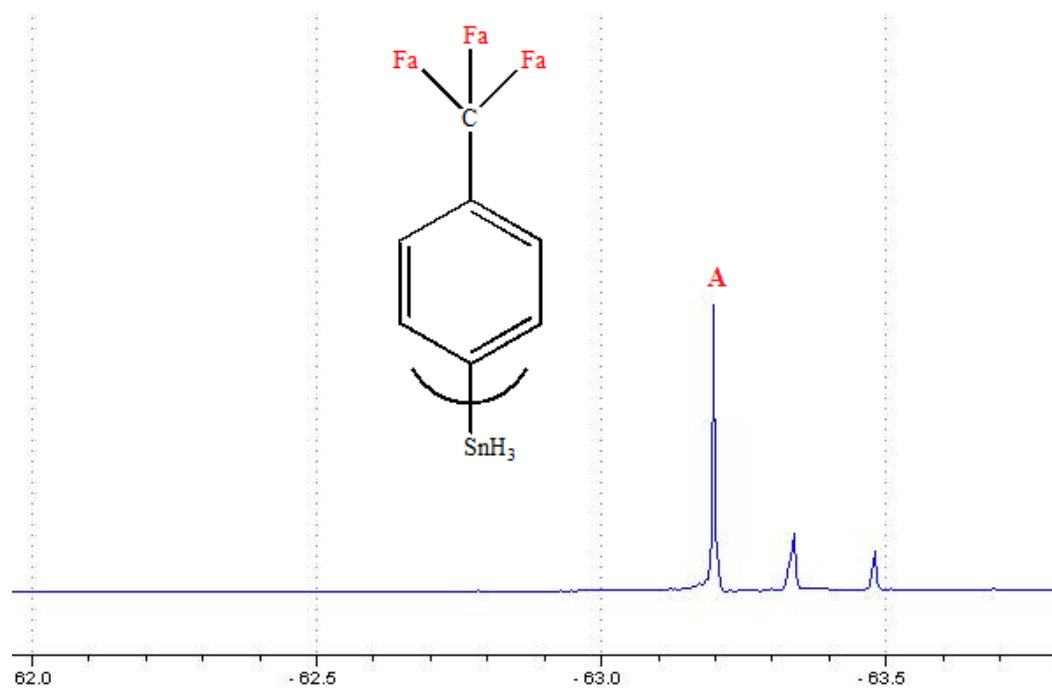


Figure 59:  $^{19}\text{F}$ -NMR spectrum for compound 8 ( $\text{CDCl}_3$ , 376 MHz)

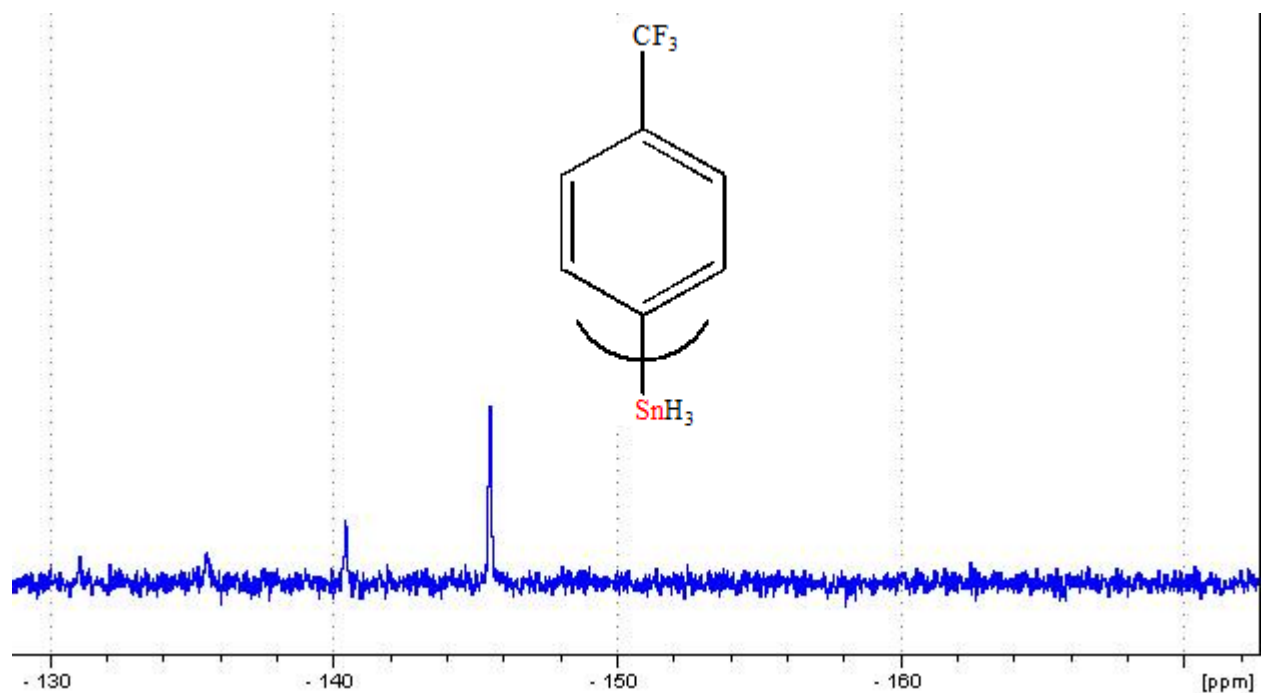


Figure 60:  $^{119}\text{Sn}$ -NMR spectrum for compound 8 ( $\text{CDCl}_3$ , 149 MHz)

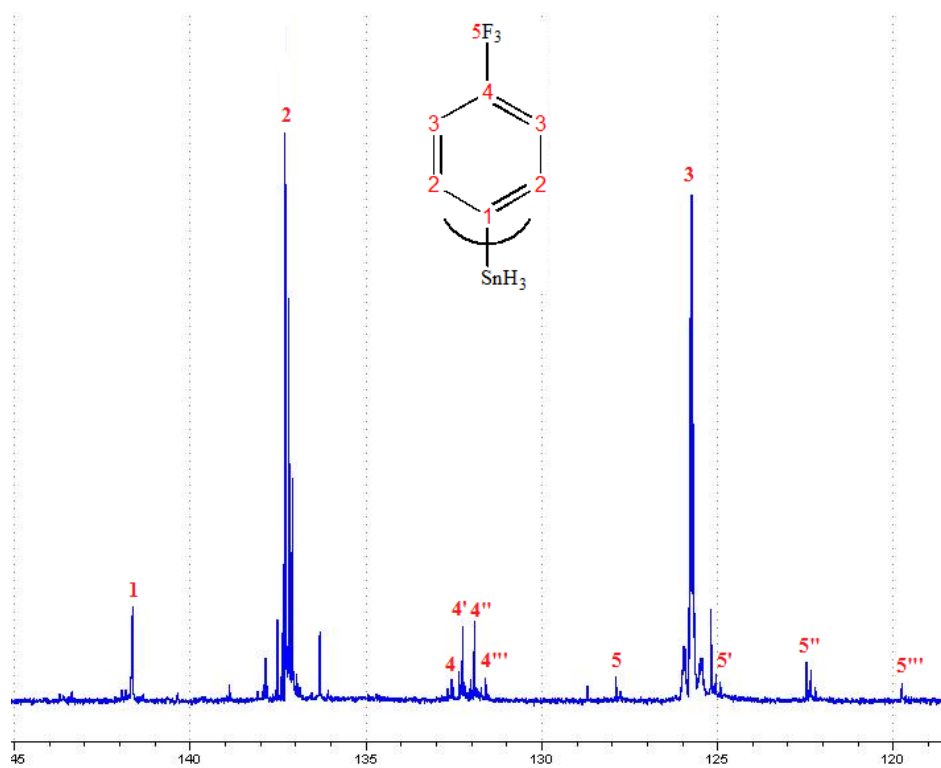


Figure 61:  $^{13}\text{C}$ -NMR spectrum for compound 8 ( $\text{CDCl}_3$ , 100 MHz)

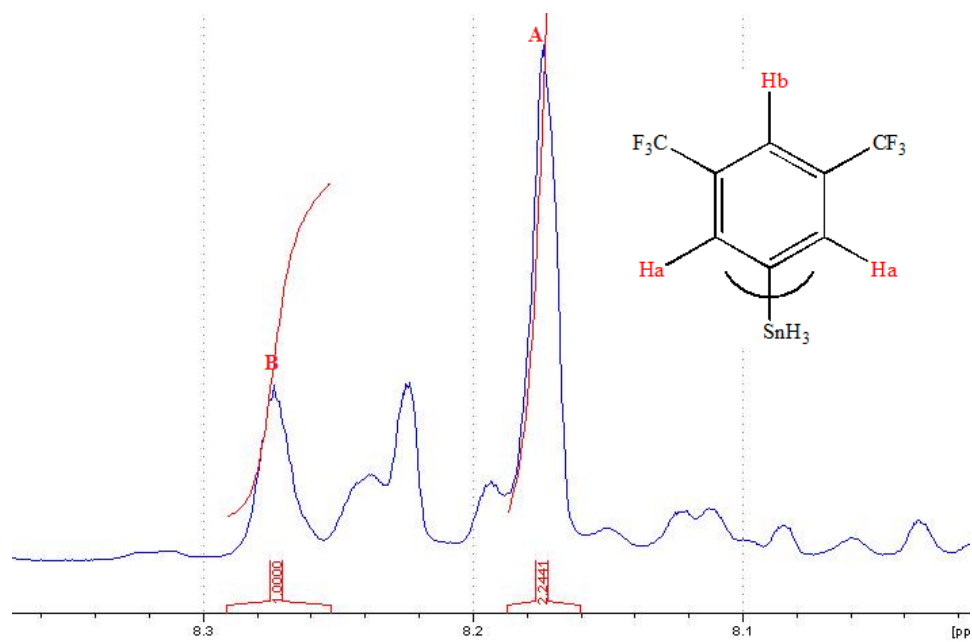


Figure 62:  $^1\text{H-NMR}$  spectrum for compound 9 ( $\text{CDCl}_3$ , 400 MHz)

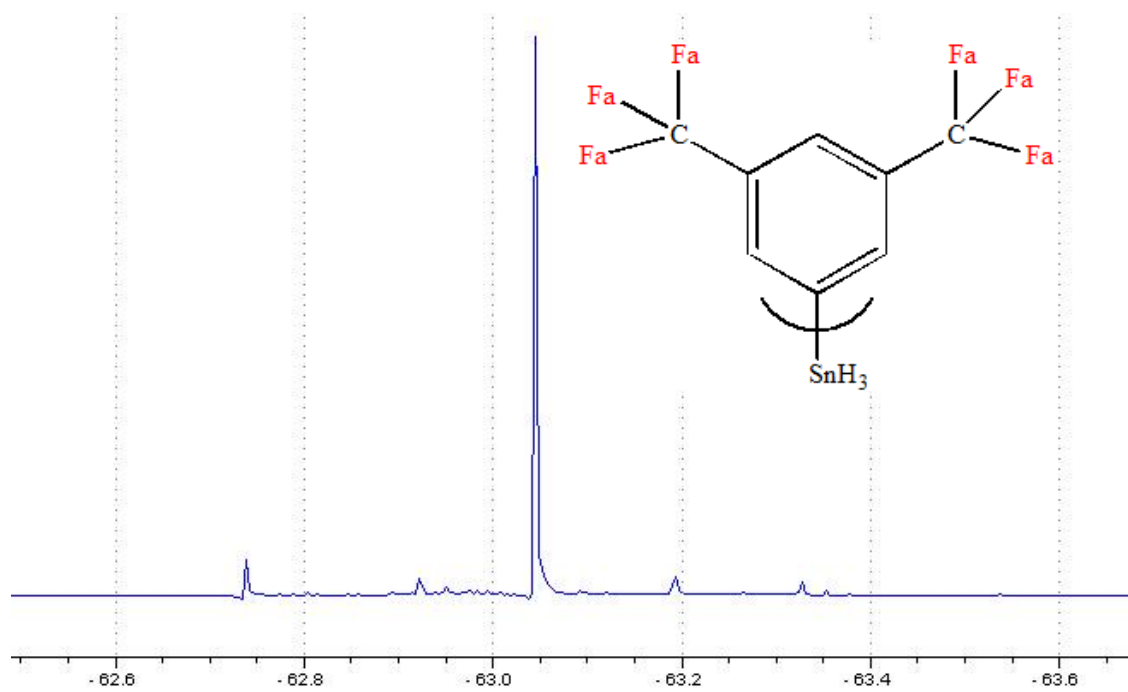


Figure 63:  $^{19}\text{F-NMR}$  spectrum for compound 9 ( $\text{CDCl}_3$ , 376 MHz)

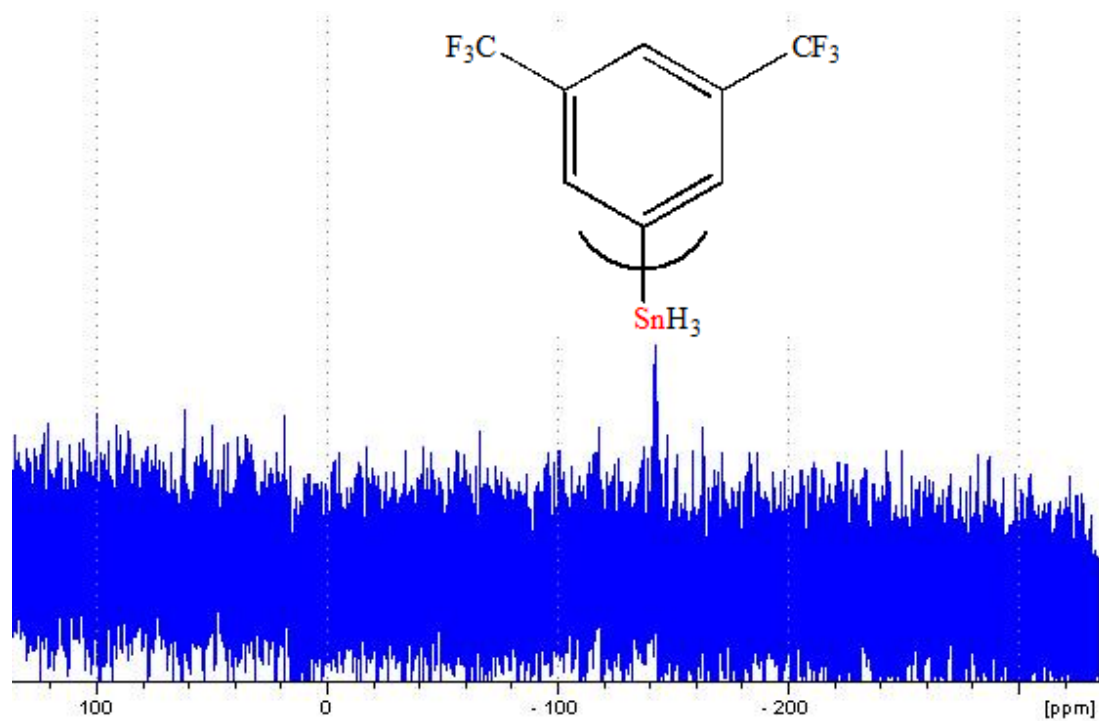


Figure 64:  $^{119}\text{Sn}$ -NMR spectrum for compound 9 ( $\text{CDCl}_3$ , 149 MHz)

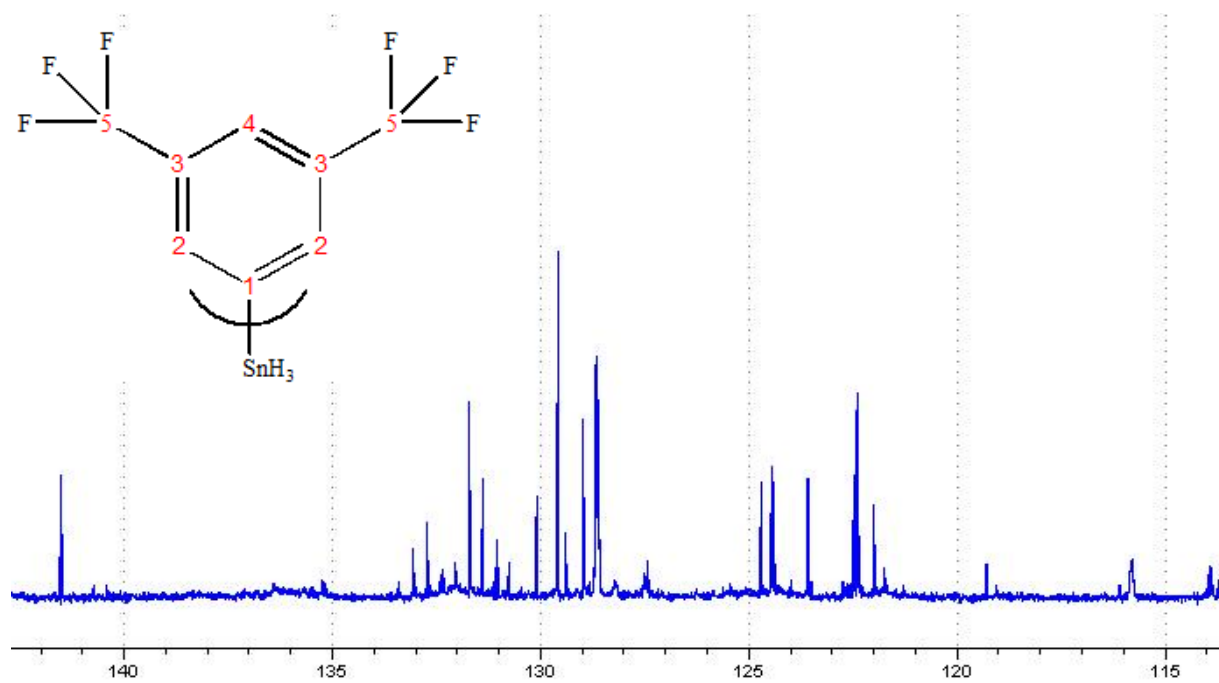


Figure 65:  $^{13}\text{C}$ -NMR spectrum for compound 9 ( $\text{CDCl}_3$ , 100 MHz)

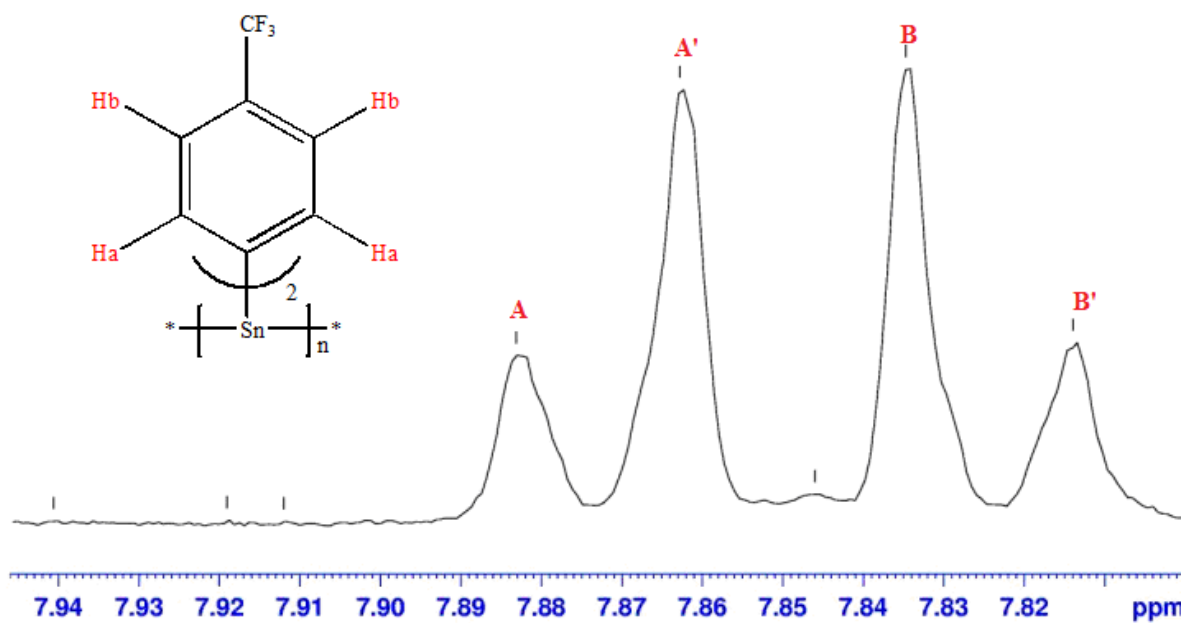


Figure 66:  $^1\text{H-NMR}$  spectrum for compound 10 ( $\text{CDCl}_3$ , 400MHz)

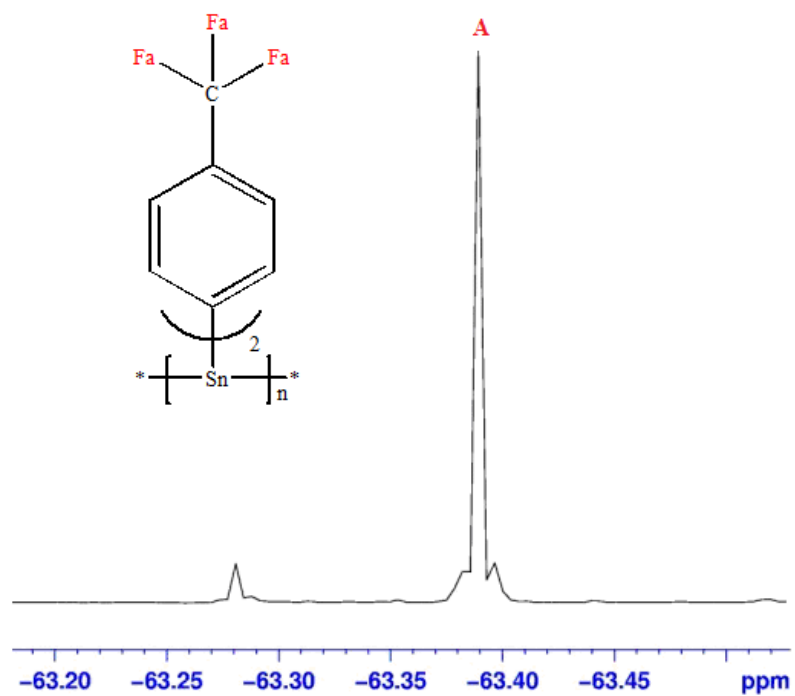


Figure 67:  $^{19}\text{F-NMR}$  spectrum for compound 10 ( $\text{CDCl}_3$ , 376MHz)

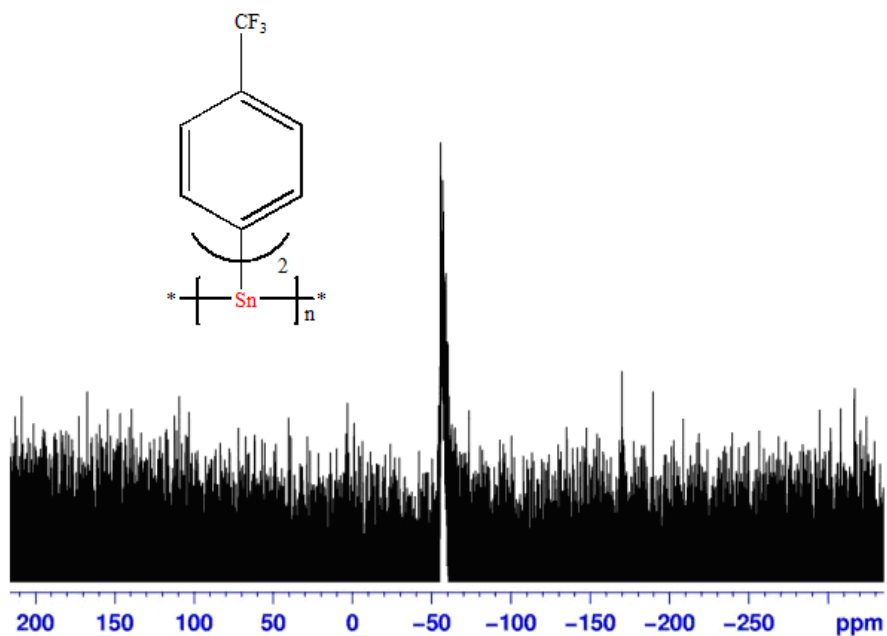


Figure 68:  $^{119}\text{Sn}$ -NMR for compound 10 ( $\text{CDCl}_3$ , 149MHz)

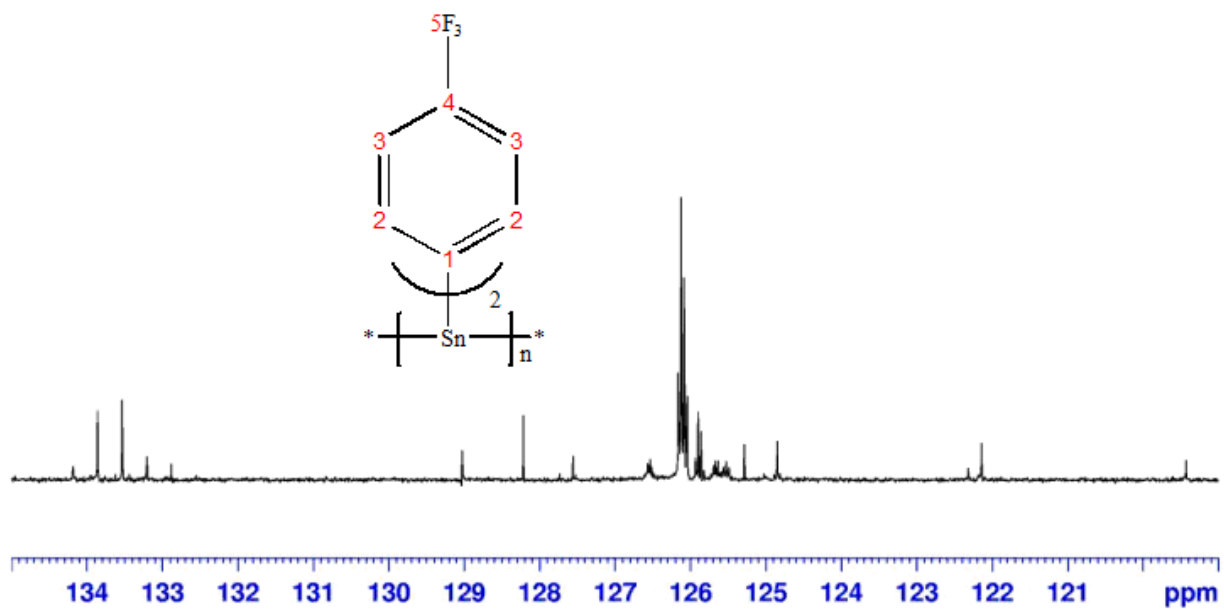


Figure 69:  $^{13}\text{C}$ -NMR spectrum for compound 10 ( $\text{CDCl}_3$ , 100MHz)

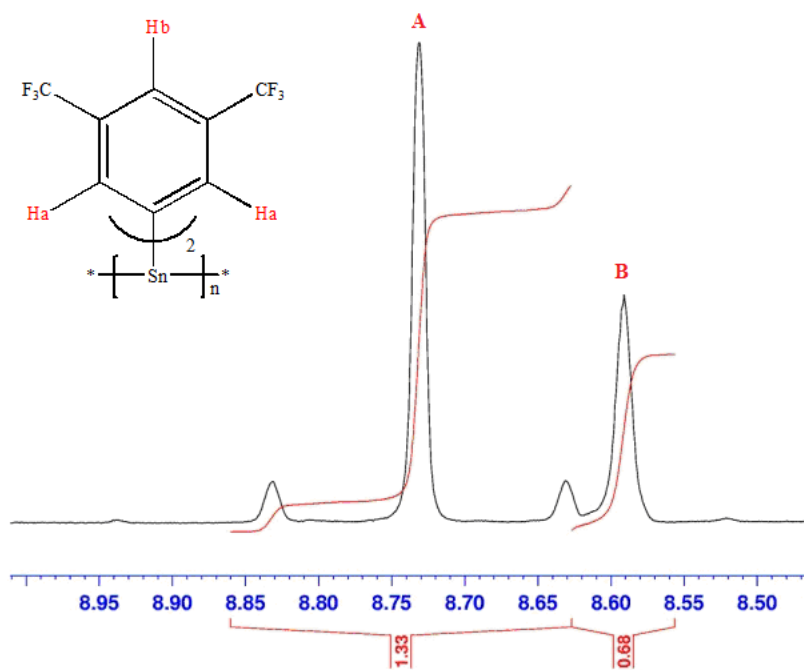


Figure 70:  $^1\text{H-NMR}$  spectrum of compound 11 ( $\text{CDCl}_3$ , 400MHz).

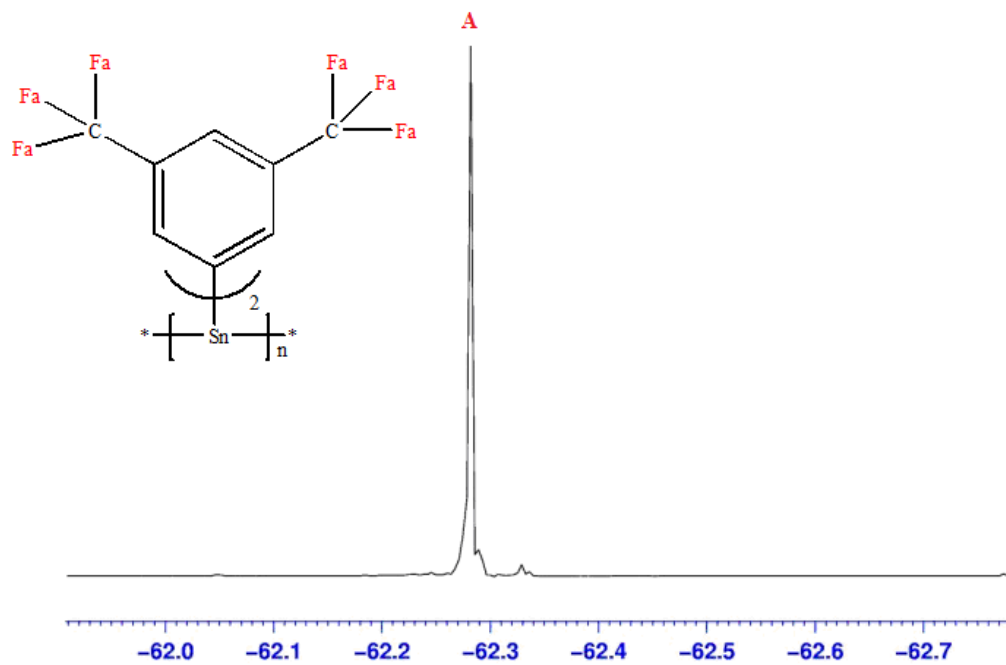


Figure 71:  $^{19}\text{F-NMR}$  spectrum for compound 11 ( $\text{CDCl}_3$ , 376MHz)

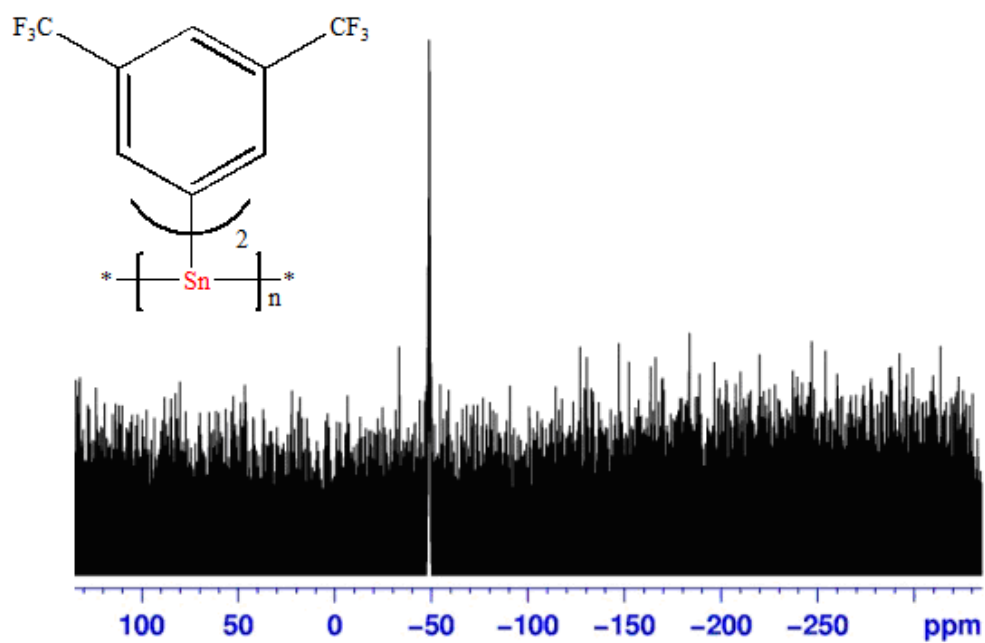


Figure 72:  $^{119}\text{Sn}$ -NMR spectrum for compound 11 ( $\text{CDCl}_3$ , 149 MHz)

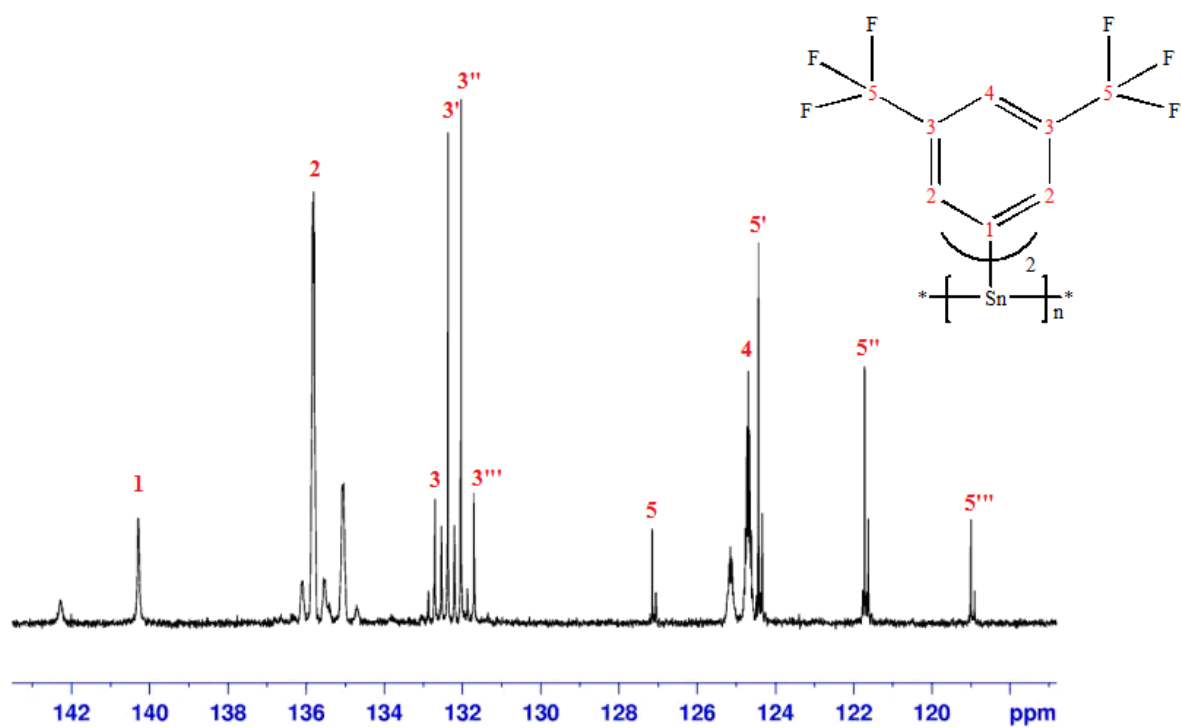


Figure 73:  $^{13}\text{C}$ -NMR spectrum for compound 11 ( $\text{CDCl}_3$ , 100MHz)

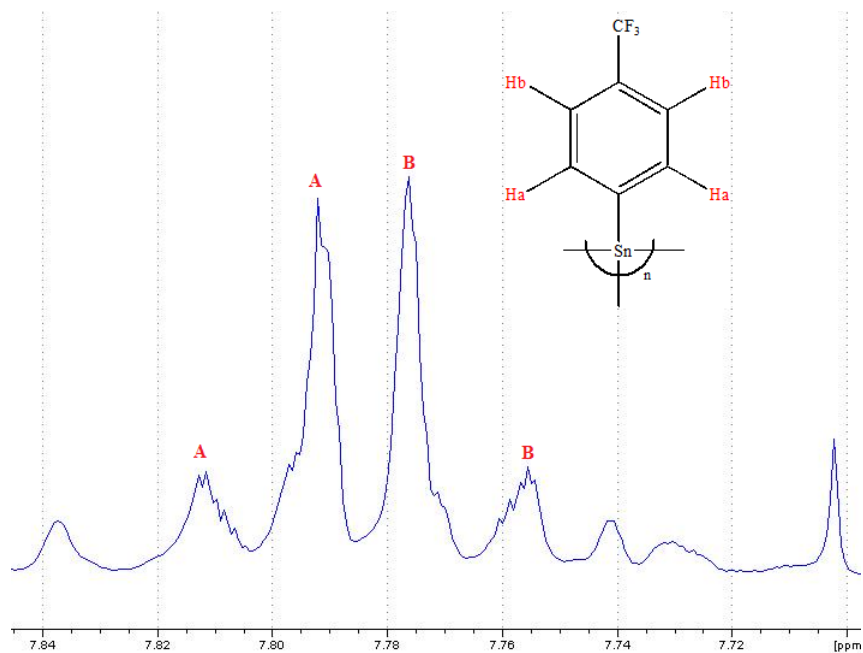


Figure 74:  $^1\text{H}$ -NMR spectrum for compound 12 ( $\text{CDCl}_3$ , 400 MHz)

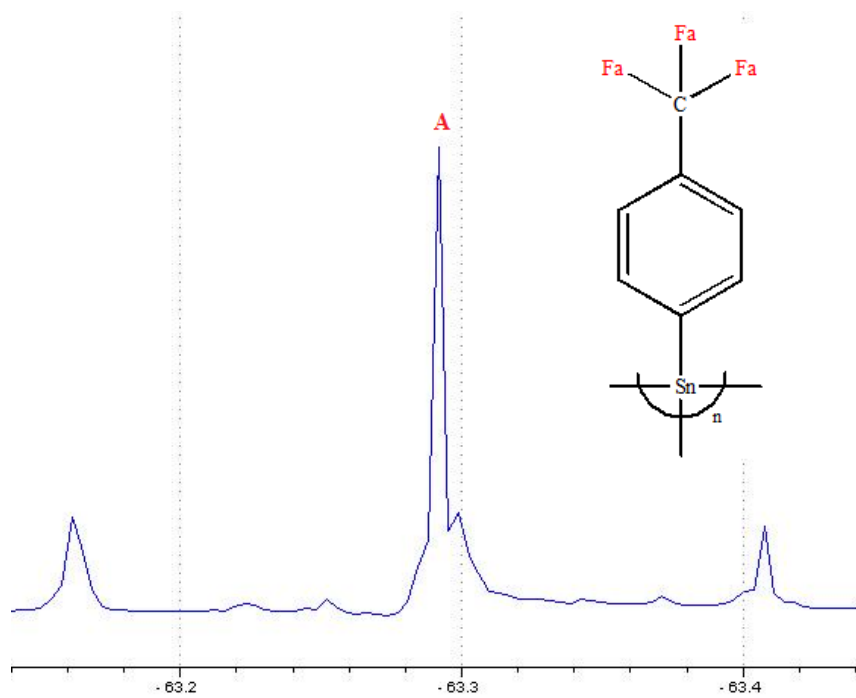


Figure 75:  $^{19}\text{F}$ -NMR spectrum for compound 12 ( $\text{CDCl}_3$ , 376 MHz)

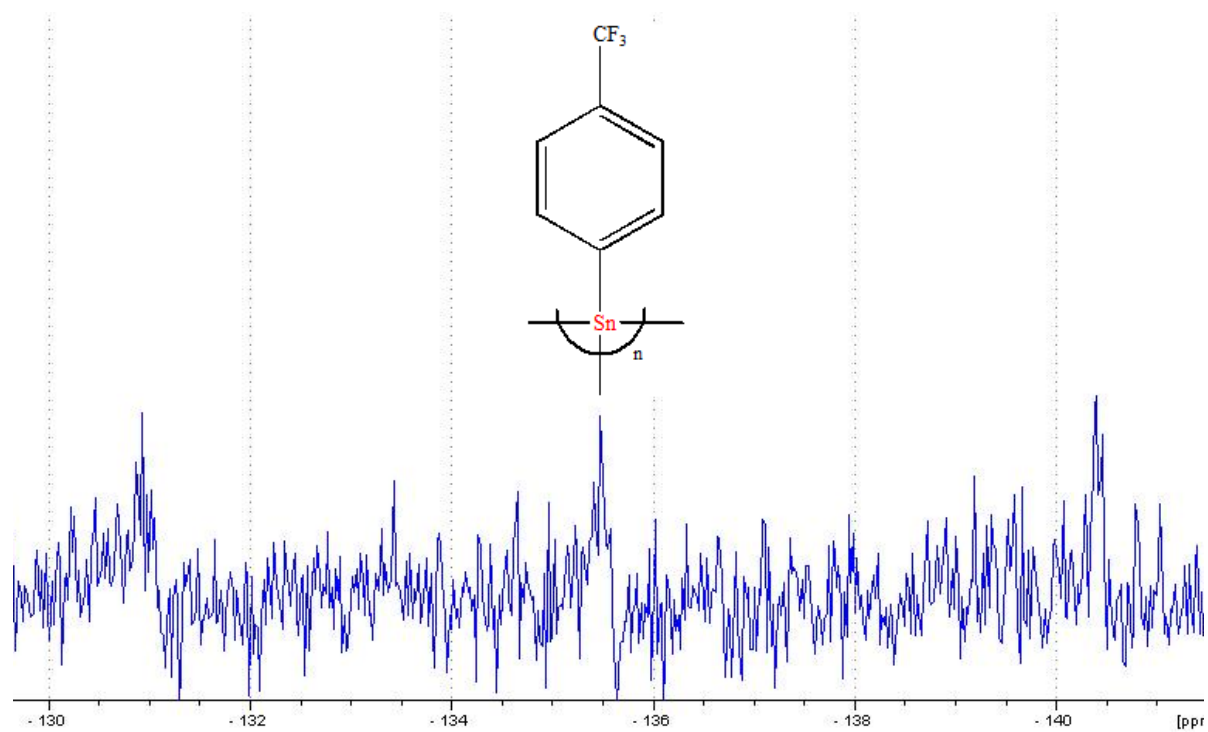


Figure 76:  $^{119}\text{Sn}$ -NMR spectrum for compound 12 ( $\text{CDCl}_3$ , 149 MHz)

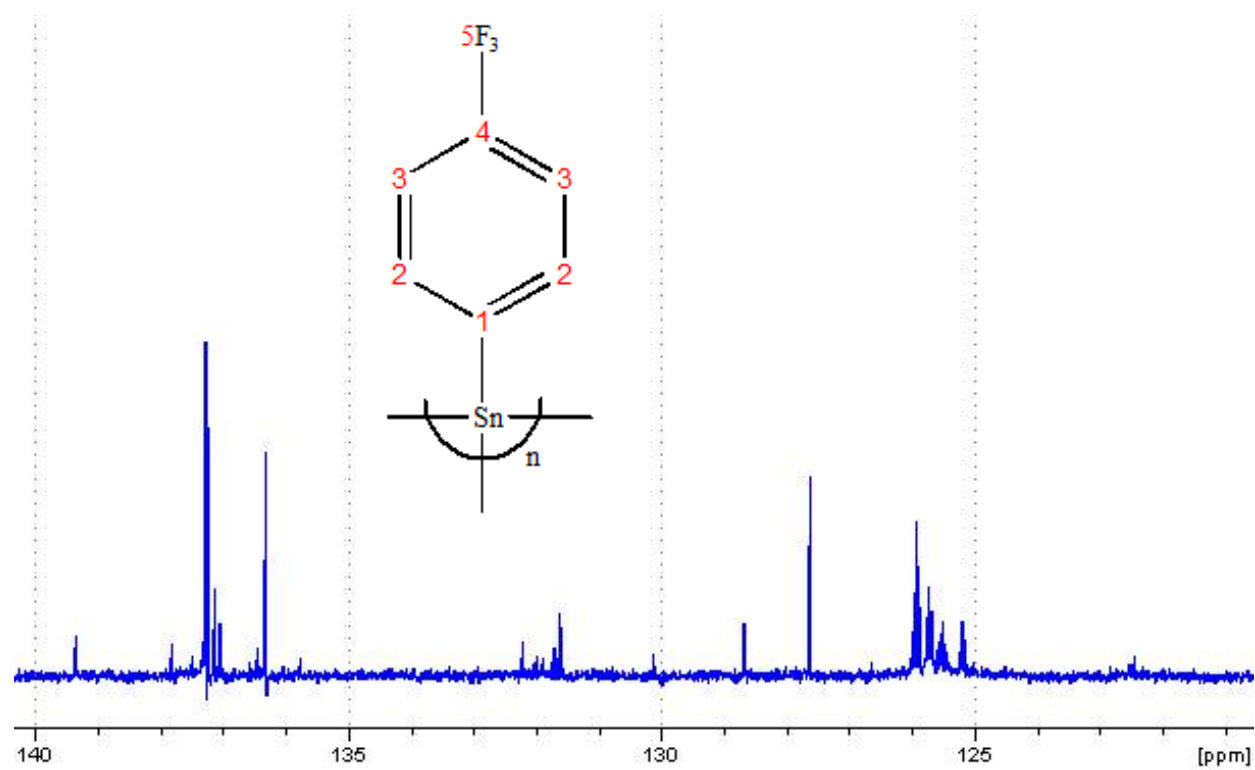


Figure 77:  $^{13}\text{C}$ -NMR spectrum of compound 12 ( $\text{CDCl}_3$ , 100 MHz)

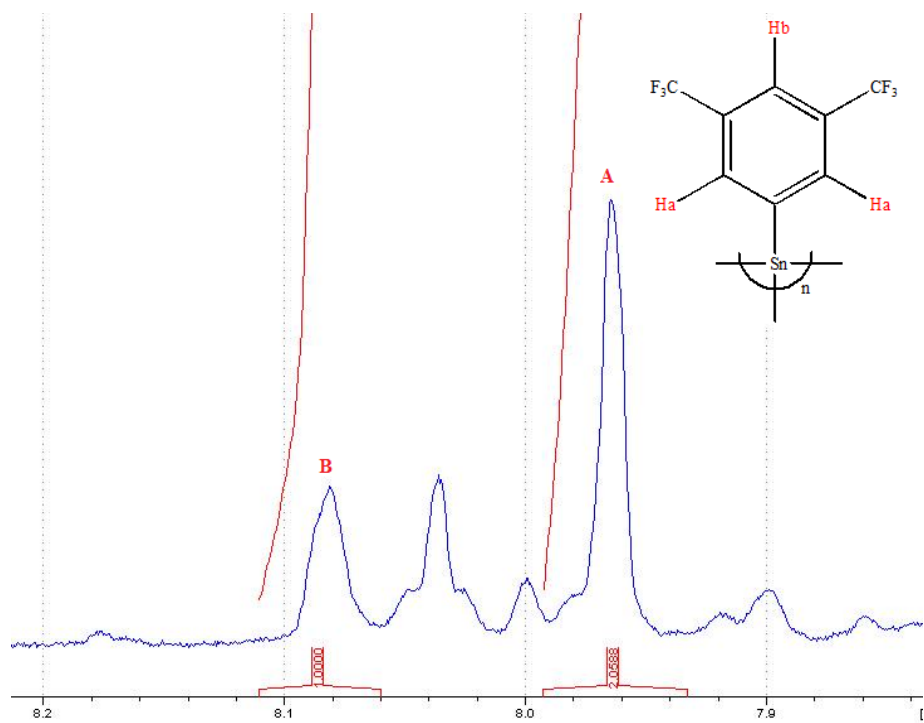


Figure 78:  $^1\text{H}$ -NMR spectrum for compound 13 ( $\text{CDCl}_3$ , 400 MHz)

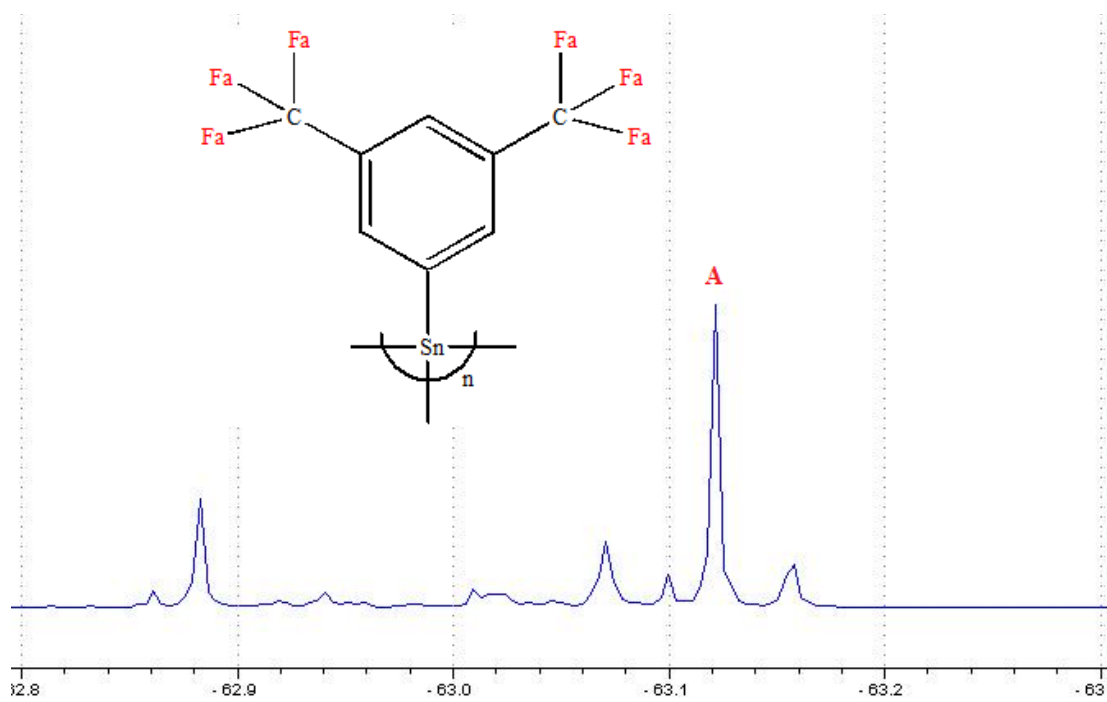


Figure 79:  $^{19}\text{F}$ -NMR spectrum for compound 13 ( $\text{CDCl}_3$ , 376 MHz)

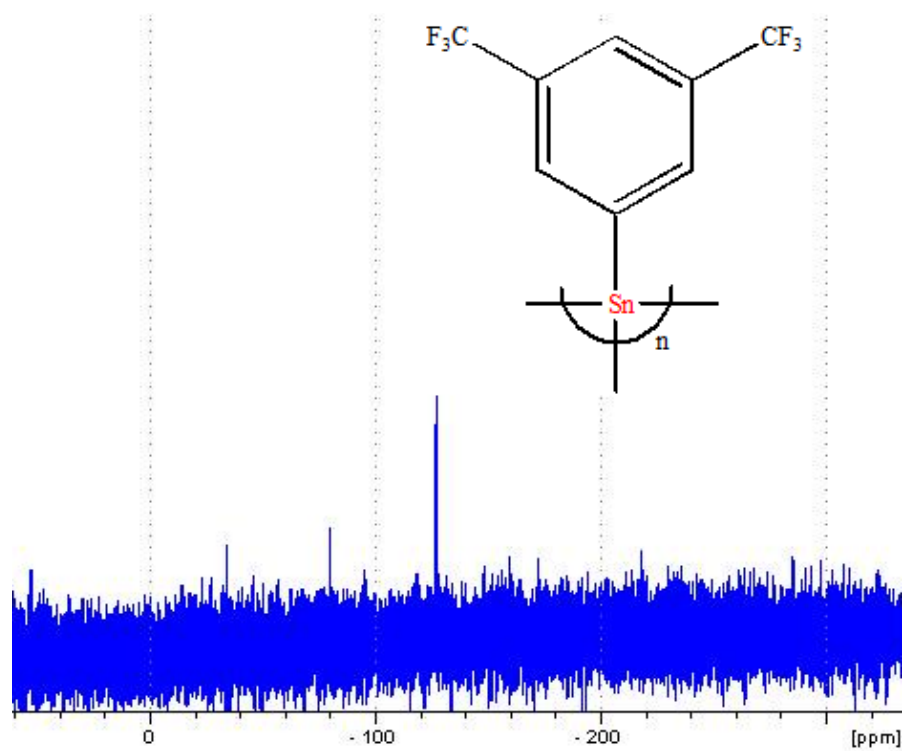


Figure 80:  $^{119}\text{Sn}$ -NMR spectrum for compound 13 ( $\text{CDCl}_3$ , 149 MHz)

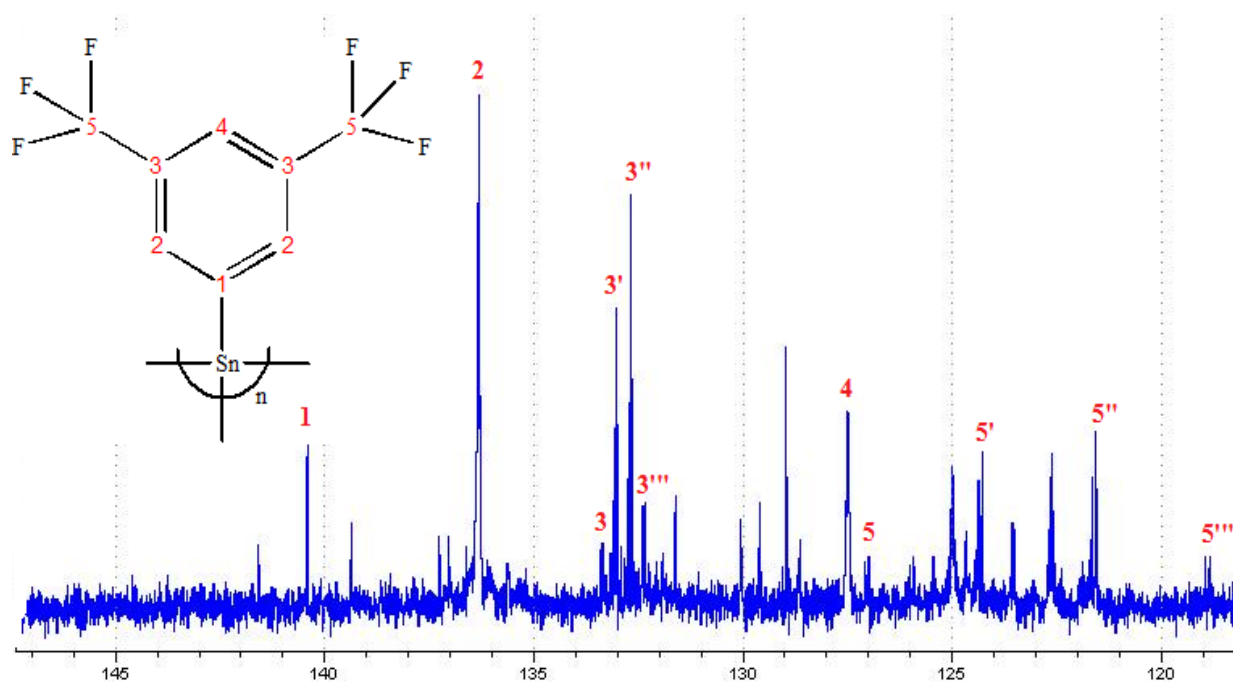
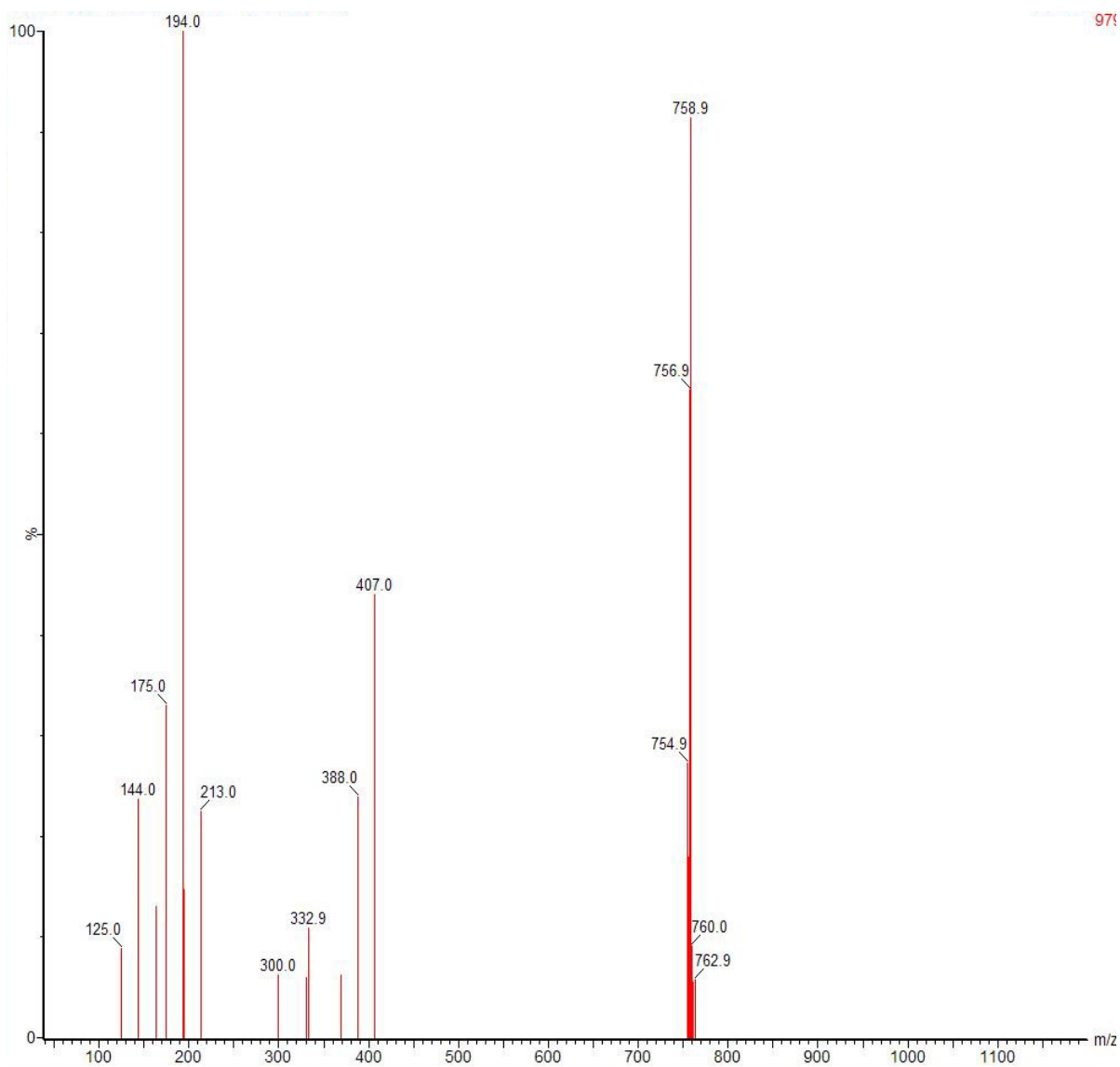
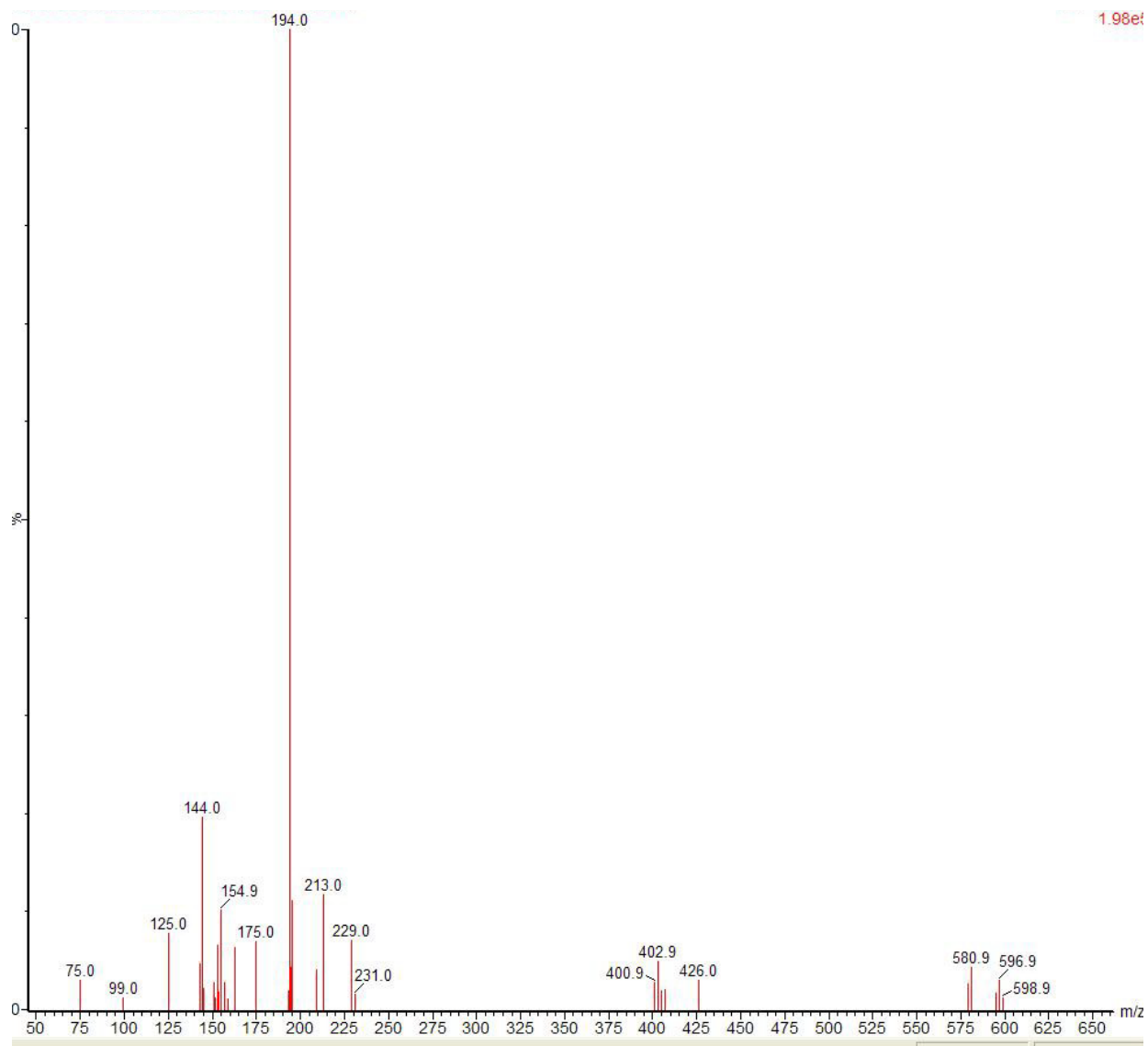


Figure 81:  $^{13}\text{C}$ -NMR spectrum for compound 13 ( $\text{CDCl}_3$ , 100 MHz)



**Figure 82: HR-E.I mass spectrum for compound 2**



**Figure 83:HR-E.I mass spectrum for compound 5**

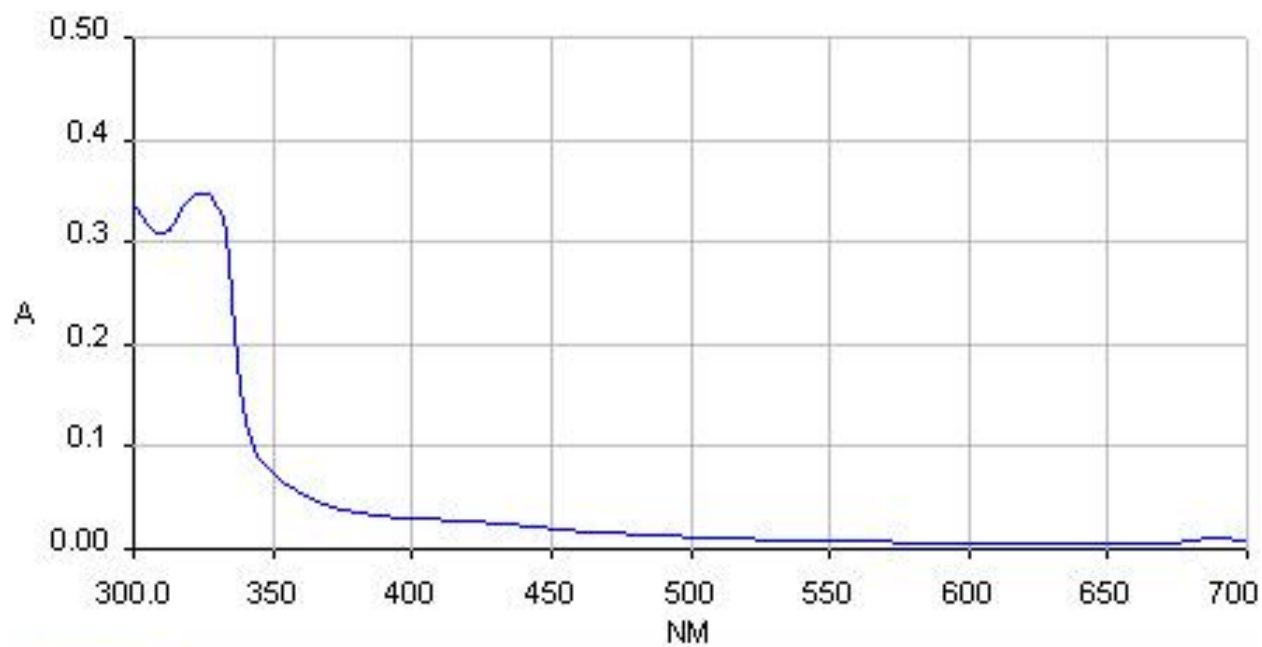


**Figure 84: UV/VIS spectrum for compound 10 in THF**

## Crystallographic data for compound 2

Table 13. Crystal data and structure refinement for compound 2

Identification code	k0951	
Empirical formula	C <sub>32</sub> H <sub>12</sub> F <sub>24</sub> Sn	
Formula weight	971.11	
Temperature	150(2) K	
Wavelength	0.71073 Å	
Crystal system	Monoclinic	
Space group	C 2/c	
Unit cell dimensions	a = 17.3506(8) Å	∠ = 90°.
	b = 20.8038(11) Å	∠ = 109.998(3)°.
	c = 9.8944(3) Å	∠ = 90°.
Volume	3356.1(3) Å <sup>3</sup>	
Z	4	
Density (calculated)	1.922 Mg/m <sup>3</sup>	
Absorption coefficient	0.920 mm <sup>-1</sup>	
F(000)	1880	
Crystal size	0.28 x 0.24 x 0.12 mm <sup>3</sup>	
Theta range for data collection	2.94 to 27.48°.	
Index ranges	-22 ≤ h ≤ 20, -24 ≤ k ≤ 26, -10 ≤ l ≤ 12	
Reflections collected	10930	
Independent reflections	3818 [R(int) = 0.0382]	
Completeness to theta = 27.48°	99.0 %	
Absorption correction	Semi-empirical from equivalents	
Max. and min. transmission	0.897 and 0.798	
Refinement method	Full-matrix least-squares on F <sup>2</sup>	
Data / restraints / parameters	3818 / 210 / 314	
Goodness-of-fit on F <sup>2</sup>	1.051	
Final R indices [I > 2σ(I)]	R1 = 0.0398, wR2 = 0.0881	
R indices (all data)	R1 = 0.0569, wR2 = 0.0977	
Largest diff. peak and hole	1.796 and -0.700 e.Å <sup>-3</sup>	

Table 14. Atomic coordinates ( $\times 10^4$ ) and equivalent isotropic displacement parameters ( $\text{\AA}^2 \times 10^3$ ) for **2**.  $U(\text{eq})$  is defined as one third of the trace of the orthogonalized  $U^{ij}$  tensor.

	x	y	z	U(eq)
Sn(1)	5000	2049(1)	2500	24(1)
C(1)	4488(2)	2560(2)	3882(3)	24(1)
C(2)	4192(2)	2178(2)	4754(3)	31(1)
C(3)	3864(2)	2454(2)	5721(4)	36(1)
C(4)	3826(2)	3117(2)	5822(4)	38(1)
C(5)	4109(2)	3501(2)	4942(3)	30(1)
C(6)	4441(2)	3224(2)	3984(3)	27(1)
C(7)	3563(3)	2032(2)	6671(5)	52(1)
C(8)	4071(3)	4216(2)	5054(4)	42(1)
C(9)	4017(2)	1455(1)	1187(3)	23(1)
C(10)	3210(2)	1574(2)	1095(3)	23(1)
C(11)	2565(2)	1209(1)	197(3)	24(1)
C(12)	2712(2)	723(2)	-642(3)	25(1)
C(13)	3514(2)	603(2)	-558(3)	27(1)
C(14)	4159(2)	962(2)	350(3)	27(1)
C(15)	1714(2)	1338(2)	164(3)	31(1)
C(16)	3678(2)	76(2)	-1447(4)	40(1)
F(1)	3258(5)	1488(3)	6078(8)	95(3)
F(2)	2895(3)	2314(2)	6904(6)	64(2)
F(3)	4080(3)	1949(4)	7888(6)	116(4)
F(1A)	3017(8)	1657(10)	6015(18)	100(8)
F(2A)	3514(16)	2275(5)	7771(18)	116(8)
F(3A)	4242(7)	1554(7)	7346(15)	87(5)
F(4)	3442(12)	4407(9)	5400(30)	114(5)
F(5)	4725(10)	4474(6)	5981(11)	79(4)
F(6)	3980(8)	4522(6)	3801(8)	62(2)
F(4A)	3654(14)	4399(16)	5880(30)	81(5)
F(5A)	4837(9)	4429(9)	5740(20)	66(4)
F(6A)	3800(18)	4473(12)	3855(13)	96(8)
F(7)	1638(1)	1265(1)	1440(2)	61(1)

F(8)	1481(1)	1948(1)	-251(3)	59(1)
F(9)	1154(1)	961(1)	-743(2)	46(1)
F(10)	3779(2)	-490(1)	-768(3)	72(1)
F(11)	3080(2)	11(2)	-2707(3)	83(1)
F(12)	4361(2)	159(1)	-1746(3)	57(1)

---

Table 15.

Bond lengths [Å] and angles [°] for **2**.

---

Sn(1)-C(9)	2.147(3)
Sn(1)-C(9)#1	2.147(3)
Sn(1)-C(1)	2.150(3)
Sn(1)-C(1)#1	2.150(3)
C(1)-C(6)	1.390(5)
C(1)-C(2)	1.392(4)
C(2)-C(3)	1.393(5)
C(3)-C(4)	1.387(5)
C(3)-C(7)	1.504(5)
C(4)-C(5)	1.389(5)
C(5)-C(6)	1.391(4)
C(5)-C(8)	1.496(5)
C(7)-F(1A)	1.228(14)
C(7)-F(2A)	1.228(10)
C(7)-F(3)	1.243(6)
C(7)-F(1)	1.301(7)
C(7)-F(2)	1.387(6)
C(7)-F(3A)	1.511(11)
C(8)-F(6A)	1.238(15)
C(8)-F(5)	1.305(10)
C(8)-F(4)	1.310(11)
C(8)-F(4A)	1.316(15)
C(8)-F(5A)	1.343(14)
C(8)-F(6)	1.353(10)
C(9)-C(14)	1.392(4)

C(9)-C(10)	1.393(4)
C(10)-C(11)	1.392(4)
C(11)-C(12)	1.385(4)
C(11)-C(15)	1.490(4)
C(12)-C(13)	1.389(4)
C(13)-C(14)	1.388(4)
C(13)-C(16)	1.494(5)
C(15)-F(7)	1.322(4)
C(15)-F(9)	1.329(4)
C(15)-F(8)	1.354(4)
C(16)-F(12)	1.328(4)
C(16)-F(11)	1.328(4)
C(16)-F(10)	1.337(5)

C(9)-Sn(1)-C(9)#1	109.73(16)
C(9)-Sn(1)-C(1)	104.69(11)
C(9)#1-Sn(1)-C(1)	108.38(11)
C(9)-Sn(1)-C(1)#1	108.38(11)
C(9)#1-Sn(1)-C(1)#1	104.69(11)
C(1)-Sn(1)-C(1)#1	120.76(17)
C(6)-C(1)-C(2)	118.6(3)
C(6)-C(1)-Sn(1)	125.8(2)
C(2)-C(1)-Sn(1)	115.6(2)
C(1)-C(2)-C(3)	121.0(3)
C(4)-C(3)-C(2)	120.0(3)
C(4)-C(3)-C(7)	119.9(3)
C(2)-C(3)-C(7)	120.1(3)
C(3)-C(4)-C(5)	119.4(3)
C(4)-C(5)-C(6)	120.5(3)
C(4)-C(5)-C(8)	119.5(3)
C(6)-C(5)-C(8)	120.0(3)
C(1)-C(6)-C(5)	120.6(3)
F(1A)-C(7)-F(2A)	117.1(9)
F(1A)-C(7)-F(3)	126.4(10)
F(2A)-C(7)-F(1)	128.0(9)

F(3)-C(7)-F(1)	111.3(5)
F(3)-C(7)-F(2)	105.4(4)
F(1)-C(7)-F(2)	102.0(4)
F(1A)-C(7)-C(3)	114.2(10)
F(2A)-C(7)-C(3)	117.3(7)
F(3)-C(7)-C(3)	113.4(4)
F(1)-C(7)-C(3)	113.6(4)
F(2)-C(7)-C(3)	110.3(4)
F(1A)-C(7)-F(3A)	99.1(7)
F(2A)-C(7)-F(3A)	99.1(8)
F(2)-C(7)-F(3A)	140.7(5)
C(3)-C(7)-F(3A)	105.9(5)
F(6A)-C(8)-F(5)	116.8(15)
F(5)-C(8)-F(4)	107.1(7)
F(6A)-C(8)-F(4A)	111.0(12)
F(6A)-C(8)-F(5A)	109.2(12)
F(4)-C(8)-F(5A)	122.4(12)
F(4A)-C(8)-F(5A)	104.4(9)
F(5)-C(8)-F(6)	104.6(6)
F(4)-C(8)-F(6)	104.3(8)
F(4A)-C(8)-F(6)	120.8(16)
F(6A)-C(8)-C(5)	111.7(11)
F(5)-C(8)-C(5)	114.3(7)
F(4)-C(8)-C(5)	112.4(9)
F(4A)-C(8)-C(5)	112.4(15)
F(5A)-C(8)-C(5)	107.8(9)
F(6)-C(8)-C(5)	113.2(6)
C(14)-C(9)-C(10)	118.0(3)
C(14)-C(9)-Sn(1)	121.2(2)
C(10)-C(9)-Sn(1)	120.7(2)
C(11)-C(10)-C(9)	121.0(3)
C(12)-C(11)-C(10)	120.5(3)
C(12)-C(11)-C(15)	120.1(3)
C(10)-C(11)-C(15)	119.3(3)
C(11)-C(12)-C(13)	118.8(3)

C(14)-C(13)-C(12)	120.8(3)
C(14)-C(13)-C(16)	120.2(3)
C(12)-C(13)-C(16)	119.1(3)
C(13)-C(14)-C(9)	120.9(3)
F(7)-C(15)-F(9)	106.7(3)
F(7)-C(15)-F(8)	106.3(3)
F(9)-C(15)-F(8)	106.0(3)
F(7)-C(15)-C(11)	112.3(3)
F(9)-C(15)-C(11)	113.5(3)
F(8)-C(15)-C(11)	111.5(3)
F(12)-C(16)-F(11)	106.0(3)
F(12)-C(16)-F(10)	104.7(3)
F(11)-C(16)-F(10)	108.0(3)
F(12)-C(16)-C(13)	113.5(3)
F(11)-C(16)-C(13)	112.5(3)
F(10)-C(16)-C(13)	111.7(3)

---

Symmetry transformations used to generate equivalent atoms: #1 -x+1,y,-z+1/2

Table 16. Anisotropic displacement parameters ( $\text{\AA}^2 \times 10^3$ ) for **2**. The anisotropic displacement factor exponent takes the form:  $-2\pi^2 [ h^2 a^{*2} U^{11} + \dots + 2 h k a^* b^* U^{12} ]$

---

	U11	U22	U33	U23	U13	U12
Sn(1)	23(1)	25(1)	25(1)	0	10(1)	0
C(1)	20(1)	30(2)	23(1)	-1(1)	8(1)	1(1)
C(2)	35(2)	30(2)	29(2)	-1(1)	13(1)	-1(1)
C(3)	41(2)	39(2)	32(2)	-4(2)	17(2)	-6(2)
C(4)	41(2)	43(2)	33(2)	-8(2)	19(2)	-3(2)
C(5)	29(2)	30(2)	31(2)	-8(1)	10(1)	-2(1)
C(6)	24(2)	29(2)	28(2)	-1(1)	8(1)	0(1)
C(7)	72(3)	51(3)	47(2)	1(2)	39(2)	-8(2)
C(8)	53(2)	31(2)	45(2)	-10(2)	22(2)	-2(2)
C(9)	24(1)	22(2)	22(1)	0(1)	9(1)	0(1)
C(10)	24(2)	24(2)	22(1)	1(1)	8(1)	0(1)

C(11)	26(2)	23(2)	22(1)	4(1)	9(1)	3(1)
C(12)	27(2)	26(2)	22(2)	1(1)	6(1)	0(1)
C(13)	32(2)	24(2)	27(2)	-2(1)	11(1)	3(1)
C(14)	26(2)	28(2)	30(2)	0(1)	12(1)	1(1)
C(15)	28(2)	36(2)	31(2)	-5(1)	10(1)	-1(1)
C(16)	34(2)	38(2)	47(2)	-13(2)	13(2)	4(2)
F(1)	178(8)	37(3)	126(6)	-15(3)	123(6)	-22(4)
F(2)	67(3)	74(3)	75(3)	4(2)	53(3)	-2(2)
F(3)	49(3)	224(10)	71(4)	93(5)	14(2)	-5(4)
F(1A)	37(6)	145(18)	96(12)	61(11)	-6(6)	-50(8)
F(2A)	250(20)	65(8)	93(12)	-7(8)	133(15)	-7(12)
F(3A)	104(10)	84(9)	110(10)	69(7)	86(8)	39(7)
F(4)	129(7)	37(4)	228(13)	-3(9)	131(8)	20(5)
F(5)	121(8)	44(4)	41(4)	-11(3)	-14(4)	-4(5)
F(6)	103(5)	29(3)	57(5)	-4(3)	33(4)	-2(3)
F(4A)	135(12)	44(8)	107(11)	-26(7)	99(9)	-2(9)
F(5A)	59(7)	31(5)	115(12)	-32(6)	39(7)	-28(4)
F(6A)	151(14)	47(9)	42(8)	13(6)	-29(9)	28(10)
F(7)	41(1)	111(2)	41(1)	-10(1)	26(1)	2(1)
F(8)	31(1)	41(1)	104(2)	4(1)	20(1)	9(1)
F(9)	25(1)	54(1)	57(1)	-18(1)	13(1)	-7(1)
F(10)	107(2)	27(1)	109(2)	-6(1)	71(2)	7(1)
F(11)	61(2)	101(2)	67(2)	-58(2)	-3(1)	21(2)
F(12)	64(2)	55(2)	69(2)	-22(1)	46(1)	-1(1)

---

Table 17. Hydrogen coordinates ( $\times 10^4$ ) and isotropic displacement parameters ( $\text{\AA}^2 \times 10^3$ )

for **2**.

---

	x	y	z	U(eq)
H(2A)	4215	1723	4688	37
H(4A)	3608	3307	6487	45
H(6A)	4638	3491	3395	32
H(10A)	3099	1909	1654	28
H(12A)	2271	477	-1264	30
H(14A)	4704	869	401	32

---

## Crystallographic data for compound 4

Table 18. Crystal data and structure refinement for compound 4.

Identification code	k09260	
Empirical formula	C <sub>14</sub> H <sub>8</sub> Cl <sub>2</sub> F <sub>6</sub> Sn	
Formula weight	479.79	
Temperature	150(1) K	
Wavelength	0.71073 Å	
Crystal system	Monoclinic	
Space group	P 2 <sub>1</sub> /c	
Unit cell dimensions	a = 13.3883(4) Å	∠ = 90°.
	b = 5.81970(10) Å	∠ = 103.8730(12)°.
	c = 21.2604(7) Å	∠ = 90°.
Volume	1608.20(8) Å <sup>3</sup>	
Z	4	
Density (calculated)	1.982 Mg/m <sup>3</sup>	
Absorption coefficient	1.975 mm <sup>-1</sup>	
F(000)	920	
Crystal size	0.20 x 0.12 x 0.06 mm <sup>3</sup>	
Theta range for data collection	2.80 to 27.50°.	
Index ranges	-17 ≤ h ≤ 17, -7 ≤ k ≤ 7, -27 ≤ l ≤ 27	
Reflections collected	10434	
Independent reflections	3664 [R(int) = 0.0501]	
Completeness to theta = 27.50°	99.2 %	
Absorption correction	Semi-empirical from equivalents	
Max. and min. transmission	0.891 and 0.696	
Refinement method	Full-matrix least-squares on F <sup>2</sup>	
Data / restraints / parameters	3664 / 0 / 234	
Goodness-of-fit on F <sup>2</sup>	1.059	
Final R indices [I > 2σ(I)]	R <sub>1</sub> = 0.0376, wR <sub>2</sub> = 0.0865	
R indices (all data)	R <sub>1</sub> = 0.0538, wR <sub>2</sub> = 0.0967	
Largest diff. peak and hole	1.397 and -0.881 e.Å <sup>-3</sup>	

Table 19. Atomic coordinates ( $\times 10^4$ ) and equivalent isotropic displacement parameters ( $\text{\AA}^2 \times 10^3$ ) for **4**. U(eq) is defined as one third of the trace of the orthogonalized  $U^{ij}$  tensor.

	x	y	z	U(eq)
Sn(1)	5819(1)	968(1)	6624(1)	31(1)
Cl(1)	6487(1)	-738(2)	5811(1)	42(1)
Cl(2)	5368(1)	-2248(2)	7154(1)	37(1)
C(7)	9774(4)	5693(9)	8444(3)	54(1)
F(1)	9871(4)	5296(13)	9074(2)	112(2)
F(2)	9731(4)	7952(8)	8417(4)	121(3)
F(3)	10609(3)	5080(11)	8311(3)	115(3)
F(1A)	9629(17)	6930(50)	8826(12)	41(7)
F(2A)	10260(20)	7010(50)	8093(12)	60(9)
F(3A)	10370(20)	4120(40)	8763(14)	54(8)
C(14)	1722(4)	5382(9)	4893(2)	47(1)
F(4)	1417(4)	7267(9)	5120(2)	105(2)
F(5)	1823(3)	5877(11)	4312(2)	101(2)
F(6)	909(3)	3999(9)	4799(3)	111(2)
F(4A)	988(17)	5350(50)	5140(11)	40(7)
F(5A)	1823(17)	7540(40)	4739(12)	46(7)
F(6A)	1390(20)	4320(40)	4382(14)	53(8)
C(1)	7101(3)	2559(6)	7249(2)	31(1)
C(2)	7523(3)	1677(8)	7861(2)	42(1)
C(3)	8393(3)	2699(8)	8252(2)	44(1)
C(4)	8821(3)	4608(8)	8028(2)	42(1)
C(5)	8403(3)	5470(8)	7425(2)	49(1)
C(6)	7545(3)	4447(7)	7031(2)	41(1)
C(8)	4441(3)	2510(6)	6091(2)	30(1)
C(9)	3494(3)	1484(7)	6062(2)	41(1)
C(10)	2605(3)	2426(8)	5671(2)	43(1)
C(11)	2655(3)	4360(7)	5309(2)	35(1)
C(12)	3601(3)	5444(7)	5353(2)	37(1)
C(13)	4490(3)	4493(7)	5736	36(1)

Table 20. Bond lengths [ $\text{\AA}$ ] and angles [ $^\circ$ ] for **4**

---

Sn(1)-C(1)	2.116(4)
Sn(1)-C(8)	2.119(4)
Sn(1)-Cl(2)	2.3369(9)
Sn(1)-Cl(1)	2.3478(10)
C(7)-F(1A)	1.14(2)
C(7)-F(3)	1.268(6)
C(7)-F(3A)	1.29(2)
C(7)-F(2)	1.317(7)
C(7)-F(1)	1.334(7)
C(7)-F(2A)	1.34(3)
C(7)-C(4)	1.505(6)
C(14)-F(4A)	1.22(2)
C(14)-F(6A)	1.24(3)
C(14)-F(4)	1.303(6)
C(14)-F(5)	1.307(6)
C(14)-F(5A)	1.32(2)
C(14)-F(6)	1.330(7)
C(14)-C(11)	1.472(6)
C(1)-C(6)	1.380(6)
C(1)-C(2)	1.387(5)
C(2)-C(3)	1.392(6)
C(3)-C(4)	1.386(6)
C(4)-C(5)	1.366(7)
C(5)-C(6)	1.384(6)
C(8)-C(13)	1.389(5)
C(8)-C(9)	1.390(6)
C(9)-C(10)	1.391(6)
C(10)-C(11)	1.374(6)
C(11)-C(12)	1.399(6)
C(12)-C(13)	1.386(6)
C(1)-Sn(1)-C(8)	128.44(15)
C(1)-Sn(1)-Cl(2)	108.22(11)

C(8)-Sn(1)-Cl(2)	107.75(11)
C(1)-Sn(1)-Cl(1)	104.60(11)
C(8)-Sn(1)-Cl(1)	102.81(10)
Cl(2)-Sn(1)-Cl(1)	101.76(3)
F(1A)-C(7)-F(3)	130.4(12)
F(1A)-C(7)-F(3A)	105.2(18)
F(3)-C(7)-F(3A)	56.7(13)
F(1A)-C(7)-F(2)	52.0(13)
F(3)-C(7)-F(2)	107.6(6)
F(3A)-C(7)-F(2)	138.0(12)
F(1A)-C(7)-F(1)	52.1(14)
F(3)-C(7)-F(1)	107.3(6)
F(3A)-C(7)-F(1)	56.8(13)
F(2)-C(7)-F(1)	102.1(6)
F(1A)-C(7)-F(2A)	102.8(18)
F(3)-C(7)-F(2A)	57.9(14)
F(3A)-C(7)-F(2A)	112.1(18)
F(2)-C(7)-F(2A)	54.9(13)
F(1)-C(7)-F(2A)	135.6(12)
F(1A)-C(7)-C(4)	114.8(12)
F(3)-C(7)-C(4)	114.8(5)
F(3A)-C(7)-C(4)	110.1(12)
F(2)-C(7)-C(4)	111.7(4)
F(1)-C(7)-C(4)	112.4(4)
F(2A)-C(7)-C(4)	111.6(12)
F(4A)-C(14)-F(6A)	102.5(18)
F(4A)-C(14)-F(4)	59.9(12)
F(6A)-C(14)-F(4)	132.1(12)
F(4A)-C(14)-F(5)	133.4(11)
F(6A)-C(14)-F(5)	51.4(14)
F(4)-C(14)-F(5)	106.1(5)
F(4A)-C(14)-F(5A)	105.4(16)
F(6A)-C(14)-F(5A)	107.3(17)
F(4)-C(14)-F(5A)	49.2(11)
F(5)-C(14)-F(5A)	60.9(12)

F(4A)-C(14)-F(6)	48.7(12)
F(6A)-C(14)-F(6)	57.3(15)
F(4)-C(14)-F(6)	104.3(5)
F(5)-C(14)-F(6)	105.0(5)
F(5A)-C(14)-F(6)	132.2(10)
F(4A)-C(14)-C(11)	112.9(11)
F(6A)-C(14)-C(11)	113.4(12)
F(4)-C(14)-C(11)	114.4(4)
F(5)-C(14)-C(11)	113.0(4)
F(5A)-C(14)-C(11)	114.4(10)
F(6)-C(14)-C(11)	113.0(4)
C(6)-C(1)-C(2)	119.9(4)
C(6)-C(1)-Sn(1)	119.2(3)
C(2)-C(1)-Sn(1)	120.9(3)
C(1)-C(2)-C(3)	119.8(4)
C(4)-C(3)-C(2)	119.5(4)
C(5)-C(4)-C(3)	120.4(4)
C(5)-C(4)-C(7)	119.7(4)
C(3)-C(4)-C(7)	119.8(4)
C(4)-C(5)-C(6)	120.3(4)
C(1)-C(6)-C(5)	120.1(4)
C(13)-C(8)-C(9)	119.6(4)
C(13)-C(8)-Sn(1)	119.6(3)
C(9)-C(8)-Sn(1)	120.6(3)
C(8)-C(9)-C(10)	119.9(4)
C(11)-C(10)-C(9)	120.6(4)
C(10)-C(11)-C(12)	119.8(4)
C(10)-C(11)-C(14)	121.3(4)
C(12)-C(11)-C(14)	118.8(4)
C(13)-C(12)-C(11)	119.7(4)
C(12)-C(13)-C(8)	120.3(4)

Symmetry transformations used to generate equivalent atoms:

Table 21. Anisotropic displacement parameters ( $\text{\AA}^2 \times 10^3$ ) for **4**. The anisotropic displacement factor exponent takes the form:  $-2\text{h}^2\text{a}^2\text{U}^{11} + \dots + 2\text{hka}^*\text{b}^*\text{U}^{12}$  ]

	U11	U22	U33	U23	U13	U12
Sn(1)	37(1)	29(1)	26(1)	1(1)	7(1)	-2(1)
Cl(1)	55(1)	42(1)	34(1)	-1(1)	21(1)	-2(1)
Cl(2)	50(1)	31(1)	33(1)	2(1)	18(1)	-1(1)
C(7)	42(3)	57(3)	59(3)	-10(3)	4(2)	-7(2)
F(1)	80(3)	177(6)	67(3)	-25(4)	-5(3)	-59(4)
F(2)	85(3)	55(3)	182(7)	-27(4)	-49(4)	-9(2)
F(3)	28(2)	157(5)	159(6)	-100(5)	21(2)	-12(2)
C(14)	41(3)	63(3)	38(2)	-1(2)	8(2)	6(2)
F(4)	115(4)	106(4)	70(3)	-26(3)	-22(3)	73(3)
F(5)	57(2)	203(7)	41(2)	43(3)	12(2)	49(3)
F(6)	46(2)	100(4)	162(6)	41(4)	-27(3)	-11(2)
C(1)	33(2)	28(2)	31(2)	-3(2)	6(2)	1(2)
C(2)	51(3)	39(2)	32(2)	4(2)	3(2)	-7(2)
C(3)	47(3)	44(2)	37(2)	-1(2)	0(2)	1(2)
C(4)	32(2)	44(2)	45(3)	-5(2)	3(2)	4(2)
C(5)	39(2)	51(3)	59(3)	4(2)	15(2)	-10(2)
C(6)	40(2)	43(2)	41(2)	9(2)	11(2)	-2(2)
C(8)	36(2)	30(2)	22(2)	-1(2)	4(2)	1(2)
C(9)	41(2)	39(2)	44(2)	4(2)	13(2)	-4(2)
C(10)	35(2)	50(3)	44(2)	-3(2)	11(2)	-4(2)
C(11)	35(2)	36(2)	37(2)	6(2)	15(2)	6(2)
C(12)	49(2)	35(2)	28(2)	6(2)	10(2)	0(2)
C(13)	40(2)	39(2)	29(2)	-1(2)	4(2)	-6(2)

Table 22. Hydrogen coordinates ( $\times 10^4$ ) and isotropic displacement parameters ( $\text{\AA}^2 \times 10^3$ ) for **4**.

	x	y	z	U(eq)
H(2)	7219	379	8012	50
H(3)	8691	2092	8670	53
H(5)	8703	6778	7275	59
H(6)	7261	5044	6610	50
H(9)	3453	143	6309	49
H(10)	1958	1725	5653	51
H(12)	3635	6826	5121	45
H(13)	5137	5201	5755	44

Table 23. Crystal data and structure refinement for **5**.

Identification code	k09195a	
Empirical formula	C <sub>16</sub> H <sub>6</sub> Cl <sub>2</sub> F <sub>12</sub> Sn	
Formula weight	615.80	
Temperature	120(1) K	
Wavelength	0.71073 Å	
Crystal system	Orthorhombic	
Space group	P b c n	
Unit cell dimensions	a = 26.7066(3) Å	□ = 90°.
	b = 7.4695(4) Å	□ = 90°.
	c = 9.8798(11) Å	□ = 90°.
Volume	1970.9(2) Å <sup>3</sup>	
Z	4	
Density (calculated)	2.075 Mg/m <sup>3</sup>	
Absorption coefficient	1.679 mm <sup>-1</sup>	
F(000)	1176	
Crystal size	0.34 x 0.18 x 0.12 mm <sup>3</sup>	
Theta range for data collection	3.05 to 27.48°.	
Index ranges	-28 ≤ h ≤ 34, -9 ≤ k ≤ 9, -12 ≤ l ≤ 12	
Reflections collected	11445	
Independent reflections	2234 [R(int) = 0.0704]	
Completeness to theta = 27.48°	98.8 %	
Absorption correction	Semi-empirical from equivalents	
Max. and min. transmission	0.825 and 0.572	
Refinement method	Full-matrix least-squares on F <sup>2</sup>	
Data / restraints / parameters	2234 / 0 / 141	
Goodness-of-fit on F <sup>2</sup>	1.092	
Final R indices [I > 2σ(I)]	R1 = 0.0453, wR2 = 0.1109	
R indices (all data)	R1 = 0.0716, wR2 = 0.1303	
Largest diff. peak and hole	1.651 and -0.899 e.Å <sup>-3</sup>	

Table 2. Atomic coordinates ( $\times 10^4$ ) and equivalent isotropic displacement parameters ( $\text{\AA}^2 \times 10^3$ ) for **5**.  $U(\text{eq})$  is defined as one third of the trace of the orthogonalized  $U^{ij}$  tensor.

	x	y	z	U(eq)
Sn(1)	5000	5340(1)	7500	38(1)
Cl(1)	4961(1)	7370(2)	9301(1)	46(1)
F(1)	3043(1)	4360(4)	4313(3)	68(1)
F(2)	2606(1)	4756(4)	6097(3)	64(1)
F(3)	3128(1)	6747(3)	5449(3)	64(1)
F(4)	3816(2)	-113(4)	9749(3)	67(1)
F(5)	3817(1)	-1452(4)	7839(3)	64(1)
F(6)	3133(1)	-392(4)	8643(4)	71(1)
C(1)	4298(2)	4049(6)	7286(4)	35(1)
C(2)	3930(2)	4875(5)	6507(4)	38(1)
C(3)	3457(2)	4108(5)	6397(4)	36(1)
C(4)	3350(2)	2498(5)	7047(4)	38(1)
C(5)	3723(2)	1682(6)	7798(4)	37(1)
C(6)	4195(2)	2424(5)	7917(5)	40(1)
C(7)	3058(2)	5008(6)	5575(5)	41(1)
C(8)	3614(2)	-76(6)	8504(5)	45(1)

Table 25. Bond lengths [ $\text{\AA}$ ] and angles [ $^\circ$ ] for **5**.

for 4.

---

Sn(1)-C(1)	2.119(4)
Sn(1)-C(1)#1	2.119(4)
Sn(1)-Cl(1)	2.3399(11)
Sn(1)-Cl(1)#1	2.3399(11)
F(1)-C(7)	1.338(6)
F(2)-C(7)	1.325(5)
F(3)-C(7)	1.318(5)
F(4)-C(8)	1.343(5)
F(5)-C(8)	1.335(5)
F(6)-C(8)	1.313(5)
C(1)-C(2)	1.391(6)
C(1)-C(6)	1.393(6)
C(2)-C(3)	1.391(6)
C(3)-C(4)	1.393(6)
C(3)-C(7)	1.500(6)
C(4)-C(5)	1.382(6)
C(5)-C(6)	1.382(6)
C(5)-C(8)	1.515(6)
C(1)-Sn(1)-C(1)#1	125.9(2)
C(1)-Sn(1)-Cl(1)	109.35(11)
C(1)#1-Sn(1)-Cl(1)	104.96(11)
C(1)-Sn(1)-Cl(1)#1	104.96(11)
C(1)#1-Sn(1)-Cl(1)#1	109.35(11)
Cl(1)-Sn(1)-Cl(1)#1	99.23(6)
C(2)-C(1)-C(6)	119.7(4)
C(2)-C(1)-Sn(1)	118.5(3)
C(6)-C(1)-Sn(1)	121.8(3)
C(1)-C(2)-C(3)	120.1(4)
C(2)-C(3)-C(4)	120.4(4)
C(2)-C(3)-C(7)	120.2(4)
C(4)-C(3)-C(7)	119.4(4)
C(5)-C(4)-C(3)	118.7(4)

C(4)-C(5)-C(6)	121.7(4)
C(4)-C(5)-C(8)	119.4(4)
C(6)-C(5)-C(8)	118.8(4)
C(5)-C(6)-C(1)	119.4(4)
F(3)-C(7)-F(2)	107.9(4)
F(3)-C(7)-F(1)	105.9(4)
F(2)-C(7)-F(1)	106.5(4)
F(3)-C(7)-C(3)	113.0(4)
F(2)-C(7)-C(3)	111.9(4)
F(1)-C(7)-C(3)	111.3(4)
F(6)-C(8)-F(5)	108.1(4)
F(6)-C(8)-F(4)	107.0(4)
F(5)-C(8)-F(4)	105.8(4)
F(6)-C(8)-C(5)	113.0(4)
F(5)-C(8)-C(5)	111.3(4)
F(4)-C(8)-C(5)	111.3(4)

---

Symmetry transformations used to generate equivalent atoms: #1  $-x+1,y,-z+3/2$

Table 4. Anisotropic displacement parameters ( $\text{\AA}^2 \times 10^3$ ) for k09195a. The anisotropic displacement factor exponent takes the form:  $-2\sigma^2 [ h^2 a^2 U^{11} + \dots + 2 h k a^* b^* U^{12} ]$

	U11	U22	U33	U23	U13	U12
Sn(1)	31(1)	42(1)	40(1)	0	0(1)	0
Cl(1)	45(1)	50(1)	41(1)	-6(1)	-2(1)	6(1)
F(1)	75(2)	84(2)	44(2)	-8(1)	-16(2)	23(2)
F(2)	36(2)	79(2)	77(2)	23(2)	2(1)	4(1)
F(3)	59(2)	42(2)	90(2)	11(2)	-18(2)	4(1)
F(4)	95(3)	56(2)	49(2)	18(1)	-7(2)	-9(2)
F(5)	84(2)	35(1)	73(2)	-1(1)	9(2)	6(1)
F(6)	54(2)	54(2)	105(3)	30(2)	7(2)	-5(1)
C(1)	24(2)	38(2)	43(2)	-3(2)	1(2)	-1(2)
C(2)	38(2)	36(2)	38(2)	-2(2)	2(2)	1(2)
C(3)	38(2)	34(2)	37(2)	0(2)	1(2)	4(2)
C(4)	38(2)	38(2)	39(2)	-4(2)	4(2)	0(2)
C(5)	42(2)	33(2)	36(2)	-2(2)	3(2)	3(2)
C(6)	44(2)	38(2)	40(2)	-1(2)	-1(2)	4(2)
C(7)	32(2)	45(2)	44(2)	6(2)	0(2)	2(2)
C(8)	47(3)	40(2)	50(3)	2(2)	1(2)	1(2)

Table 5. Hydrogen coordinates ( $\times 10^4$ ) and isotropic displacement parameters ( $\text{\AA}^2 \times 10^{-3}$ ) for **5**.

	x	y	z	U(eq)
H(2A)	4002	5964	6050	45
H(4A)	3028	1970	6976	46
H(6A)	4447	1830	8426	49